FACULTÉ
DE MÉDECINE

UNIVERSITÉ LIBRE DE BRUXELLES

Clinical implementation of a Monte Carlo-based platform for the validation of stereotactic and intensity-modulated radiation therapy

Thesis submitted by Antoine WAGNER
in fulfilment of the requirements of the PhD Degree in Biomedical Sciences
("Docteur en Sciences Biomédicales")
Academic year 2019-2020

Supervisor: Professor Dirk VAN GESTEL

Co-supervisor: Professor Nick REYNAERT

Laboratoire de Radiophysique Médicale, ULB

Thesis jury:

Christian MELOT (ULB, Chair)
Dirk VAN GESTEL (ULB, Secretary)
David GALL (ULB)
Serge GOLDMAN (ULB)
Pasquale NARDONE (ULB)
Nick REYNAERT (ULB)
Michaël VOUCHE (ULB)
Edmond STERPIN (KUL)
Dirk VERELLEN (UAntwerp)

Faculté de Médecine – Université Libre de Bruxelles

Clinical implementation of a Monte Carlo-based platform for the validation of stereotactic and intensity-modulated radiation therapy

Thesis submitted by Antoine WAGNER
in fulfilment of the requirements of the PhD Degree in Biomedical Sciences
("Docteur en Sciences Biomédicales")
Academic year 2019-2020

Supervisor: Professor Dirk VAN GESTEL

Co-supervisor: Professor Nick REYNAERT

Laboratoire de Radiophysique Médicale, ULB

Thesis jury:

Christian MELOT (ULB, Chair)
Dirk VAN GESTEL (ULB, Secretary)
David GALL (ULB)
Serge GOLDMAN (ULB)
Pasquale NARDONE (ULB)
Nick Reynaert (ULB)
Michaël VOUCHE (ULB)
Edmond STERPIN (KUL)
Dirk VERELLEN (UAntwerp)

Remerciements

Je tiens tout d'abord à remercier mon promoteur, le professeur Dirk Van Gestel, d'avoir accepté de me superviser dans ce travail. J'ai pu grandement apprécier ses conseils avisés et son aide tout au long de ma thèse.

Je remercie également mon co-promoteur, le professeur Nick Reynaert, de m'avoir encouragé à me lancer dans ce travail, et de m'avoir suivi et sauvé des impasses dans lesquelles je me perdais parfois. Que ce soit depuis mon arrivée à Lille il y a maintenant quelques années, ou plus tard après son retour au pays, Nick a toujours répondu présent à mes appels à l'aide, et rien de ceci n'aurait été possible sans son indéfectible soutien et son optimisme sans faille (même s'il m'a obligé à écouter ses innombrables créations musicales en contrepartie).

Je remercie les membres de mon jury d'avoir accepté de lire et juger ce travail de thèse.

Je tiens aussi à remercier le professeur Eric Lartigau, qui m'a donné la possibilité de progresser sur ce travail malgré des activités cliniques souvent chargées au Centre Oscar Lambret.

Je remercie particulièrement Thomas, Frederik, Kévin et Erwann pour leur aide sur les différents articles, pour le temps passé à mesurer, à expliquer ou encore à relire. Leurs retours toujours rapides et pertinents m'ont souvent remis sur la voie et évité bien des obstacles. Je remercie également Pauline, Julien, Romain, Ludovic, Camille, Benjamin, Thierry, François et Christina, qui ont été un soutien permanent au long de ce travail, et pour avoir accepté que mon temps soit parfois détourné de la routine du département.

Je remercie aussi l'équipe médicale et les manipulateurs du département de radiothérapie du Centre Oscar Lambret, pour leur disponibilité et leur gentillesse.

Ayant la faiblesse de croire que les activités extra-professionnelles constituent une contribution indirecte mais néanmoins essentielle pour mener à bien un tel projet, je tiens à remercier Jérôme, Julien, Julieng, Folki, Guillaume L, Benoît, et Guillaume T pour les nombreuses heures passées à nous détruire les tympans, que ce soit dans des caves, des bars douteux, ou des tremplins obscurs... Je remercie mes sympathiques futurs ex-voisins Bertrand et Sophie. Je remercie aussi (en vrac) Alex, Pef, Kenza, Nico, Béné, Xav, Abel, Romaric, Guillaume M, Younes, Bruno, Karim, Paul, Tarek, Alba, Conan, Joseph, Rheu, Roland et bien d'autres de Lille, de Bruxelles ou d'ailleurs...

Je termine par ma famille, pour leur soutien éternel, et pour avoir toujours fait semblant que mon sujet leur paraissait intéressant. Je remercie particulièrement mes parents, mon frère, Camille, les innombrables oncles/tantes/cousin(e)s, ma tante Anne, ma Omi et mon oncle Raymond.

Résumé

En radiothérapie, le niveau de précision de la dose délivrée au patient au cours de son traitement est d'une importance essentielle dans l'évolution vers une amélioration de la qualité et de la cohérence des données de suivi. L'une des premières étapes vers un système de support à la décision clinique (Clinical-Decision Support System CDSS) est la reconstruction précise de cette dose délivrée, en prenant en compte les nombreux facteurs pouvant générer des déviations significatives entre la dose planifiée visualisée à l'écran par l'utilisateur et la dose réellement accumulée lors des séances de traitement. Ces facteurs incluent les variations de débit de l'accélérateur, les incertitudes d'étalonnage, de calcul de dose, les mouvements du patient et des organes, etc.

L'objectif de cette étude est d'implémenter et tester une plate-forme de calcul Monte Carlo pour la validation des systèmes Cyberknife et Tomothérapie installés au Centre Oscar Lambret. L'étude d'un détecteur dédié aux petits faisceaux (la chambre d'ionisation microLion) est également incluse, ce détecteur étant particulièrement adapté aux mesures sur le système Cyberknife.

Le contexte et les concepts théoriques sont introduits dans les deux premiers chapitres. Dans le troisième chapitre, la modélisation Monte Carlo du Cyberknife et du détecteur microLion est détaillée. La quatrième partie inclut la description de la plate-forme Moderato et de son module d'évaluation. Dans le dernier chapitre, la modélisation du dernier modèle de Cyberknife (M6) équipé d'un collimateur multi-lames est décrite. Une nouvelle technique est également introduite dans le but d'accélérer la recherche des paramètres du faisceau d'électrons pour un modèle Monte Carlo, permettant une intégration plus simple et automatisée de nouveaux appareils dans Moderato.

Mots-clés

Reconstruction de dose délivrée, double calcul, Monte Carlo, Cyberknife, Tomothérapie, radiothérapie par modulation d'intensité, radiothérapie stéréotaxique

Summary

In radiation therapy, the accuracy of the dose delivered to the patient during the course of treatment is of great importance to progress towards improved quality and coherence of the outcome data. One of the first steps to evolve towards a Clinical-Decision Support System (CDSS) is to be able to accurately reconstruct that delivered dose, taking into account the range of factors that can potentially generate significant differences between the planned dose visualized on the screen of the dosimetrist, and the actually delivered dose accumulated during the treatment sessions. These factors include accelerator output variations, commissioning uncertainties, dose computation errors, patient and organ movement, etc.

The objective of this work is to implement and test a Monte Carlo platform for the validation of the Cyberknife and Tomotherapy systems installed at Centre Oscar Lambret. A study of a small field-dedicated detector (the microLion ionization chamber) is also included, this detector being particularly suited for measurements on the Cyberknife system.

The context and theoretical concepts are introduced in the first two chapters. In the third chapter, the Monte Carlo modelling of the Cyberknife and microLion detector is detailed. The fourth part includes the description of the Monte Carlo platform *Moderato* and its evaluation module. In the final chapter, the modelling of the latest MLC-equipped Cyberknife model (the M6) is described. A new technique is also introduced to accelerate the optimization of the beam electron parameters of a Monte Carlo model, thus allowing for an easier and more automated use of the *Moderato* system.

Keywords

Dose reconstruction, dose verification, Monte Carlo, Cyberknife, Tomotherapy, intensity-modulated radiation therapy, stereotactic radiation therapy

Table of contents

List of publications

Use of a liquid ionization chamber for stereotactic radiotherapy dosimetry

A. Wagner, F. Crop, T. Lacornerie, F. Vandevelde, N. Reynaert
Physics in Medicine and Biology, 2013; 58(8); 2445-2459

Characterization of recombination effects in a liquid ionization chamber used for the dosimetry of a radiosurgical accelerator

A. Wagner, F. Crop, T. Lacornerie, N. Reynaert
Journal of Visualized Experiments, 2014; 87: 51296

Use of an in-house Monte Carlo platform to assess the clinical impact of algorithm-related dose differences on DVH constraints

A. Wagner, F. Crop, X. Mirabel, C. Tailly, N. Reynaert
Physica Medica, 2017; 42; 319-326

Integration of the M6 Cyberknife in the Moderato Monte Carlo platform and prediction of beam parameters using machine learning

A. Wagner, K. Brou Boni, E. Rault, F. Crop, T. Lacornerie, D. Van Gestel, N. Reynaert
Physica Medica, 2020; 70; 123-132

Clinical implementation of a Monte Carlo based treatment plan QA platform for validation of Cyberknife and Tomotherapy treatments

N. Reynaert, B. Demol, M. Charoy, S. Bouchoucha, F. Crop, **A. Wagner**, T. Lacornerie, F. Dubus, E. Rault, P. Comte, R. Cayez, C. Boydev, D. Pasquier, X. Mirabel, E. Lartigau, T. Sarrazin
Physica Medica, 2016; 32; 1225-1237

Can we spare the pancreas and other abdominal organs at risk ? A comparison of conformal radiotherapy, helical tomotherapy and proton beam therapy in pediatric irradiation

E. Jouglar, **A. Wagner**, G. Delpon, L. Campion, P. Meingan, V. Bernier, C. Demoor-Goldschmidt, M. Mahé, T. Lacornerie, S. Supiot
PLoS ONE, 2016; 11(10):e0164643

About the non-consistency of PTV-based prescription in lung

S. Lebredonchel, T. Lacornerie, E. Rault, **A. Wagner**, N. Reynaert, F. Crop
Physica Medica, 2017; 44; 177-187

Planification de la radiothérapie du cancer de la prostate par l'imagerie par résonance magnétique

L. Vanquin, C. Boydev, J. Korhonen, E. Rault, F. Crop, T. Lacornerie**, A. Wagner**, J. Laffarguette, D. Pasquier, N. Reynaert
Cancer / Radiothérapie, 2019 ; 23 ; 281-289

MR to CT synthesis with multicenter data in the pelvic area using a conditional generative adversarial network

K. Brou Boni, J. Klein, L. Vanquin, **A. Wagner**, T. Lacornerie, D. Pasquier, N. Reynaert
Physics in Medicine and Biology, 2020, accepted

List of figures (not included in articles)

List of figures (included in articles)

Publication: Use of a liquid ionization chamber for stereotactic radiotherapy dosimetry

Publication: Use of an in-house Monte Carlo platform to assess the clinical impact of algorithm-related dose differences on DVH constraints

Publication: Integration of the M6 Cyberknife in the Moderato Monte Carlo platform and prediction of beam parameters using machine learning

List of abbreviations

3D-CRT: 3D conformal radiation therapy

AMC: Accuray Monte Carlo

ART: Accuray raytracing

CBCT: cone beam computed tomography

CDSS: clinical decision-support system

COL: Centre Oscar Lambret (Lille, France)

CT: computed tomography

CTV: clinical target volume

DNA: Deoxyribonucleic acid

DQA: Delivery quality assurance

DICOM: digital image and communications in medicine

DRR: digitally reconstructed radiograph

DVF: deformation vector field

DVH: dose volume histogram

DQA: delivery quality assurance

EPID: Electronic Portal Imaging Device

FFF: flattening filter-free

FOV: field of view

FSPB: Finite-size pencil beam

FWHM: full width at half maximum

Gy: unit of radiation dose (Gray), 1 Gy = 1 $J.kg^{-1}$

GTV: gross tumor volume

GUI: graphical user interface

HU: Hounsfield units

IGRT: image-guided radiation therapy

IJB: Institut Jules Bordet (Brussels, Belgium)

IMRT: intensity-modulated radiation therapy

ITV: internal target volume

IVDT: image value to density table

J: Joules

kV: kilovolt

kVCT: kilovoltage computed tomography

LIC: liquid ionization chamber

Linac: linear accelerator

MC: Monte Carlo

MCDE: Monte Carlo dose engine

MCTP: Monte Carlo treatment planning

MeV: Megaelectronvolt

MLC: multi-leaf collimator

MR: magnetic resonance

MRI: magnetic resonance imaging

MU: monitor unit

MV: megavolt

MVCT: megavoltage computed tomography

OAR: organ-at-risk

OCR: off-center ratio

OF: output factor

PDD: percentage depth dose

PET: positron emission tomography

PTV: planning target volume

QC: quality control

ROI: region of interest

RT: Raytracing

SAD: source-axis distance

SSD: source-skin distance or source-surface distance

SBRT: stereotactic body radiation therapy

SRS : stereotactic radiosurgery

TERMA: total energy released per unit mass

TPR: tissue-phantom ratio

TPS: treatment planning system

VMAT: volumetric modulated arc therapy

WHO: World Health Organization

xml: extensible markup language

1. Introduction

1.1. Cancer

Cancer is a disease characterized by cells undergoing abnormal growth inside a healthy tissue, thus degrading its normal function and potentially threatening the organism survival. The severity and evolution of the disease depend on the nature of the cells and the region of the body involved, but in general the term cancer refers to malignant tumors, which can spread to other parts of the body (creating metastases), in contrast to benign tumors. Many different cancers exist, the most common being lung, breast, colorectum, prostate, stomach and liver.

According to the World Health Organization, an estimated 9.6 million deaths worldwide were caused by cancer in 2018 (Figure 1). Apart from well-known causes such as tobacco use, alcohol, unhealthy diet, some bacteria and viruses, etc. the rate of cancer incidence is also linked with the increasing life expectancy, as the risk of developing the disease rises with age. By 2025, the WHO predicts a number of new cancer cases of over 20 million worldwide (to be compared with 14.1 million in 2012) [1].

After diagnosis, a treatment strategy is devised by a multidisciplinary team of physicians. Standard techniques include surgery, chemotherapy, radiation therapy, immunotherapy, or a combination of several of these modalities. Depending on the stage of the disease and the prognosis, a treatment strategy can either be curative or palliative, i.e. aimed mainly at improving the quality of life of the patient.

Studies suggest that approximately 50 % of all cancer patients might benefit from radiation therapy in the management of their disease [2,3].

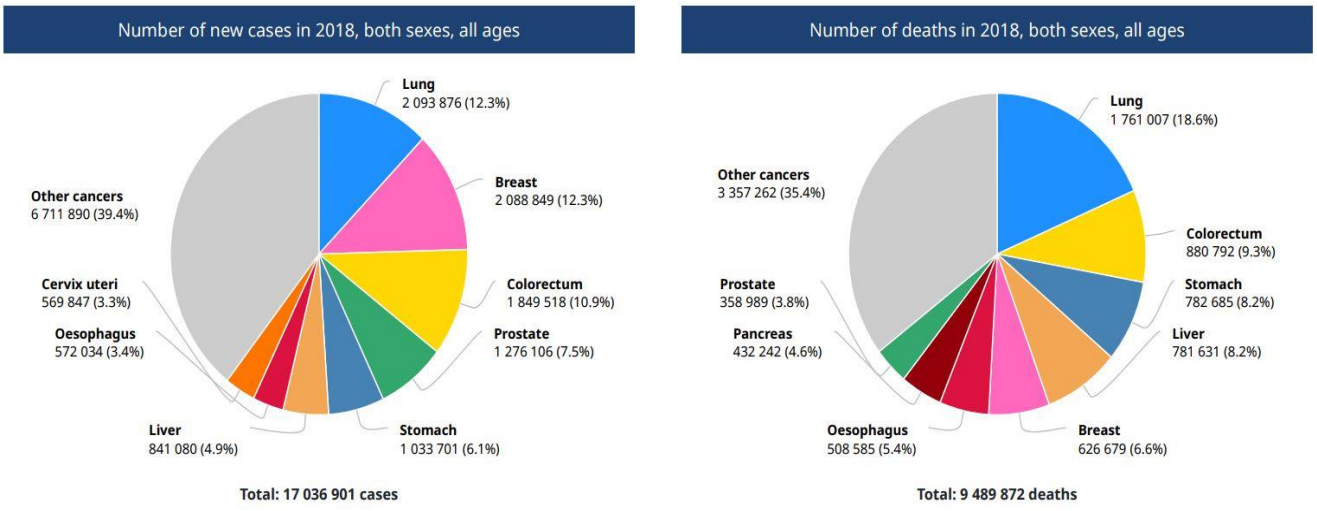

Figure 1. Left: number of new cancer cases in 2018, sorted by anatomical region. Right: number of deaths caused by cancer in 2018 (World Health Organization).

1.2. Radiation therapy

The principle of radiation therapy is to deliver a dose of ionizing radiation to that part of the patient where a tumor is located, in an attempt to kill the malignant cells and thus control the progression of the disease.

Although other techniques exist, a vast majority of radiotherapy devices are linear accelerators ("*linacs*") producing photon beams (Figure 2). They consist of a gantry rotating around a moving couch on which the patient is positioned. Inside the gantry, a focused electron beam is generated and accelerated to a high energy, ranging from 6 to 20 MeV depending on the models (1 MegaElectronVolt = 1.6 10^{-13} Joules). These electrons then impinge on a tungsten target, producing a divergent photon beam that is filtered and shaped by a chain of accessories before being delivered to the patient. Modern devices include a multi-leaf collimator (MLC) to shape the beam in conformance with the target (Figure 2). The amount of radiation deposited in the tissues is measured in Gray (Gy): it is the energy absorbed per unit mass, 1 Gy = 1 J/kg. A radiotherapy treatment can be delivered in a number of different fractionation schemes, ranging from 1 to more than 30 sessions. A typical scheme is to deliver 50 Gy to the tumor in 25 fractions of 2 Gy, spanning a period of 5 weeks with 5 fractions a week.

Figure 2. Left: a Clinac iX linear accelerator (*Varian Medical Systems Inc., Palo Alto, CA. Source:* http://varanparto.com/en/product/clinac-ix/). Right: the multi-leaf collimator (MLC) allows positioning each leaf independently to match the shape of the target volume as closely as possible (*Bortfeld T, Phys Med Biol 51, 2006*).

The radiosensitive part of the cell is the DNA (Deoxyribonucleic acid) that contains all the information necessary for its division. After irradiation by a photon beam, the DNA structure is damaged and if the dose of radiation is sufficient, the cell (or its daughters) will eventually die. The aim of a radiotherapy treatment is to sterilize all those tumour cells that are able to divide (clonogenic cells) and thus prevent tumor growth, while preserving the surrounding healthy tissues from the damages of radiation. With an adequate fractionation scheme, these tissues (called organs-at-risk or OAR) may initiate repair mechanisms, allowing the normal cells to recover between sessions. However, these organs still have tolerance levels that must be respected if one wants to avoid adverse effects, and some treatments might not be feasible depending on the desired dose to the tumor and the geometry of the patient anatomy. This is the reason for the rapidly evolving technology in radiation therapy during the last few decades, going from very simple beam arrangements to much more complex delivery modes.

Historically, a "conventional" 3D conformal radiotherapy (3D-CRT) treatment consisted of a rather simple ballistics of 1 to 6 beams, shaped with the help of the MLC to conform as much as possible to the target volume. This technique does not enable very complex isodoses (e.g. concave) and can be limited in terms of organ sparing. Nowadays, Intensity-Modulated Radiation Therapy (IMRT) is a very widespread treatment technique. The main difference with 3D-CRT is that the intensity of an IMRT beam is variable throughout the dimension of the beam itself, resulting in more complex isodose distributions (Figure 3).

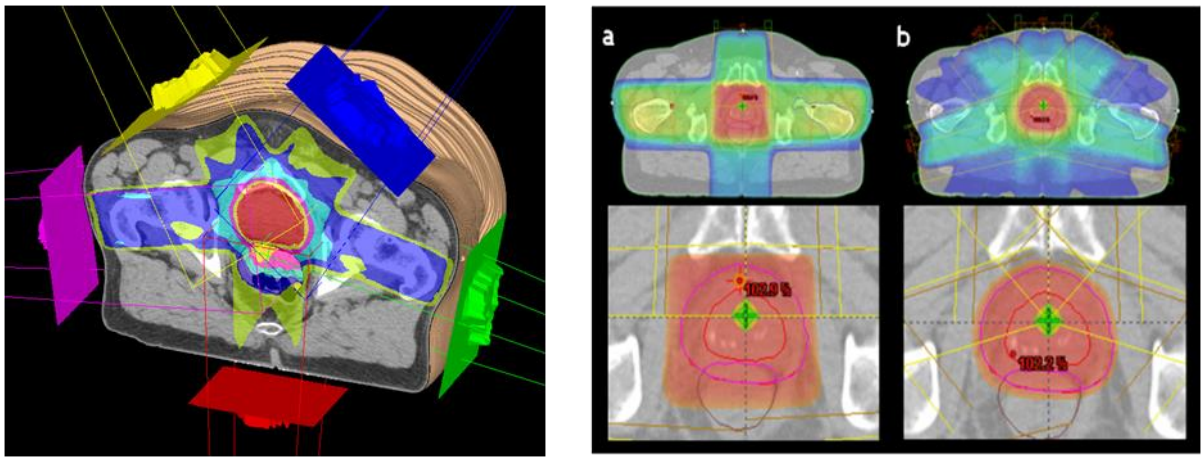

Figure 3. The left image illustrates the concept of intensity modulation: the colored profiles show very different intensity patterns from one beam to the other, depending on the angle used to target the prostate (*Cambazard et al, Discrete Applied Mathematics 160, 2012*). On the right, two CT images with dose superimposed show the difference between a simple 3D-CRT 4-beam arrangement (resulting in a "box-shaped" dose distribution) and the IMRT 5-beam ballistics, leading to a more conformal dose around the target and a better sparing of the bladder and rectum *(Eclipse Treatment Planning System, Varian).*

Most modern accelerators now offer the possibility of performing Volumetric Modulated Arc Therapy (VMAT): compared to IMRT, this technique adds the possibility of rotating the gantry arm and varying the dose rate during the irradiation, essentially speeding up the treatment session.

We will go into more technical details about the delivery techniques in the next sections of this work; for now let us introduce the general "track" that a patient undergoes after being prescribed a radiotherapy treatment (Figure 4).

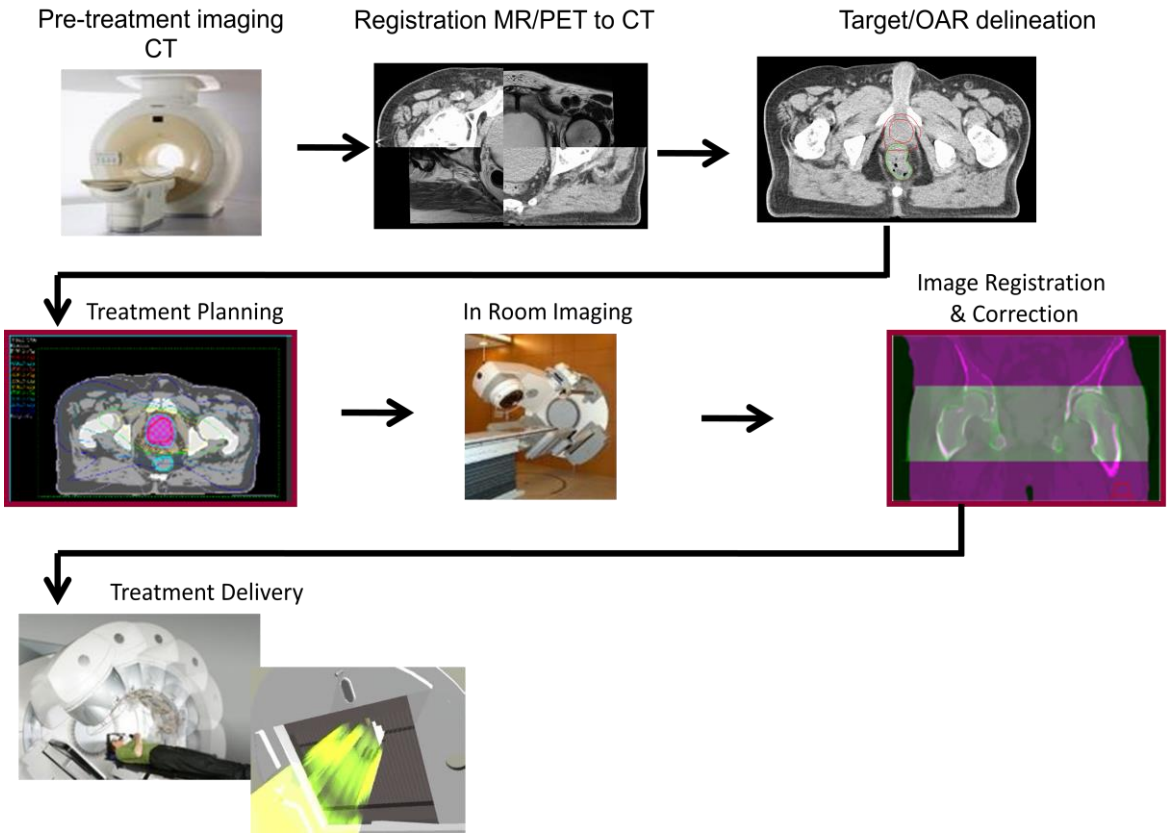

Figure 4. Treatment course in radiotherapy.

The steps are listed below:

- *Pre-treatment imaging*: the patient undergoes a Computed Tomography (CT) in the treatment position. This imaging modality provides a map of the physical densities of the internal tissues of the patient, using a rotating X-ray tube and a translating couch. The patient is positioned with specific immobilization devices that will be used throughout the course of his treatment. Lasers are employed to apply skin markers that materialize the entry points of the treatment beams.

- *Registration*: this "simulation CT" can be registered to other image series offering complementary information in terms of contrast and functional aspects, such as MRI (Magnetic Resonance Imaging) and PET (Positron Emission Tomography). This helps providing a better definition of the tumor and the organs-at-risk during the delineation phase.
  Image registration consists in superposing images of the same patient acquired at different times and possibly in different positions, using advanced image processing algorithms. These can either be rigid (i.e. allowing only translations and rotations of the patient) or deformable (including elasticity to account for the deformable aspect of a human body). Registration is a crucial aspect of the radiotherapy chain, as its accuracy greatly impacts the overall accuracy of the treatment.

- *Delineation*: the target and organs-at-risk (OARs) are contoured by the radiation oncologist (Figure 5), on the CT images and other modalities (MRI, PET…) The

target volumes follow specific conventions defined by the ICRU reports [4–7]: first the Gross Tumour Volume (GTV) is contoured, correponding to the visible extent of malignant growth. Then the Clinical Target Volume (CTV) that encompasses the sub-clinical microscopic disease is delineated, either by adding margins or including anatomical regions known to carry a risk of containing disseminating disease. The Internal Target Volume (ITV) consists of the CTV plus an internal margin taking into account the variations in the size and position of the CTV due to organ motions (e.g. breathing, bowel movements, etc.) Finally, the Planning Target Volume (PTV) is a geometrical concept including patient set-up uncertainties, machine tolerances and intra-treatment variations. It is generally created by adding a margin (not necessarily isotropic) around the CTV or ITV.

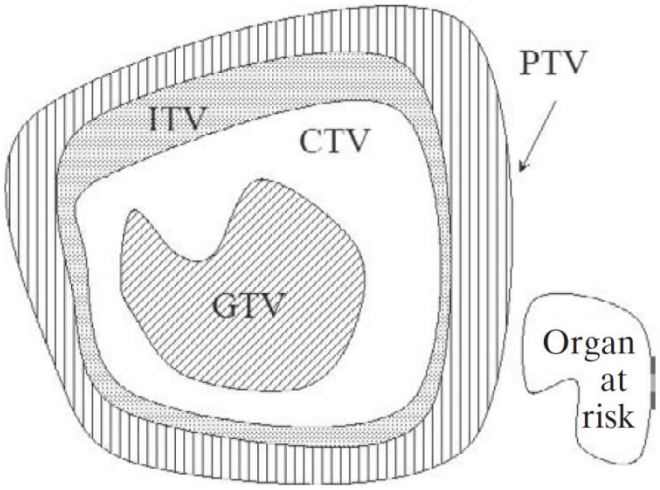

Figure 5. Representation of the regions of interest (targets and OARs) delineated on patient images before starting treatment planning, as defined in the ICRU reports 50 and 62.

- *Treatment planning*: the ballistics of the treatment is prepared by the dosimetrists and physicists on the Treatment Planning Station (TPS). Many methods exist to optimize a radiotherapy treatment plan, but the use of semi-automatic algorithms is becoming increasingly widespread, due to the growing complexity of the delivery scheme.
  The information on the tissue densities is extracted from the simulation CT, allowing the TPS to calculate the dose deposition from the photon beams. The plan is iteratively optimized and re-evaluated by visualizing the isodose lines on the patient image, and by observing the Dose-Volume Histograms (DVHs), i.e. the curves representing the dose delivered to a percentage of each of the regions of interest (ROIs).
  Once the treatment plan is considered optimal, it is validated by a radiation oncologist and a physicist, and the beam parameters are exported to the treatment console.

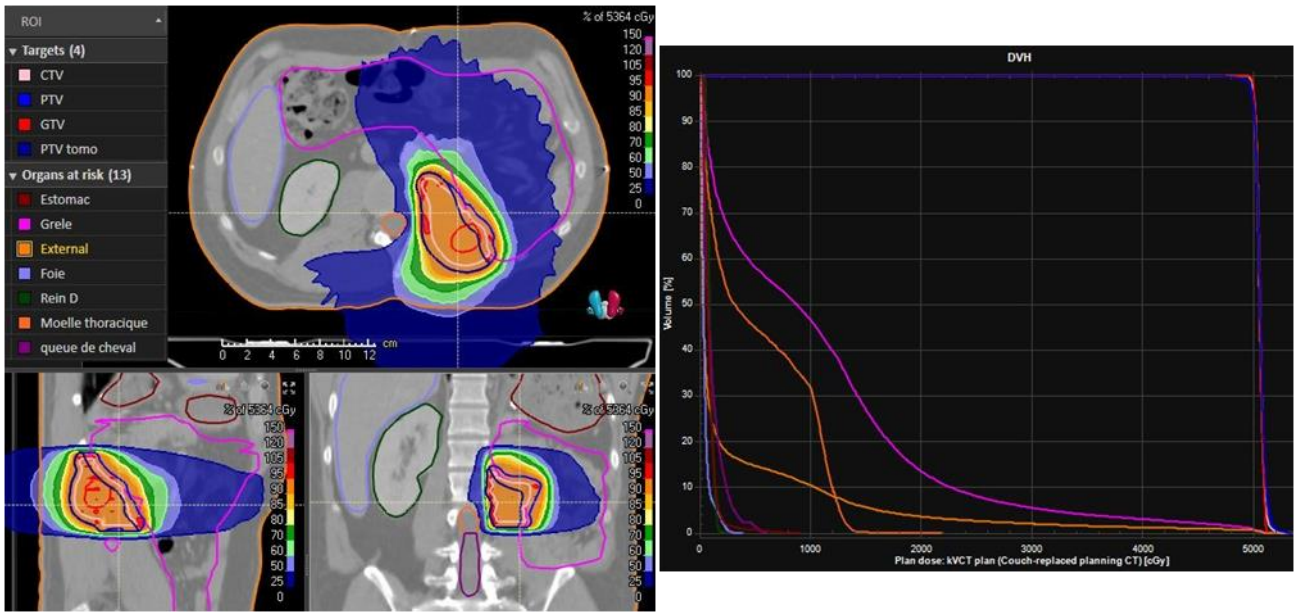

Figure 6. Typical interface of a TPS: on the left the user visualizes the CT images with the isodose lines superimposed in colors, and the list of ROIs on the left. The right part shows the DVH curve for each of the ROIs in the list: the targets appear as steep lines at the right of the graph (homogeneous doses), whereas the OARs show smoother curves with various dose levels depending on the sparing reached for this specific plan (*RayStation, RaySearch Laboratories*).

- *Treatment*: after validation, the patient starts his first treatment session. He is positioned using the same immobilization devices as in the simulation images, and the lasers/skin markers system.
  Then an image is acquired using a specific in-room imaging system (kV cone-beam CT, MVCT, portal images, etc.) and the positioning can be corrected by comparing with the images from the simulation. This is *the Image registration and correction* step.
  Finally, the treatment session is delivered.

This list highlights the fact that radiation therapy is a long serial process that is prone to errors and uncertainties, wherever they may appear in the chain introduced above: even more so considering the very fast evolution of the delivery techniques that require an ever-growing accuracy to ensure treatment safety.

1.3. Rapid learning and clinical decision support

Cancer treatment is becoming increasingly individualized. This is a natural consequence of the expanding amount of data available to diagnose disease and assess treatment outcomes, as well as the number and complexity of methods available to administer therapy [8]. This encouraging aspect however comes at the price of moving the standard of “evidence-based medicine” further away from clinical practice: clinical trials might take too long to produce results relevant within the technological context, and those results might prove too specific to be applied to the general patient population. Less than 3 % of patients treated with radiotherapy are included in clinical trials [9,10].

A proposed solution to these obstacles is the concept of "rapid learning" [8,11]. As a complement to clinical trial-based medicine, the philosophy of rapid learning is to take advantage of the high amount of data available from clinical practice. It can be viewed as an iteration loop (Figure 7): knowledge is first generated from very diverse data (multimodality imaging, disease scores, age, combined therapies, blood tests, genome information, treatment technique and outcome, cost, etc.) Given the considerable amount of information, this knowledge needs to be analyzed using computer models, i.e. performing machine learning. The model is then applied to the clinical practice using a Clinical Decision-Support System (CDSS), which is a tool designed to assist the physician and the patient in their choice of therapeutic strategy, based on the data of that specific patient and the constructed model. Finally, the system is re-evaluated as the data from new patients are fed into the model, which continuously "learns" how to improve.

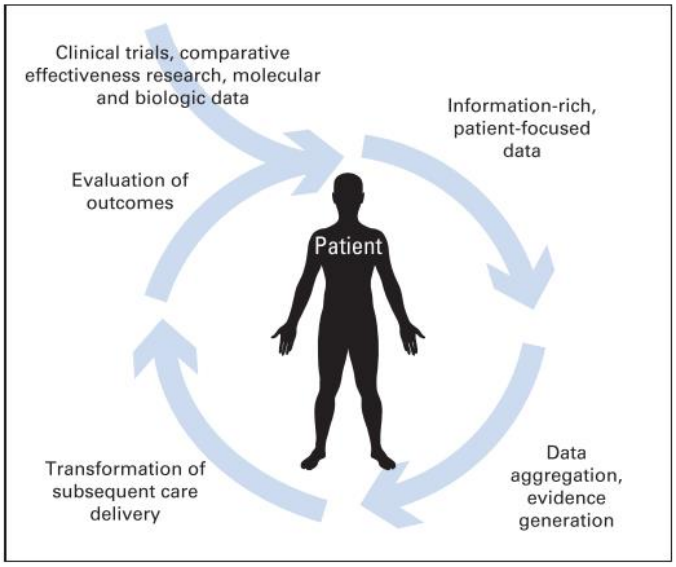

Figure 7. The rapid learning iteration loop includes four phases: patient data collection, knowledge generation, application to treatment delivery, and evaluation of outcomes [11].

Of course, to enable such a system to provide valuable predictive information and help clinical decision, the quality and accuracy of the data gathered have to be sufficient. If too many or too large uncertainties are present, biases are introduced, and the conclusions drawn are likely to be incorrect [12].

1.4. Reconstructing delivered dose

Errors and uncertainties might occur at every step in the chain of processes in radiotherapy (Figure 4). Below is a list of the main sources of uncertainty affecting the correlation between treatment strategy and outcome:

- *Delineation*: systematic uncertainties are inevitably associated with the initial contouring of the target volumes (GTV) and microscopic infiltration (CTV). The volumes can be difficult to discern on CT images that rarely present a sufficient contrast in the range of densities of soft tissues, leading to large inter- and intra-

observer variabilities in the contours [13]. These errors are propagated throughout the entire course of the treatment.
Multimodality imaging is increasingly used to mitigate these problems: the better soft-tissue contrast of MRI images and the high sensitivity of PET modality can help reducing variability [14–16]. However this approach introduces other uncertainties due to the registration process between images [17,18]. This is the reason why a great effort has been devoted to the development of MRI-only radiotherapy in recent years [19]. The research on MRI-based radiotherapy constitutes a major part of the scientific project at our institution, and is still ongoing today [20–22].

- *Accelerator*: uncertainties are associated with the dose rate, field size, laser position, on-board imaging system, gantry and couch movement, multi-leaf collimator, absolute dose calibration, etc. Periodic quality controls (QC) are performed on radiotherapy devices to test that mechanical and dosimetric parameters are within tolerance levels [23].

- *Treatment Planning System*: the TPS parameters must pass a number of verifications before calculating patient plans [24]. The commissioning phase involves performing an extensive series of dose measurements with various detectors in a water phantom (dose profiles, percentage-depth dose, output factors, etc.) and integrating these in the TPS. These "beam data" are then used by the system to calculate the dose in all the patients using the CT images. Once again, errors or inaccuracies could result in systematic over- or underdosage of the patients treated.
  Moreover, different types of algorithms exist to perform dose calculation in a TPS, with various levels of accuracy depending on their complexity. For example, simple correction-based algorithms are known to make significant dose errors when beams are targeted at tissues with many density interfaces (lung, cavum) [25]. More details will be introduced later regarding the accuracy of dose algorithms.

- *Patient*: large sources of error are associated with patient setup, and modifications of the anatomy between treatment sessions (weight loss, target volume reduction) or during the sessions (breathing motion, bowel movements, etc.)

When trying to establish a correlation between the dose given to a tumor and the treatment outcome, it is common to use the planned dose from the TPS, i.e. the dose calculated by the algorithm on the CT images. As we just saw, there are many reasons why the actually delivered dose in the tissues might differ significantly: the last three items of the list above (accelerator, TPS, and patient) directly impact the value of the actual dose in the patient (the delineation errors have a strong impact on the treatment / outcome correlation, but they would not be eliminated by the knowledge of the exact delivered dose). As none of these uncertainties are taken into account in most standard TPS, they might result in large differences between delivered and planned dose [26–30].

Some of the elements cited above can be verified using specific QC tests. Besides periodical verification measurements performed on the accelerator, the physicist can check the accelerator output for a specific plan by performing a Delivery Quality Assurance (DQA), where the treatment plan is delivered to a detector placed inside a phantom.

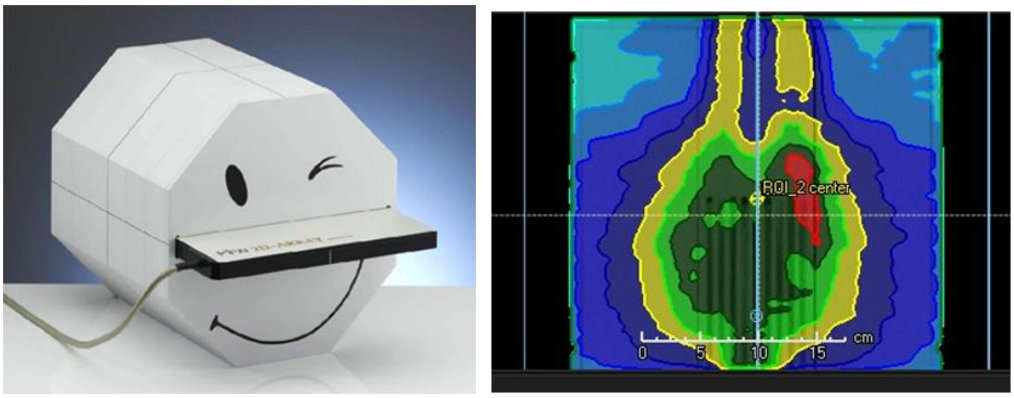

Figure 8. Left: the *Octavius* (PTW, Freibug, https://www.ptwdosimetry.com/en/products/octavius-ii/) consists of an octogonal phantom with a 2D array of ionization chamber detectors. In the TPS, the patient plan is used to re-calculate the dose in that phantom. The resulting dose distribution on the slice corresponding to the position of the matrix of detectors is displayed on the right (*Raystation TPS, Raysearch Labs*).

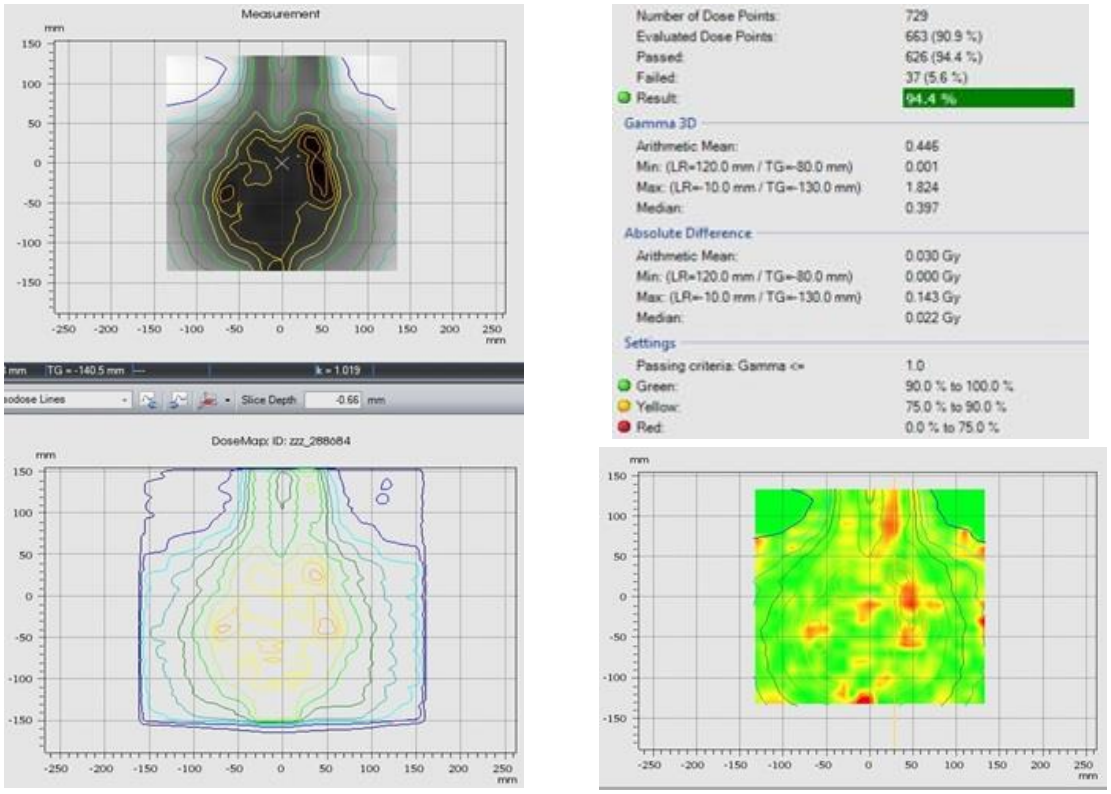

Figure 9. The measured dose matrix (upper left) is compared to the calculated dose (lower left), which is the matrix introduced in Figure 8. The right part of the figure shows the gamma-analysis of the dose. The percentage of passing points is shown above, and the gamma map is represented below (displayed with *VeriSoft* software, PTW Freiburg).

Different types of detector exist: the example of the *Octavius* (PTW, Freiburg) is given in Figure 8 and Figure 9. It consists of a 2-dimensional array of ionization chambers inserted inside an octogonal phantom [31]. Once a patient plan is optimized, it is re-calculated on the CT images of the phantom, and the 2D dose matrix corresponding to the plane of the detectors is extracted. Then the phantom /detector system is placed on the treatment

couch and the plan is delivered, which provides a new 2D dose matrix. Finally the measured and calculated matrices are compared in a dedicated software using gamma-analysis [32], a method that defines an acceptance criterion (gamma-index) based on the dose difference and distance-to-agreement at each point in the matrix.

This method provides a verification of the capacity of the machine to deliver the plan calculated by the TPS (it controls the *"Accelerator"* item from the list above). However, it is not a validation of the TPS dose calculation in the patient, as the phantom is homogeneous, whereas the patient might contain much more complex and heterogeneous media. Nor does it take into account inter- or intra-fraction variations of the patient geometry. Furthermore, the use of gamma passing rates has been shown to sometimes poorly correlate with clinically relevant dose deviations [33].

An alternative to the pre-treatment DQA is to use information collected during the treatment session by the machine, either in the form of log-files containing the actual parameters of all the components at every moment during irradiation (couch, MLC, dose rate, etc.), or using the on-board detectors to reconstruct the original fluence.

Another verification that is routinely realized is the independent calculation of the Monitor Units. The MU are measured by an ionization chamber situated inside the treatment head, and therefore are a measure of the ouput of the accelerator. At the reference conditions (a specific beam setup defined by dosimetric guidelines), the delivery of 100 MU corresponds to a dose of 1 Gy. Of course, a beam delivering 100 MU to an actual patient will not deliver exactly 1 Gy, as the absorbed dose will depend on many other factors (beam size, source-skin distance, geometry of the patient, etc.)

Re-calculating the MU requires a secondary software providing an independent calculation (i.e. using a different algorithm). It has become a legal obligation in France since 2008 [34]. Unfortunately, this method suffers from two major drawbacks. First, while a single-beam verification of the MU can be applied to the simple beams used in conventional 3D conformal radiotherapy, the beams used in more modern techniques such as Intensity-Modulated Radiation Therapy (IMRT) and Stereotactic Body Radiation Therapy (SBRT) present complex shapes and small sizes for which re-calculation is very challenging, or not available. Moreover, the simplicity of such secondary systems implies that dose differences observed between the two algorithms are often attributed to the lack of accuracy of the independent calculation itself.

The last item in the list (the patient-related variations) is probably the one generating the largest deviations, as well as the most difficult to take into account. It requires performing daily images of the patient to re-calculate the dose based on the modified anatomy. A pre-treatment image allows taking into account inter-fraction differences, but ideally several images should be obtained during the treatment, especially for long sessions (4D imaging). From this corrected fraction dose, the dose from all fractions can be accumulated to obtain the final delivered dose to the target and OARs, using deformable image registration (DIR). However, no consensus has yet been reached on which DIR algorithms to use and how to verify them [35]. Besides, new difficulties arise when accumulating dose between deformed images ("dose warping") as voxels might appear or disappear from one session to another, raising the question of how the dose in those voxels should be treated [36].

To sum up, in order to design a reliable dose reconstruction method, each of the aspects above should be addressed. An ideal system should be able to include the actual output of the machine to account for deviations of the accelerator (through log files or exit detector data), and to perform an accurate and independent dose re-calculation in the patient in his actual treatment position (including setup errors and organ motion), based on images acquired before or during the treatment session.

1.5. Description of the project

1.5.i. Context and objectives

The work presented in this manuscript is part of a larger project of personalization of the therapeutic strategy in radiotherapy, through a collaboration between the Centre Oscar Lambret (COL) in Lille and the Institut Jules Bordet (IJB) in Brussels. The long-term objective of this project is to introduce a clinical decision support system (CDSS) as introduced in section 1.3, which requires high-quality patient data.

Research is conducted on different aspects to progress towards this improvement. As briefly mentioned earlier, the departments of both centers are active in the development of MR-only treatment planning [20–22], and an MR scanner dedicated to radiotherapy was recently installed at COL. This advance is of great interest in the improvement of target and OAR delineation (eliminating registration uncertainties), but also a necessary step considering the growing interest for MR-guided radiotherapy devices.

Another aspect of interest is the reporting of dose in radiotherapy: several studies have been published on this topic. The first introduces a solution for the conversion between dose to medium and dose to water [37]. Two other studies are related to the specific problem of dose prescription and reporting for lung treatments [38,39].

The present study falls within the third part of this project, which long-term objective is the determination of the actual delivered dose on different machines, in the hope of establishing correlations between treatment and patient outcomes. As a first step, this work will consist in the clinical implementation of a Monte Carlo-based platform for the validation of stereotactic and intensity-modulated radiotherapy plans. We will give a brief definition of the terms to situate the context; more details will be provided in the next chapter.

Monte Carlo (MC) techniques are a very widespread class of methods that involve obtaining numerical results using repeated random sampling. They are often applied when specific problems are too complex or impossible to solve otherwise (in a “deterministic” manner). In the context of radiation therapy, MC algorithms provide a very accurate tool for the calculation of dose distributions (especially in the presence of tissue heterogeneities), at the cost of longer computation times [40].

A number of new radiotherapy devices have been installed at the Centre Oscar Lambret during the last decade. Today three Tomotherapy machines (Accuray, Sunnyvale, CA) and two Cyberknife systems (Accuray, Sunnyvale, CA) are used, offering a wide range of therapeutic possibilities.

Tomotherapy (Figure 10) is a dedicated Intensity-Modulated Radiation Therapy (IMRT) solution, consisting of a 6 MV accelerator rotating around a translating couch, a 40 cm wide binary MLC and an integrated MegaVoltage Computed Tomography (MVCT) imaging system. Typical indications include normofractionated treatments (from 15 to 35 fractions of 1.6 to 3 Gy) of the head and neck, pelvis, breast, brain and central nervous system tumours, sarcomas, etc. Its IMRT capacity allows it to deliver highly modulated beams that result in very complex and conformal isodoses.

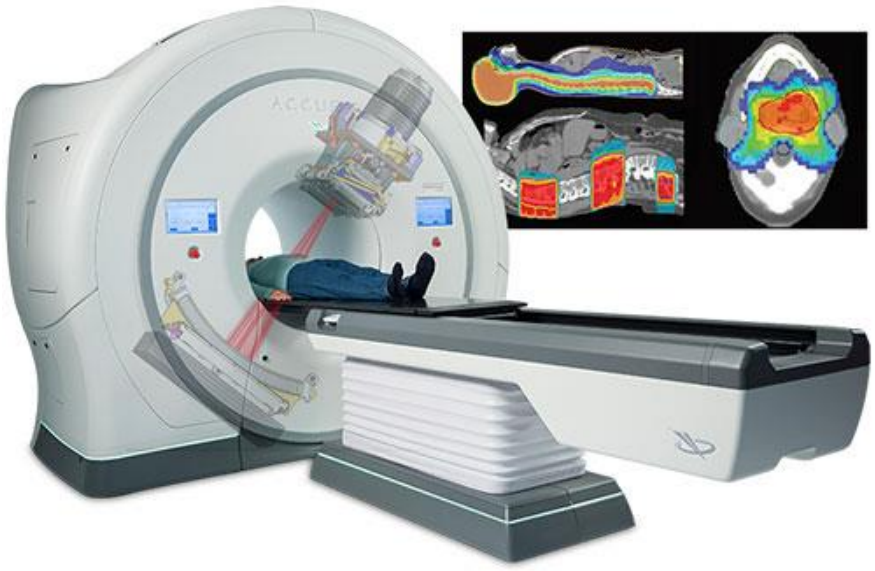

Figure 10. View of the Tomotherapy machine: with its rotating tube and moving couch, its aspect is similar to that of a CT-scanner, but the accelerator delivers a high energy 6 MV beam (instead of 120 kV for the CT). Some typical treatment isodoses are shown in the superior right corner (*Accuray*, Sunnyvale CA, https://www.accuray.com/tomotherapy/).

The Cyberknife (Figure 11), on the other hand, is a Stereotactic Body radiation Therapy (SBRT) device. A 6 MV linac is mounted on a robotic arm with six axes of rotation, providing many possibilities of treatment position and angle. The couch is also supported by a robotic arm allowing for translations and small rotations. Patient position can be verified using two kV imagers positioned at 45° and an optical system. A typical Cyberknife treatment involves 1 to 9 fractions of 4 to 20 Gy (it is *hypofractionated*). The most commonly treated areas include the brain, lung, liver, prostate, spine, and head and neck. In general, targets are of much smaller volume than the ones treated with Tomotherapy (thus allowing for higher doses per fraction), making the two systems complementary.

Figure 11. View of the Cyberknife M6 system, with the robotic treatment head and couch, and the dose images for a stereotactic treatment on the right (small target in the abdomen). Source: https://delraynewspaper.com/wp-content/uploads/2018/07/cyberknife.jpeg

The goal pursued in this work will thus consist in integrating these two machines in a MC calculation platform, allowing for accurate and consistent re-calculation of the dose distributions coming from their different TPS. Besides offering an independent calculation tool to validate clinical treatment plans, this solution will also form the first step towards the reconstruction of the delivered dose to the patient introduced in section 1.4.

1.5.ii. Overview of existing studies

A large number of studies deal with the problem of the re-calculation of planned and/or delivered dose. Some are focused on one of the main three uncertainty factors cited in section 1.4 (i.e. (1) verifying/correcting the output of the accelerator, (2) verifying/correcting the dose calculated by the commercial TPS and (3) taking into account the modifications associated with the patient anatomy/movements), while some try to combine several of these aspects. We will give an overview of a selection of these studies for the sake of brevity.

As introduced earlier, accelerator output can be verified through measurements before or during the treatment.
Chen et al. [41] and Sevillano et al. [42] used exit detector data from Tomotherapy to assess deviations between planned and actual leaf open times of the MLC. Deshpande et al. [43] performed pre-treatment exit data measurements to re-calculate dose distributions on patients planning CTs.
Saito et al. [44] and Sun et al. [45] evaluated methods of 3D dose reconstruction for VMAT treatments. The principle of such methods is somewhat similar to the phantom QC described in section 1.4 (Figure 8 and Figure 9), with the exception that instead of comparing 2D dose distributions, a complete 3D dose is reconstructed, allowing to perform 3D gamma analysis as well as comparison of the planned and "measured" DVHs to targets and OARs.

To verify the dose calculation algorithm of the TPS, an independent dose computation has to be performed.

Handsfield et al [46] developed a Tomotherapy QA process (MCLogQA) combining the exit detector data and a pretreatment Monte Carlo secondary dose calculation on the patient planning CT (based on the TomoPen MC algorithm[47]). This allows comparing the planned dose from the TPS, the MC re-calculated planned dose, and the MC re-calculated dose based on exit detector data.
Commercial solutions for VMAT patient dose reconstruction exist that are based on log-files and EPID (Electronic Portal Imaging Device: a detector placed in front of the treatment head allowing to perform an image using the high-energy treatment beam). *Mobius3D* (Mobius Medical Systems, USA) [48–50] and *PerFraction* (Sun Nuclear Corporation, USA) [48,51,52] are softwares that perform dose re-calculation with a superposition/convolution method (more details are given on this type of algorithm in the next chapter), thus providing independent calculation besides taking into account the linac output. More recently, Monte Carlo-based solutions were introduced to verify dose calculations, such as *SciMoCa* (IBA Dosimetry, Germany), *VeriQA* (PTW, Freiburg) and *RadCalc* (LAP, Germany).

To assess the uncertainties associated with the patient, one has to perform some form of verification during the treatment session.
In vivo dosimetry refers to the measurement of the radiation dose received by the patient during treatment. Many distinct methods exist, offering very different information, from simple point dose verification to much more complex 3D patient dose reconstruction.
In vivo dosimeters have been used for decades [53]: some provide a real-time dose measurement (silicon diodes, MOSFETs) whereas others such as TLDs (thermoluminescent dosimeters) have to be processed after irradiation to obtain the dose. A common way of performing *in vivo* dosimetry is to place the detector on the patient, on the beam axis, and to compare the measured dose to a dose calculated in the TPS. This verification may be useful to detect errors in patient setup, as well as other problems associated with the accelerator (MLC, wedges, etc.) or the TPS (errors in linac modelling). However, it does not provide any information on the dose distribution inside the patient, and it is difficult to implement to complex IMRT techniques such as the ones discussed in this thesis, because of the presence of strong dose gradients preventing from achieving accurate point measurements.
Portal dosimetry (EPID) consists in the acquisition of megavoltage images during patient treatment using an amorphous silicon detector panel. This information can be used to verify the dose at the beam entrance [54] or to reconstruct the 3D dose distribution inside the patient geometry by back-projecting the measured fluence [55]. Portal dosimetry is not present on the Tomotherapy and Cyberknife devices.
Cone beam computed tomography (CBCT) systems can be employed to image the patient before a treatment session. A CBCT is a CT where the fan beam is replaced with a divergent conical beam, thus imaging a volume of the patient instead of a slice. It can be mounted on an accelerator to acquire a 3D image from a single rotation of the gantry, either before or during the treatment irradiation. Several teams have exploited CBCT images to reconstruct delivered dose during treatments [27,28,30,56].
The Helical Tomotherapy system is equipped with a megavoltage computed tomography (MVCT) system, which allows acquiring a CT image of the patient using the MV beam (with a reduced energy and a low dose rate) before delivering the actual treatment. Chao et al. used MVCT images to reconstruct the dose from tomotherapy total-body irradiation (TBI) [57]. Branchini et al. [58] used deformable image registration to re-

calculate delivered dose for 8 head and neck patients. Thomas et al [59] developed a method of dose re-calculation on MVCT images to provide a "dose of the day" information, with an independent algorithm based on a RayTrace technique [60]. This process was applied in a later study from the same group (Shelley et al [29]) to re-calculate and accumulate the dose to the rectum throughout all the treatment sessions for 109 prostate patients.

1.5.iii. Plan of the thesis

In the second chapter, more details will be provided on the tools and radiotherapy techniques studied. We will describe the technical aspects of the Tomotherapy and Cyberknife systems more specifically, and discuss the algorithms used in their respective TPS to compute the dose in the patient. The specific Monte Carlo methods used in this work will also be described. Finally, the problems associated with the measurement of the so-called "small fields" will be introduced as well, as both devices fall within that category.

The third chapter introduces the MC modelling of the first Cyberknife system installed at the Centre Oscar Lambret. This modelling is then used to perform the characterization of a detector specifically introduced for the measurements of small fields: the PTW microLion detector, which is a liquid ionization chamber. This detector is also modelled using Monte Carlo methods, allowing to obtain correction factors to apply to the chamber readings to account for perturbation effects.

The fourth chapter introduces the Monte Carlo platform *Moderato*: the MC models for the Cyberknife (obtained in the previous chapter) and the Tomotherapy (realized by another researcher from our team) are integrated in a user-friendly, automated platform allowing for the re-calculation of patient plans in a simple graphical user interface.
An additional module is then introduced in *Moderato*: the "prescription – validation" module, allowing for automated generation of contraints on organs-at-risk based on the fractionation scheme, and a visual warning system in case of constraints violations. A study is realized on a number of Cyberknife and Tomotherapy plans to determine the dose differences arising from the MC re-calculations of the plans, and their impact on the constraints to the OARs.

In the fifth chapter, the MC modelling of the more recent MLC-equipped Cyberknife M6 device is realized. The model is also integrated in *Moderato* and patient plans are re-calculated. Film measurements are performed for specific cases of complex peripheral beams to assess the accuracy of the algorithms.
A new method is then introduced, inspired by the difficulties in modelling this type of device: a Machine Learning (ML) algorithm is built that allows predicting the parameters of an unknown primary electron beam based on dose profile measurements, saving a considerable amount of research time.

Finally, in the last chapter, we emphasize the contributions of the present work, and give an overview of the perspectives and the projects to come.

2. Tools and theoretical aspects

2.1. Linear accelerator

The vast majority of external radiation therapy devices used nowadays is based on the concept of the linear accelerator. An electron beam is produced and accelerated to a high energy, comprised between 4 and 25 MeV. Accelerating electrons to a higher energy requires a longer accelerator tube: it is situated inside the horizontal part of the gantry pictured in Figure 12, and a bending magnet is used to deflect the electron beam by 90° and orient it in the direction of the treatment couch (this is not the case for Tomotherapy and Cyberknife, where the lower energy of 6 MV allows using a straight design).

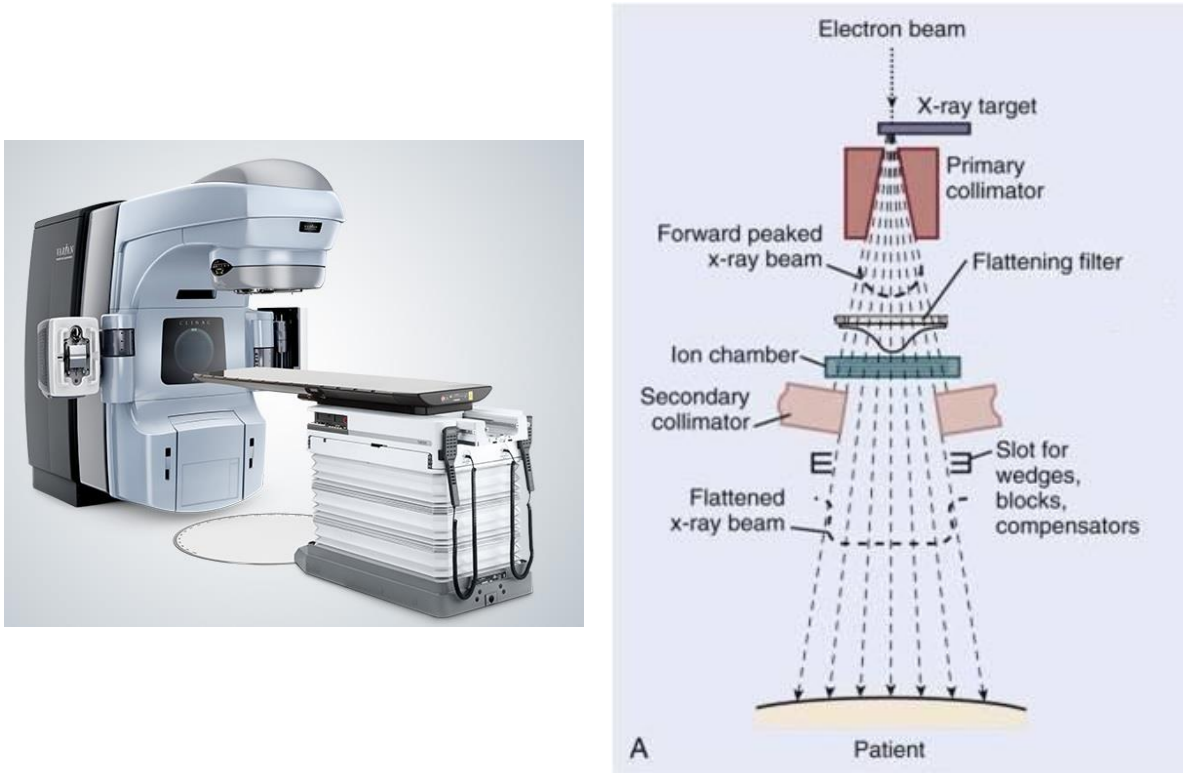

Figure 12. General overview of the components used to generate, monitor and shape a photon beam in a medical linear accelerator. Left: https://img.medicalexpo.fr/images_me/photo-mg/70440-8852662.jpg Right: Tsechanski et al, Phys Med Biol 43, 1998.

The high-energy electron beam then hits a tungsten X-ray target, producing a divergent forward-peaked photon beam due to electron deceleration (bremsstrahlung). This beam then passes through a series of components as depicted on the right side of Figure 12.

The primary collimator removes the part of the beam produced with a very large angle with respect to the electron beam axis. In conventional linear accelerators such as the model visible on the left side, the next component is the flattening filter: its purpose is to

compensate for the forward-projected intensity of the photon beam by inserting a higher attenuation on the central axis, thus providing a nearly flat intensity profile at its exit. It is worth noting that the flattening filter is no longer present in many modern devices (including Tomotherapy and Cyberknife), which are therefore know as flattening filter-free, or "FFF". Next, the beam passes through the monitor chamber, an ionization chamber that continuously measures the output the linac and sends the signal to stop irradiation once the correct number of monitor units (MU) is delivered. Finally, the secondary collimation includes the jaws and MLC that define the shape of the beam that enters the patient anatomy.

2.2. Helical Tomotherapy

Three Tomotherapy (*Accuray, Sunnyvale, CA*) machines have been installed at Centre Oscar Lambret since 2008. As briefly introduced in the previous chapter, this device is a dedicated IMRT modality, consisting of a 6 MV *FFF* linear accelerator rotating around a couch that translates during dose delivery. This setup results in a "helical" irradiation, i.e. the patient is treated slice by slice with a narrow opening of the beam in the craniocaudal direction.

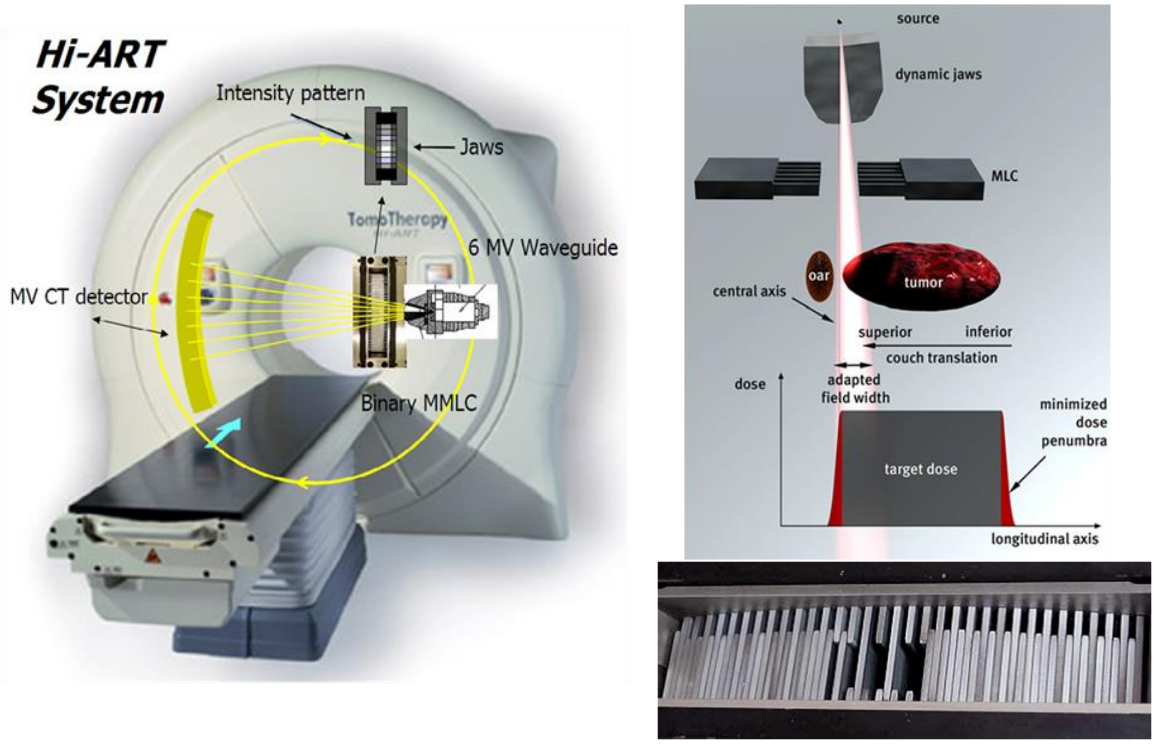

Figure 13. Left: schematic view of the Tomotherapy system and its major components (from https://digitalcommons.lsu.edu/gradschool_theses/2491). Upper right: principle of the dynamic jaws (Sterzing et al, IJROBP 76 (4), 2010). Lower right: view of the binary MLC (from https://www.researchgate.net/profile/Tomas_Kron/publication/237472416).

This craniocaudal extension is defined by the jaws, which present three possible widths at isocenter: 5 cm, 2.5 cm or 1 cm. These jaws gradually open when the moving couch brings the target volume in front of the beam, and close when reaching the end of the

target extension, allowing to spare the tissues directly above or under the tumor [61] (Figure 13).

A binary MLC is used to block parts of the beam during the rotation, each leaf being either fully closed or fully open. The changes in this MLC pattern from one incidence to the other provide Tomotherapy with its high modulation capacities.
The system is also equipped with MVCT (MegaVoltage Computed Tomography) detectors, allowing to perform a tridimensional density image in a manner similar to a classical CT, although with a much lower tissue contrast due to the higher energy of the beam. After the patient has been positioned based on skin markers and lasers, an MVCT image is performed and registered with the planning kVCT (Figure 14). This information allows to correct the initial setup by applying translations and/or rotations with the treatment couch and the tube.

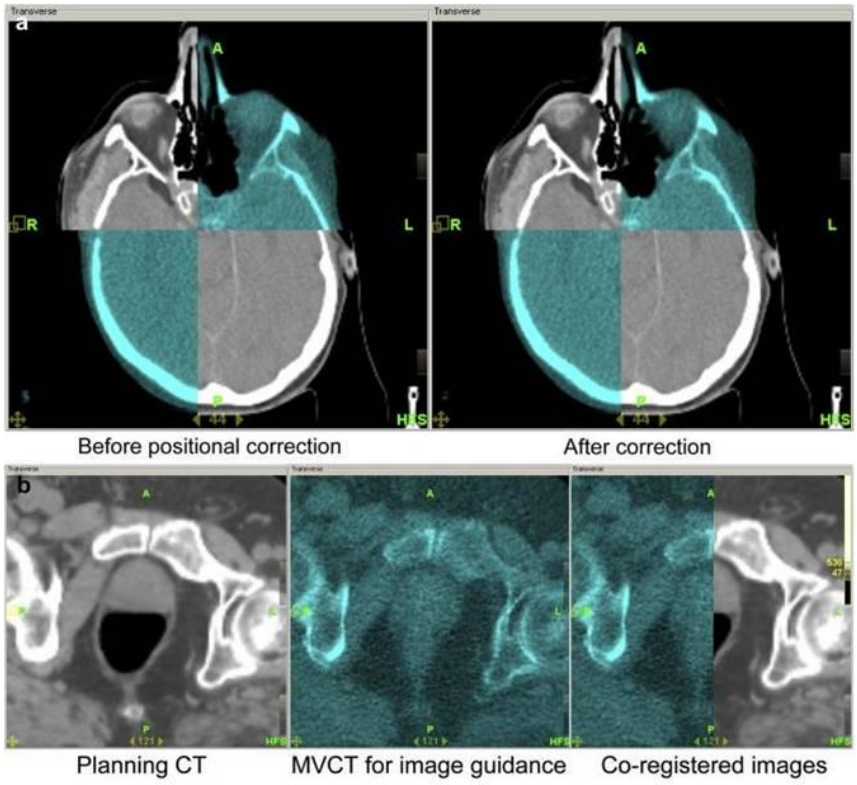

Figure 14. Use of MVCT images (shown in blue) to apply setup corrections based on the registration with the planning CT (grey).

The most frequent indications of Tomotherapy are head and neck tumors, pelvis, central nervous system, breast, brain, lung and limbs. A major advantage resides in the very large treatment range in the craniocaudal direction (160 cm), in particular when treating lower limbs or medulloblastoma.
An example of a head and neck treatment with Tomotherapy is given in Figure 15. The prescription contains an "integrated boost" with two dose levels of 54 and 60 Gy, delivered respectively to a "low-risk" and a "high-risk" CTV. This means that these two regions receive different dose during each session.
Depending on their situation and sensitivity, the organs-at-risk (OARs) receive more or less dose as indicated by the curves in the Dose-Volume Histogram (DVH). For example, it can be seen on the transversal and coronal views that a low-dose region has been forced around the spinal cord, with a dose limit at 25 Gy. In order to achieve this, the

user allowed the system to apply a significant amount of modulation (large time differences in leaf openings), as illustrated by the high modulation factors and gantry period.

The Monte Carlo modelling of the Tomotherapy system will not be described in full details in this work as it was performed by another member of our team, but a brief description will be provided in chapter 4.

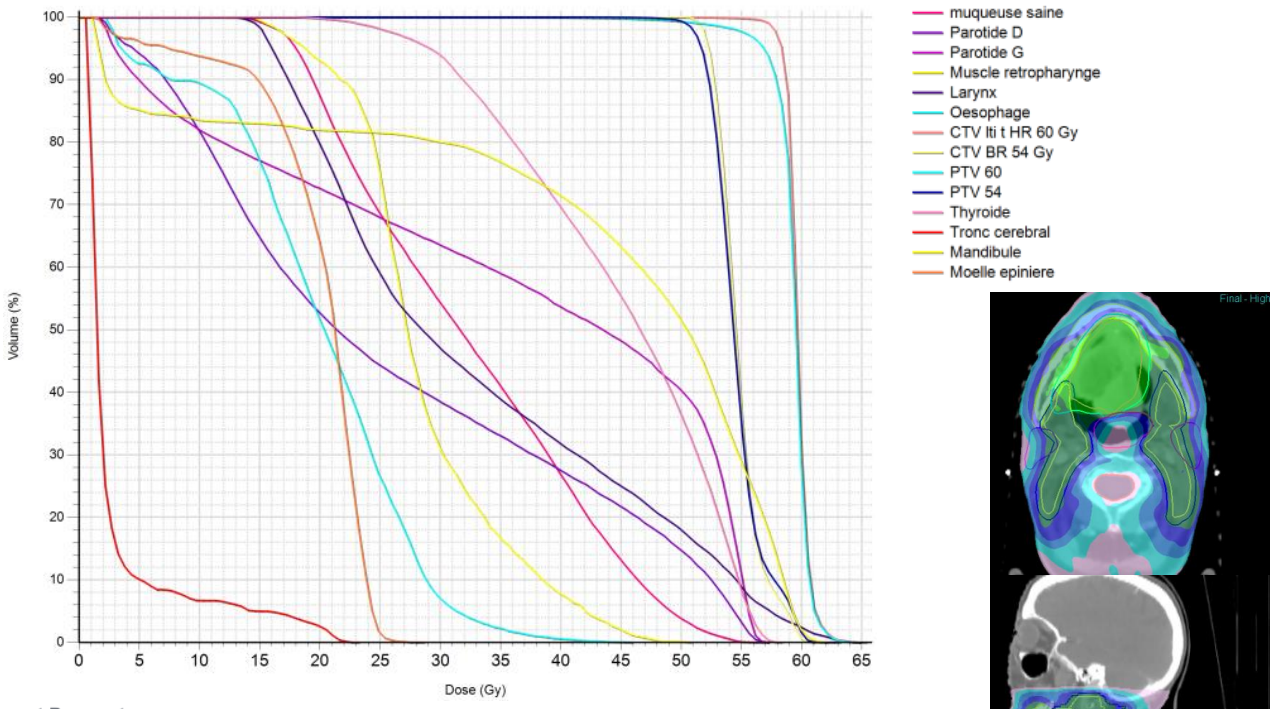

Treatment Parameters

Treatment Machine:	0210260 1180 MU/min, rev 342	**Patient Position:**	HFS
Treatment Machine Serial No.:	210260	**Field Width (cm):**	2.5, Dynamic
Planned Fractions:	30	**Pitch:**	0.431
Plan Delivery Type (Mode):	Helical (IMRT)	**Modulation Factor (Actual):**	2.600 (1.7)
Gantry Period (sec):	17.1	**Beam On Time (sec):**	264.5
Gantry Rotations:	15.4	**Couch Travel (mm):**	167.4
		Couch Speed (mm/sec):	0.6

Prescription Details

Prescription:	Median of PTV OPT 54, 54.00 Gy	**Reference Point (IECp, mm):**	X: 9.2 Y: -32.0 Z: 26.2
Maximum Dose (Gy):	64.88	**Reference Dose (Gy):**	64.88
Prescribed Dose per Fraction (Gy):	1.80		
MU per Fraction:	3831.5		
Dose Calculation Algorithm:	Convolution-Superposition		
Dose Calculation Resolution	High (Final)		

Figure 15. A typical plan report for a Helical Tomotherapy treatment (images from the *Precision* TPS, *Accuray*). The DVH is a graphical view where each curve represents the cumulative dose delivered to the targets (denoted "CTV" or "PTV" in the legend) and OARs (shown here in French). The treatment parameters are included below the DVH: the number of fractions, the gantry period (time needed for the tube to perform one complete rotation around the couch), the field width (set here at 2.5 cm), the pitch (defined similarly as in CT imaging), the total beam on time for one session, the total and fraction dose prescription, and the algorithm used for dose calculation. Finally, the right part contains transversal, sagittal and coronal views of the patient CT with the isodoses superimposed. The dark green isodose corresponds to 54 Gy and covers the larger low-risk CTV, whereas the light green area corresponds to the high-risk CTV irradiated with a dose of 60 Gy.

2.3. Cyberknife

The Cyberknife (*Accuray, Sunnyvale, CA*) is a dedicated stereotactic body radiation therapy (SBRT) system. Unlike Tomotherapy, its principle is based on hypofractionation, which is the delivery of higher doses per fraction (generally from 4 to 20 Gy) to much smaller target volumes. This is achieved through the use of a very large number of angular incidences (including non-coplanar angles), and therefore of strong dose gradients around the targets that allow a better sparing of OARs in their immediate vicinity. However, this principle no longer holds if the target becomes too large, as the irradiated normal tissue around it would not tolerate such high doses per fraction.

Two different Cyberknife devices are currently used at Centre Oscar Lambret. The first one is the "VSI" model, installed in 2007, and the second is the "M6" model installed in 2017. The main difference between both machines is the introduction of a multi-leaf collimator (MLC) in the M6.

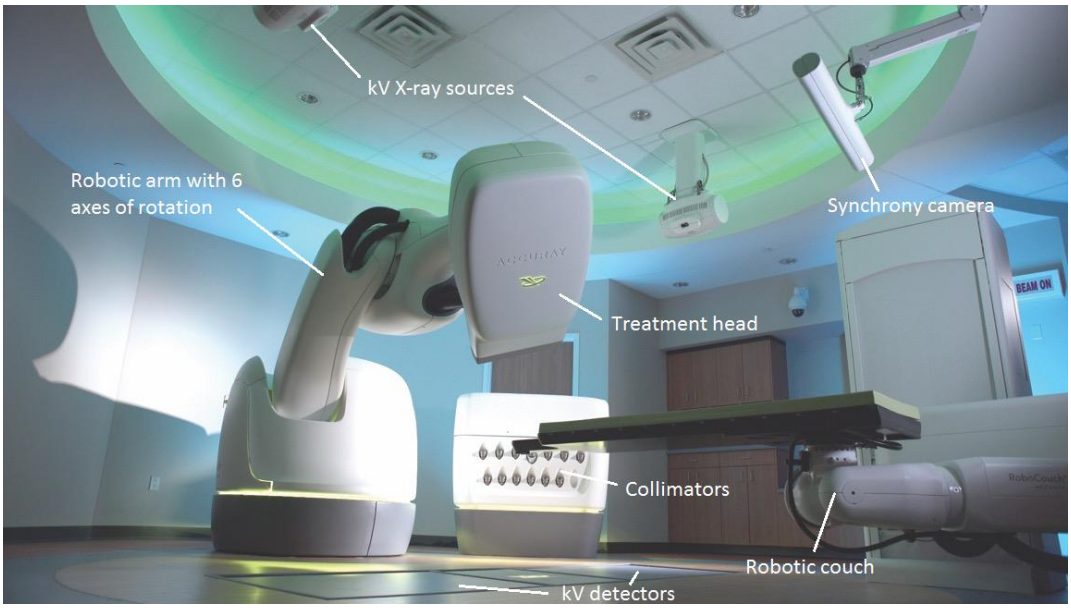

Figure 16. The M6 Cyberknife, with its main components highlighted.

The 6 MV *FFF* treatment head is mounted on a robotic arm with 6 axes of rotation, allowing it to be placed in a large number of positions around the patient ("nodes") and using many different angles to target the lesion. This feature results in higher dose gradients around the tumor, which explains why larger doses per fraction can be administered without damaging the surrounding tissue.
Several collimation options are available (Figure 17): the 12 fixed circular collimators have a diameter that varies from 5 to 60 mm at isocenter (at 80 cm source-axis distance or "SAD"). These have to be changed manually when the plan requires different collimator sizes.
The iris collimator, on the other hand, consists of two banks of leaves arranged as a diaphragm, thus allowing to deliver beams of variable size during a treatment session without any manual change. The available sizes of the beams are the same as for the fixed system. While the actual shape of the beam defined by the iris is a dodecagon, the

difference with the circular shape is small especially when moving farther away from the source (e.g. inside the patient or phantom).

Figure 17. Left : fixed 40 mm collimator. The actual collimator opening is close to 20 mm as it is placed at approximately 40 cm from the source, thus forming a 40 mm beam size at 80 cm distance. Right: view of the iris collimator from below the treatment head. The two banks of leaves can be seen (https://www.slideshare.net/JustinVinci/cyberknife-at-saint-raphaels-campusrevb).

This small difference however has strong consequences in the Monte Carlo modelling of the iris collimator, as will be detailed later.

The M6 version of the Cyberknife also includes a MLC that consists of two banks of 26 leaves each, with a 3.85 mm width at 80 cm SAD. The maximum size of the beam is 115x100 mm (allowing to treat larger targets and to speed up some treatments). To block parts of the beam, one bank is fully closed while the other is fully retracted (Figure 18).

Figure 18. The M6 treatment head includes a MLC, consisting of two banks of 26 leaves each (https://www.accuray.com/cyberknife/cyberknife-treatment-delivery-2/).

When viewed from the side, the leaves are focused on the radiation source (the tungsten target) before the entire collimator is rotated by 0.5° to minimize interleaf leakage. Each leaf has a height of 9 cm in the direction of the beam, and the tip consists of three flat surfaces focused on the source at fully retracted, mid-travel, and fully closed positions.

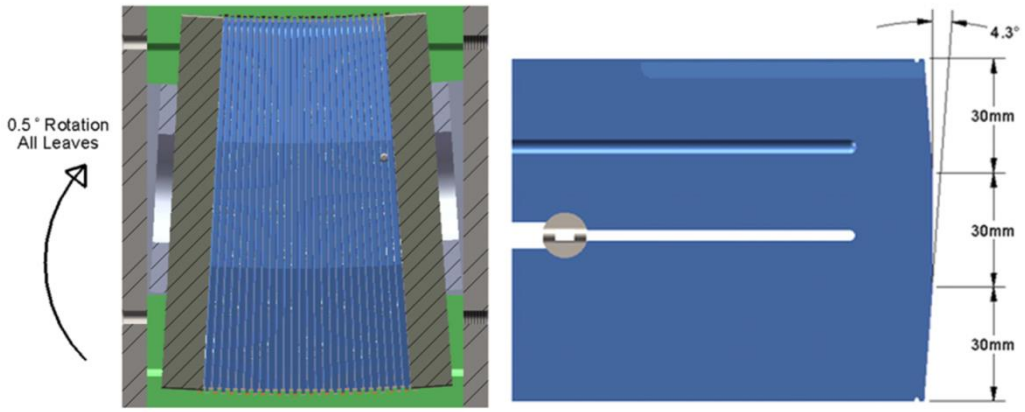

Figure 19. Right : the MLC bank as seen from one side, showing the focus of the leaves on the radiation source and the subsequent 0.5° rotation. Left: view of the tip of a leaf with the three flat surfaces (data from Accuray).

Different setup techniques are available depending on the body area to be treated. The initial positioning is based on lasers and on the kV imaging system (two X-ray tubes placed at 45°), which can also be used to correct patient positioning during the session. This imaging system registers DRR (Digitally Reconstructed Radiograph) images generated from the planning CT with the images from the orthogonal X-ray tubes. This registration provides translation and rotation correction values that are applied using the robotic couch, and the process is reiterated until the patient is positioned properly.
For brain and spine lesions, setup is solely based on these orthogonal X-ray images as they offer a high image quality for fixed bony structures (allowing to position the patient with an accuracy of the order of a millimeter). For prostate and liver patients, fiducials are implanted close to the target to monitor motion during the treatment session. For lung treatments, breathing motion can be tracked using the Synchrony optical camera that visualizes light emitting diodes placed on the patient chest, and sends a signal to the treatment head to synchronize its movement with the breathing pattern.

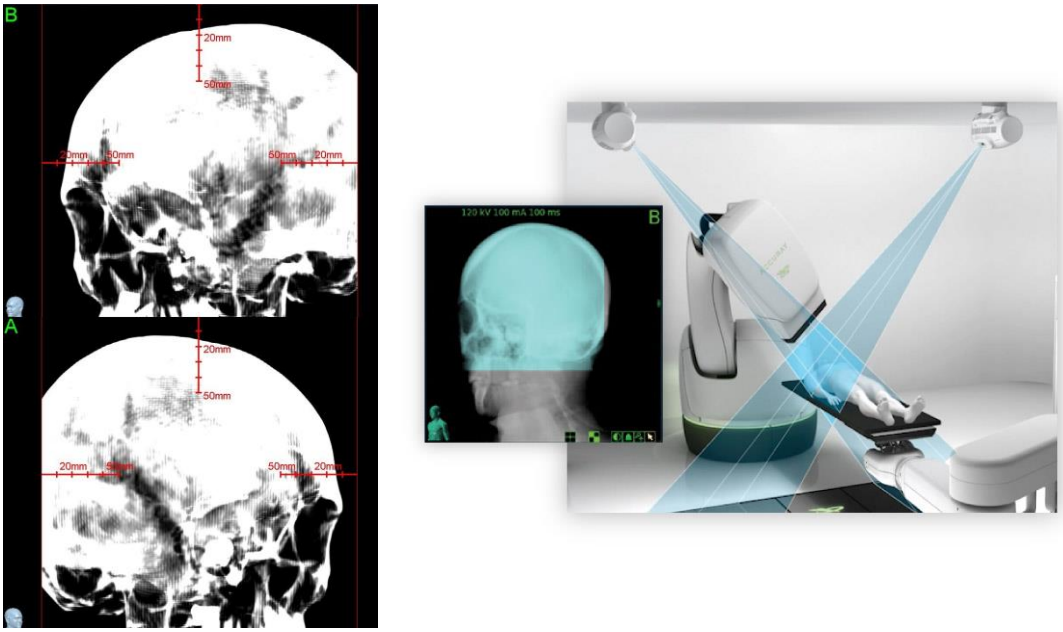

Figure 20. Example of DRR images for a brain treatment (left). These orthogonal images generated in the TPS are later used to position the patient through registration with the X-ray images from the in-room kV system (right, https://www.accuray.com/wp-content/uploads/frameless-stereotactic-targeting-srs.jpg).

A typical Cyberknife treatment involves a few sessions with a higher dose per fraction than in Tomotherapy. Frequent fractionation schemes include 1x20 Gy (small brain metastases), 3x9 Gy (larger brain metastases), 3x15 Gy (liver tumors), 3x18 Gy (lung metastases), 6x6 gy (head and neck reirradiations), 9x4 Gy (brain targets close to sensitive OARs), etc. The number of beams can range from 20 to more than 300, resulting in variabilities in fraction time, between 15 and 90 minutes. The number of beams has a higher impact on treatment time than the dose per fraction itself, because moving the head from one node to the next is generally more time-consuming than delivering the beam itself.

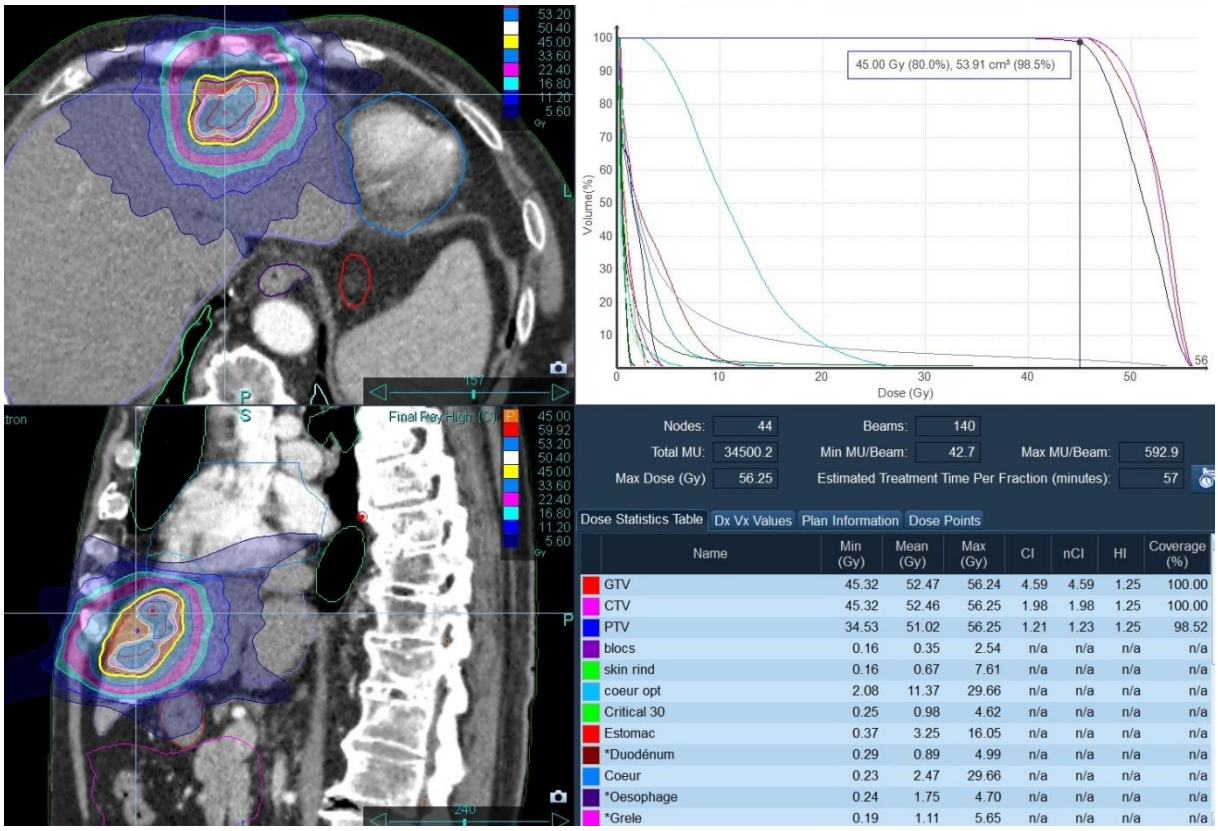

Name	Min (Gy)	Mean (Gy)	Max (Gy)	CI	nCI	HI	Coverage (%)
GTV	45.32	52.47	56.24	4.59	4.59	1.25	100.00
CTV	45.32	52.46	56.25	1.98	1.98	1.25	100.00
PTV	34.53	51.02	56.25	1.21	1.23	1.25	98.52
blocs	0.16	0.35	2.54	n/a	n/a	n/a	n/a
skin rind	0.16	0.67	7.61	n/a	n/a	n/a	n/a
coeur opt	2.08	11.37	29.66	n/a	n/a	n/a	n/a
Critical 30	0.25	0.98	4.62	n/a	n/a	n/a	n/a
Estomac	0.37	3.25	16.05	n/a	n/a	n/a	n/a
*Duodénum	0.29	0.89	4.99	n/a	n/a	n/a	n/a
Coeur	0.23	2.47	29.66	n/a	n/a	n/a	n/a
*Oesophage	0.24	1.75	4.70	n/a	n/a	n/a	n/a
*Grele	0.19	1.11	5.65	n/a	n/a	n/a	n/a

Figure 21. Illustration of a Cyberknife liver treatment, consisting of 3 fractions of 15 Gy each (images from the *Precision* TPS, *Accuray*). The DVH displays the total dose to the PTV (45 Gy) and the OARs. The plan includes 44 nodes (treatment head positions) and 140 beams. The estimated fraction time is 57 minutes, and includes the initial setup as well as the head travel time between nodes.

An important and original part of this work consisted in realizing the Monte Carlo modelling of the two Cyberknife systems installed at Centre Oscar Lambret (VSI and M6): this will be detailed in the next chapters.

2.4. Patient modelling and dose calculation

2.4.i. Computed Tomography

In order to calculate the dose delivered to the tissues by an impinging radiation beam, one has to model the patient in the TPS using the CT images of the patient.

The principle of Computed Tomography is to measure the transmission of X-rays through the body in order to build a 3D map of the densities inside the subject. This is achieved by rotating an-X-ray tube (with a typical tension of 120 kV) and an opposing detector around a translating couch, then reconstructing the images using specific algorithms.

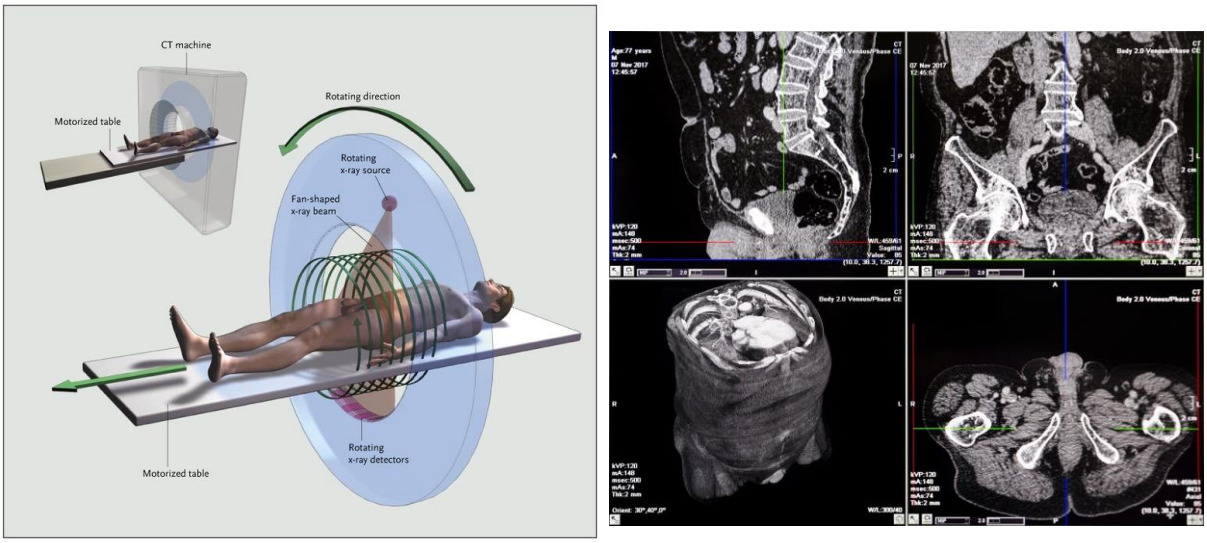

Figure 22. The principle of Computed Tomography: a rotating tube delivers a fan-beam of X-rays to the patient, and the transmitted fraction of this beam is measured in the opposing detector (left). After reconstruction, the densities of the tissues (bone, muscle, soft tissue, etc.) can be visualized as slices in the 3 directions (sagittal, coronal of transverse).

The numeric values contained in the voxels of a CT image are in Hounsfield Units (HU), defined as

$$HU = 1000\left(\frac{\mu}{\mu_{eau}} - 1\right)$$

where μ is the energy-dependent linear attenuation coefficient of the tissue in that voxel, which can be found in the relation $I = I_0 \exp(-\mu x)$ giving the intensity of a parallel monoenergetic beam with intensity I_0 after exiting a medium of width x.

To model the patient in most TPS, the bilinear relation between the HU and the mass density of the tissues is exploited. A phantom containing inserts of different densities is imaged using the CT-scan, and an image-value to density table (IVDT) is built (Figure 23). This curve allows the TPS to assign a physical density to each voxel in the image based on its HU value. This IVDT depends on the energy spectrum and can be different from one acquisition protocol to another (and more so between different CT devices).

It is worth noting that despite being essential for the dose calculation in radiotherapy, CT imaging offers poor soft-tissue contrast in comparison to MRI, and both modalities are often combined to provide sufficient information. However this introduces some uncertainties due to the registration process, which is why a great effort is being made in the research on "MRI-only" radiotherapy, i.e. finding a method to obtain tissue densities directly from MR images [19–22].

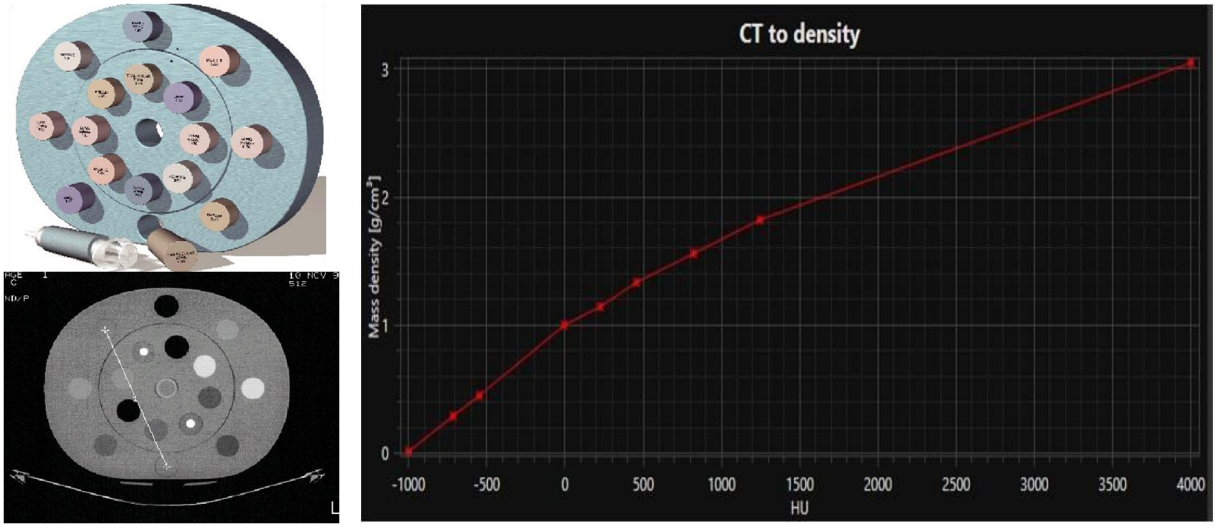

Figure 23. Acquisition of an IVDT: a phantom containing inserts of known variable densities (upper left) is scanned to obtain a CT image (lower left) in which the HU of each insert is measured, providing a bilinear correlation between the HU and the mass density (curve on the right).

2.4.ii. Commercial dose calculation algorithms

Many different dose calculation algorithms exist, and their full description is beyond the scope of the present study. We will limit ourselves to an introduction of the algorithms used in the Tomotherapy and Cyberknife TPS.

The Tomotherapy planning station (called *Precision*) is equipped with a "collapsed cone" algorithm. Introduced by Ahnesjö in 1989 [62], the collapsed cone convolution can be viewed as an approximation designed to speed up calculations in a convolution / superposition [63] algorithm. In this type of method (depicted in Figure 24), the dose deposited at a point $\vec{r}$ from all points situated at positions $\vec{r}'$ is calculated as the convolution of the TERMA (Total Energy Released per unit MAss) with a translational invariant dose kernel $k(\vec{r},\vec{r}',E')$:

$$D(\vec{r}) = \int dE' \int d^3r'\ T(\vec{r}',E')\ k(\vec{r},\vec{r}',E')$$

The TERMA is the energy locally released by the primary photons, and available for secondary particles emerging from point of interaction $\vec{r}$:

$$T(\vec{r}) = \frac{\mu}{\rho}(\vec{r})\ \Psi(\vec{r})$$

Where μ denotes the attenuation coefficient, ρ is the density of the medium and $\Psi(\vec{r})$ the energy fluence. The dose kernel $k(\vec{r},\vec{r}',E')$ describes the fraction of absorbed energy in water at a coordinate $\vec{r}$, created by interactions of primary photons of energy E at coordinates $\vec{r}'$.

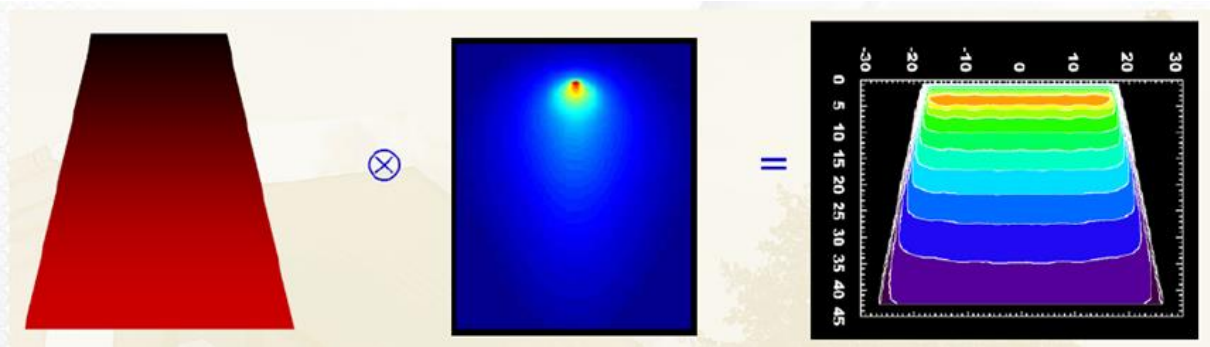

Figure 24. Principle of convolution/superposition: the TERMA in red is convolved with the point-spread dose kernel to give the absorbed dose distribution in the whole geometry (documentation from *Accuray*).

Dose calculation becomes much more complex in the presence of inhomogeneities: the dose kernels are no longer spatially invariant and need to be individually rescaled in order to take into account the effect of varying densities along the secondary particles trajectories. This leads to substantially increased computation times.
Collapsed cone convolution was introduced to overcome this issue [64]: an angular discretization of the kernel is applied, and the approximation is made that all the energy released into the cone in a certain direction from volume elements on the cone axis is transported and deposited on that axis (in other words, the cones are collapsed onto their axes as pictured in Figure 25).

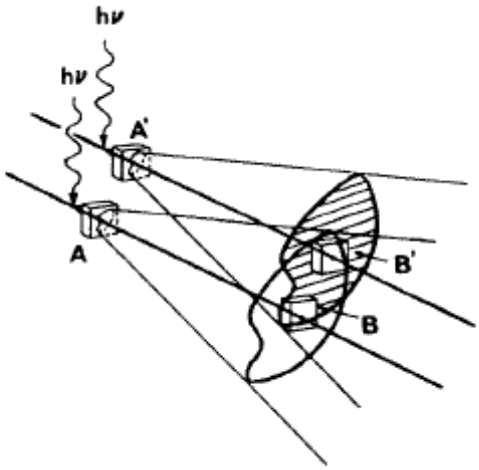

Figure 25. Collapsed cone approximation: the energy that should have been deposited from voxel A to voxel B' is collapsed to voxel B. This approximation is valid as the dose kernel decreases rapidly with distance (most energy is released close to the interaction point), and total energy is conserved (Ahnesjö, Med Phys 16, 1989).

These approximations allowed reducing dose computation times to values acceptable in clinical routine (from a few seconds to a few minutes depending on the spatial resolution and size of the geometry). Collapsed cone is now implemented in several TPS used in the clinic.

The Cyberknife treatment planning system offers three different options for dose calculations [65], namely Accuray RayTracing (ART), Accuray Monte Carlo (AMC) and Finite-Size Pencil Beam (FSPB). The FSPB algorithm is only available for the MLC plans

with the M6 Cyberknife model, whereas ART can be used for fixed and iris plans. AMC is available for all collimators.

The ART algorithm only accounts for primary path heterogeneity corrections (i.e. it does not take into account heterogeneity effects on the scattered dose and secondary electrons). An effective depth is used by summing the contributions of voxels along the ray using the CT electron density. The algorithm utilizes beam data tables that are built from measurements of tissue-phantom ratios (TPR), off-center ratios (OCR) and output factors (OF). The TPR is defined as the the ratio between the dose at a point on the central axis of the beam in a phantom, and the dose at the reference depth in that phantom. It can be viewed as a measure of the beam attenuation with depth. The OCR is the dose profile of the beam along the direction perpendicular to the beam axis. Finally, the OF is defined as the ratio of the central dose at the reference depth for a given collimator with the dose at that same point for the reference collimator (the 60 mm fixed collimator in the case of the Cyberknife).

The dose is then evaluated with the ART algorithm in a simple manner following the equation

$$D = OCR \times \left(\frac{800}{SAD}\right)^2 \times TPR \times OF$$

The ART algorithm is very simple and gives satisfactory results for situations where few inhomogeneities are present in the vicinity of the target volume.

Monte Carlo methods for dose computation in radiation therapy use probability distributions of the interactions of electrons and photons to simulate their transport through matter [25]. After a large number of histories (particles) have been generated, an estimation of the dose deposition can be obtained with an associated uncertainty. This class of algorithms is inherently slower than analytical methods, although the increase in processing power and the availability of variance reduction techniques have considerably accelerated simulations. Widely used Monte Carlo codes include BEAMnrc/EGSnrc, PENELOPE, Geant4, MCNP, etc.

The AMC algorithm was implemented by Accuray in collaboration with the team that developed MCDOSE [66,67] and is very similar to that code. The source model is generated from data measured during the commissioning (installation) of the accelerator, namely OF and PDD (Percentage Depth Dose) measurements. The PDD gives the fraction of dose deposited on the central beam axis in function of the depth, and provides information about the energy of the beam.

The calculation time is longer than that of the ART algorithm, and it depends on the options selected by the user, such as the grid resolution and the statistical uncertainty desired.

Finite size pencil beam algorithms are introduced in [68]. The principle of FSPB is that a beamlet (a very small beam element used for dose calculation in IMRT) can be considered as the difference of two broad beams with a change in the position of one leaf. A *pencil kernel* is thus formed from the difference of two exponential functions (Figure 26).

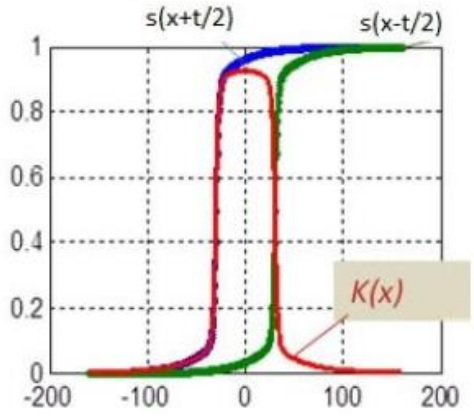

Figure 26. Pencil kernel (red curve) constructed as the difference of two exponential functions (*Physics Essentials Guide, Accuray*).

Once again parameters are obtained during the accelerator commissioning. Kernels are stored to be used by the algorithm depending on the field size. The user has the option of including lateral scatter correction in the calculation.

2.4.iii. Monte Carlo codes used in this work

A brief introduction of the concepts of Monte Carlo calculations was given in the previous section. In the next chapters, we will focus more specifically on the EGSnrc code [69].

The acronym comes for *Electron Gamma Shower*, and it was developed by the National Research Council of Canada. It is a general-purpose package for the Monte Carlo simulation of the transport of electrons and photons in an arbitrary geometry. It is very widely used in radiation therapy, and integrates several modules designed for specific applications.

The accelerator is modelled using BEAMnrc [70,71], a code offering several elementary geometries known as "component modules" (e.g. jaws, chamber, cones, MLC, etc.). The combination of these modules offers a great versatility in accelerator modelling. The transport in the patient or phantom is performed with DOSXYZnrc [72], which is a code for 3D absorbed dose calculations. The geometry can be a Cartesian volume with user-defined voxels (such as a water phantom), or a patient CT that is fed into the code in DICOM format. The DOSRZnrc [73] user code is also used in the next chapter, and is very similar to DOSXYZnrc with the exception that voxels are organized as concentric cylinders. The detector modelling is performed using CSCavity (for "correlated sampling", see chapter 3), that is designed to perform simulations in cavities such as ionization chambers.

The use of *phase-space files* is well-spread in Monte Carlo codes. The principle of a phase-space is to create a file containing a large amount of particle data (position, energy, direction) at a certain plane in the accelerator. The position of the plane can vary depending on the intended use: for example, a phase-space can be created above the MLC to avoid repeating simulations inside the treatment head, and simply transporting particles inside the collimator (that has a variable shape from one plan to another). Alternatively, some designs allow to store a phase-space below the secondary collimator, if the latter has a finite number of possible shapes. This is the case for the iris and fixed collimators of the Cyberknife.

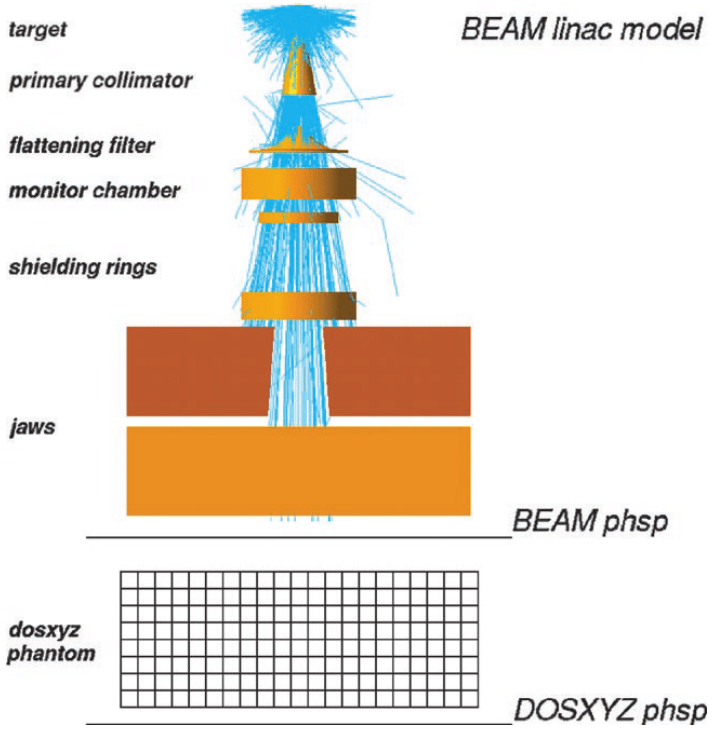

Figure 27. Principle of a phase-space file: the particles in the plane below the secondary collimation are stored in a file, and can be used later on to be transported in the phantom without re-simulating transport in the linac head (Spezi et al, Physics in Medicine and Biology, 46 (11) 2001).

2.5. Small fields

The generalization of IMRT, which is based on the superposition of small MLC segments, and SBRT, where small field sizes are used to treat small targets with higher doses, made the accurate modelling of small fields very critical. Indeed, specific problems are associated with the measurement of fields of small dimension [74,75].

The radiation source has a finite (albeit small) size, and reaching very small beam sizes requires closing the collimator down to a point where part of the source itself will not be longer viewed from the detector. This has the effect of reducing the measured signal

compared to the beams where the source is not partially concealed. Moreover, field size is overestimated as the FWHM (full width at half maximum) increases.

The difficulties are also caused by the loss of charged particle equilibrium, as megavoltage photon beams produce electrons with a considerable range. When field size is reduced to a value close to that range, penumbras start to overlap, perturbing the results in a similar way as source obstruction

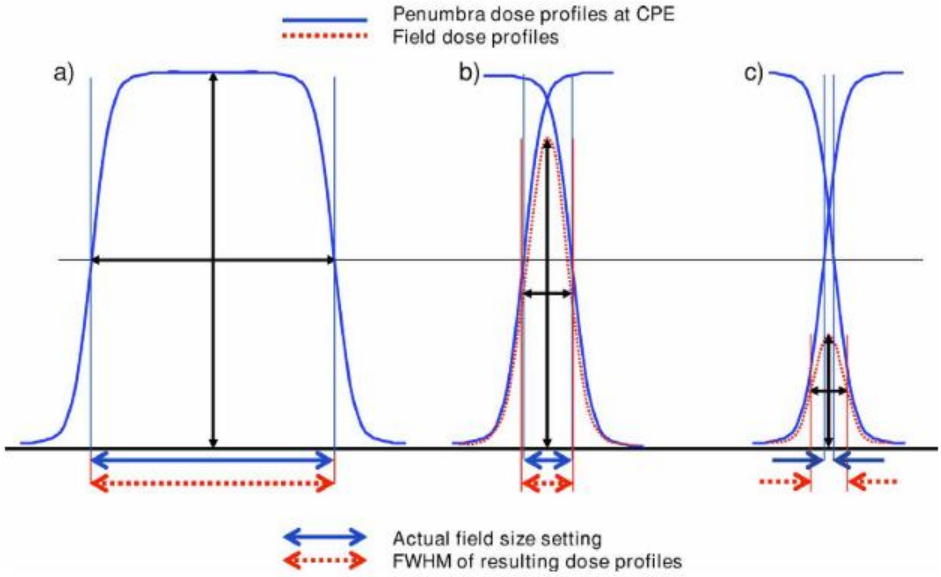

Figure 28. (a) With a large field size, charge particle equilibrium is achieved and the source is entirely viewed, leading to a correct evaluation of the field size. In (b) and (c), the reduction in field dimensions causes the penumbras to overlap and the field size determination becomes inaccurate (Small Field Dosimetry, Journal of the ICRU, 14 (2), 2014).

The detector can be another source of error: first, the assumption that the cavity (i.e. the ionization chamber) does not perturb the beam might no longer hold when the size of the detector becomes close to the field dimensions. Moreover, the materials of the detector (wall, electrode) play as perturbing factors in the measurement.

These considerations justify the use of other types of detectors, such as diodes or liquid ionization chambers (LICs). More details will be provided on this subject in the next chapter.

3. Modelling of the Cyberknife and microLion detector

3.1. Introduction

The article in the next section was published in *Physics in Medicine and Biology* [76].

The paper is divided up in three parts. The first one focuses on characterizing the ion recombination effects perturbing the dose measurements of the microLion detector, a liquid ionization detector specifically designed for the measurements of small fields. The necessity of this characterization is related to the fact that a liquid-filled cavity undergoes superior recombination effects than a gas-filled detector due to the higher density of the liquid, and that the theory and methods developed for correcting these effects in gaseous detectors does not apply to liquid ionization chambers (LICs).

In the second part of the paper, a Monte Carlo model is built for the Cyberknife accelerator (in its earlier VSI version) using the BEAMnrc / EGSnrc code system. This model is the one that is used in the Moderato platform, as will be introduced in chapter 4.

In the third part, additional perturbation effects are studied that might influence the LIC response: the cavity volume, and the detector materials (electrode, wall, isooctane). In order to do this, a Monte Carlo model is built for the detector itself using the EGSnrc code CSCavity, which is dedicated to the modelling of ionization chambers.

To fully characterize the detector, correction factors are generated to account for these recombination, volume and material effects. These factors are compared with the results from other detectors, as well as with results published in the literature.
These corrections are now applied when performing measurements with the LIC in our department, e.g. for the commissioning of the second Cyberknife installed in 2017 (the M6 model).

For the sake of readability, the references of the article are included directly at its end, in the original *PMB* format.

3.2. Article

Use of a liquid ionization chamber for stereotactic radiotherapy dosimetry

A Wagner[1], F Crop[1], T Lacornerie[1], F Vandevelde[1], N Reynaert[1,2]

[1]*Centre Oscar Lambret, Department of Medical Physics, Lille, France*

[2]*Institut Jules Bordet, Department of Medical Physics, Brussels, Belgium*

Abstract

Liquid ionization chambers (LICs) offer an interesting tool in the field of small beam dosimetry, allowing better spatial resolution and reduced perturbation effects. However, some aspects remain to be addressed, such as the higher recombination and the effects from the materials of the detector. Our aim was to investigate these issues and their impact. The first step was the evaluation of the recombination effects. Measurements were performed at different SSDs to vary the dose per pulse, and the collection efficiency was obtained. The BEAMnrc code was then used to model the Cyberknife head. Finally, the liquid ionization chamber itself was modelled using the EGSnrc-based code Cavity allowing the evaluation of the influence of the volume and the chamber materials. The liquid ionization charge collection efficiency is approximately 0.98 at 1.5 mGy pulse−1, the highest dose per pulse that we have measured. Its impact on the accuracy of output factors is less than half a per cent. The detector modelling showed a significant contribution from the graphite electrode, up to 6% for the 5 mm collimator. The dependence of the average electronic mass collision stopping power of iso-octane with beam collimation is negligible and thus has no influence on output factor measurements. Finally, the volume effect reaches 5% for the small 5 mm collimator and becomes much smaller (<0.5%) for diameters above 10 mm. LICs can effectively be used for small beam relative dosimetry as long as adequate correction factors are applied, especially for the electrode and volume effects.

1. Introduction

Conventional air-filled detectors are widely used to perform dosimetric measurements in many radiation therapy devices. However, they reach their limits when beams of small dimensions are used (Das *et al* 2008). In order to obtain accurate dose results in a small field, a very high spatial resolution is needed if one wants to avoid partial volume effects. This can be achieved by reducing the detector size. On the other hand, if the cavity becomes too small, the response of the chamber is very low and no precise measurement can be performed.

A possible solution to address this problem is to use a diode detector, which offers a higher resolution through its very small front area (1 mm^2), while maintaining a high response due to its solid state. But these detectors suffer from other sources of errors (Yin *et al* 2004, Griessbach *et al* 2005), such as scattering effects arising from the metallic shielding

introduced to compensate for over-response to low-energy scattered photons that interact through the photoelectric effect in silicon.

In light of these elements, liquid ionization chambers (LICs) (Wickmann and Nystrom 1992) appear as an interesting candidate to solve some of the issues posed by small field measurements. The higher density of the liquid greatly increases the ionization density and thus the sensitivity of the chamber compared to that of a gas-filled detector of the same volume. This allows a significant reduction of the size of the cavity and improved spatial resolution while maintaining sufficiently large signals. Second, the perturbation effects on the fluence arising from the introduction of an air cavity in the field are no longer present, as the liquids used have a density very close to that of water. In addition, unlike gas-filled chambers, the energy dependence is negligible as the collision mass stopping power ratio water-to-liquid is almost independent of the electron energy over the range used in medical accelerators. These features have led to an increasing interest in using LICs in the field of nonstandard dosimetry (Chung *et al* 2011, Francescon *et al* 2012).

However, some drawbacks remain that might compromise the interest of using LICs in small beam dosimetry. First, these devices are subject to much larger recombination effects (Johansson *et al* 1997, Andersson and Tölli 2010, Tölli *et al* 2010). Two types of recombination exist. When an electron recombines with its mother ion, we called this *initial* recombination. Obviously, the importance of the effect depends on the voltage applied on the electrodes. But it does not depend on the dose rate, as opposed to the *general* or *volumetric* recombination, which refers to the recombination of two ions coming from different ionization events.

The general collection efficiency f *is* used to quantify recombination effects. It is defined as the ratio of the measured charge to the charge produced by the incident radiation and escaping initial recombination:

$$f = \frac{Q_c}{Q_0} \tag{1}$$

In air-filled chambers, recombination effects are usually evaluated using the two-voltage method derived from the theory of Boag (1950, 1952). The chamber is used in its saturation region where the initial recombination can be considered negligible, and the collection efficiency is obtained from the chamber readings after measuring a dose at two different voltages.

Due to the reduced ion mobility in non-polar room temperature liquids, the transit time between electrodes is large (considering the mobility $k = 3 \times 10^{-8}$ m^2 s^{-1} V^{-1}, the transit time $t_{tr} = d^2/Uk$ is around 5 ms for a voltage $U = 800$ V and a distance $d = 0.35$ mm between the electrodes), and the charge density is much higher than that in a gas. This increases the probability of two ions recombining before being detected. In particular, the general recombination could present impeding effects on dose measurements given the high dose rates delivered by the existing stereotactic radiotherapy pulsed beams. The dose per pulse will depend on different factors (such as distance, depth of measurement and collimator) and will vary during the measurements, thus also varying the collection efficiency. If this variation is large enough, the data will need to be corrected for the recombination effects and these corrections will depend on the dose rate.

To evaluate the collection efficiency in LICs, the two-voltage method cannot be directly applied as in gas detectors, because there is no saturation of charge collection at high voltage (Stewart *et al* 2007). Thus, the influence of initial recombination remains important and cannot be made negligible by increasing the voltage. Tölli *et al* (2010) proposed an

alternative method, which we used in this work, consisting in varying the dose rate (or in the case of a pulsed beam, the dose per pulse) to assess the effect of general recombination.

Another potentially hindering aspect in the use of LICs for small beam measurements is the volume effect. Indeed, while these devices are designed to have very high spatial resolution in one direction, this is not necessarily true for the other dimensions. The detector studied in this work presents a cylindrical cavity with a small height (0.35 mm) even compared to the smallest beams used, e.g., in radiosurgical applications, but its larger diameter (2.5 mm) could potentially degrade the measurements in the transverse direction. This means that the results will strongly depend on the type of measurement and the orientation of the detector with respect to the beam.

Finally, one should pay attention to the possible perturbing effects of the liquid used for detection and of the chamber wall and electrode. These could also affect the response of the detector and their influence should be studied before relying upon the measurements realized with LICs.

Both these effects (volume and material) are difficult to evaluate by simple measurements. Monte Carlo simulations seem to be an effective tool to isolate the influence of the different elements and possibly be able to derive correction factors (Araki *et al* 2006, Crop *et al* 2009, Bouchard *et al* 2009, Francescon *et al* 2011, 2012). Combined with knowledge of the collection efficiency, this would allow us to better comprehend the underlying processes of liquid ionization detection for small fields.

2. Materials and methods

2.1. Recombination effects

Before proceeding to the modelling of the LIC, the recombination effects were investigated in detail as these are not taken into account in the simulations. As mentioned earlier, it is not possible to increase the voltage to a point such that the initial recombination would become negligible, as is the case in conventional gas-filled chambers. Hence, the conditions to apply the two-voltage method cannot be met.

An alternative method consists in realizing measurements while varying the dose per pulse. This way, it is possible to isolate the effect of general recombination that depends on the dose rate, whereas the initial recombination does not. This allows us to establish a relationship between the dose per pulse and the recombination effect (given that the voltage and pulse repetition frequency are kept constant). This is the method that we used in this work.

The detector studied is the PTW 31018 microLion chamber. Its geometry (depicted in figure 1) consists of a thin cylindrical cavity of 2.5 mm diameter and 0.35 mm height (giving a sensitive volume of 1.7 mm^3). It is filled with iso-octane (2.2.4-trimethylpentane) having the density 0.688 g cm^{-3}. The reference point is located 0.957 mm behind the entrance window. The electrometer is a PTW Unidos Webline with an external HV supply used to obtain a tension of 800 V. The experimental setup was realized 1 h prior to starting the measurements, in order to stabilize the detector temperature and the voltage. A pre-irradiation dose of 3000 MU was delivered to the detector to achieve a stable response (Stewart *et al* 2007).

The two-dose rate method consists in delivering 100 MU at an SSD (source-surface distance) varying from 58.5 to 198.5 cm, at 1.5 cm depth in water. The 60 mm collimator was used to avoid any volume effect. Ten measurements were performed at each step to assess the uncertainty. This setup is particularly convenient on the Cyberknife as the treatment head can

be moved along the vertical axis with a high accuracy. A 0.125 cm^3 ionization chamber was placed next to the LIC in order to provide a reference for the LIC measurements.

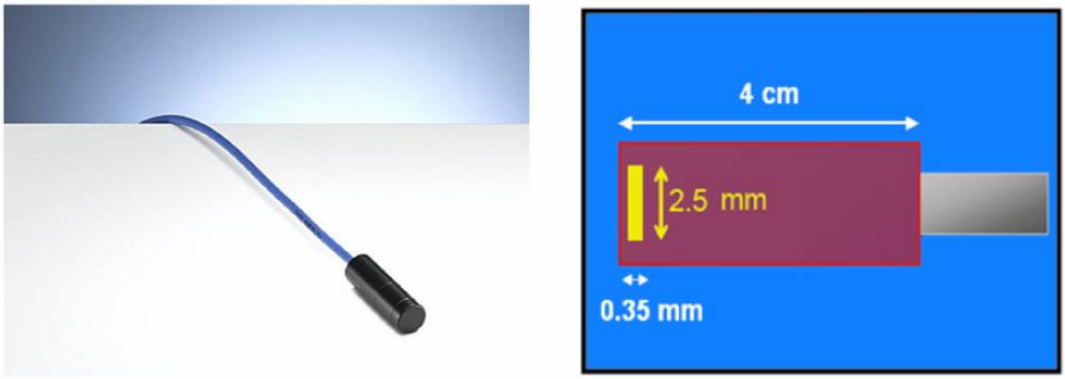

Figure 1. MicroLion chamber geometry.

Under the reference conditions (78.5 cm SSD, 60 mm collimator), the dose per pulse is given by the relation

$$D/\text{pulse} = \frac{800\ (\text{cGy min}^{-1})}{150\ (\text{Hz}) \times 60\ (\text{s min}^{-1})} \tag{2}$$

After correcting for the distance, this gives a value of 1.58 mGy $pulse^{-1}$ at 58.5 cm SSD and 0.14 mGy $pulse^{-1}$ at 198.5 cm SSD. This represents a range wide enough to observe significant recombination effects. The repetition rate of the accelerator was fixed during our measurements; in those accelerators where the dose rate can be varied through the modification of the linac repetition rate, the collection efficiency could also be investigated by varying the linac pulse frequency.

Some additional tests were run to assess leakage current magnitude and its stability, by acquiring charges with no irradiation for a duration equal to that of the measurements (7.5 s for 100 MU). The leakage charge after zeroing was found to be under 0.03% of the lowest charge (highest SSD) measured with the beam on, which we considered negligible.

The results were analysed using two different approaches. The first one (method A), based on Stewart *et al* (2007), simply consists of correcting the LIC readings with the values from the gas detector, thus taking into account the same attenuation, distance and scatter effects. This way the variation of the corrected LIC response with SSD should only be dependent on the recombination effect, and the collection efficiency can be plotted against the dose per pulse. This is of course only true if recombination effects do not significantly affect the 0.125 cm^3 chamber. This was verified by performing the same series of measurements with the 0.125 cm^3 detector alone placed in air with a build-up cap, thus eliminating attenuation and scatter effects, and correcting the reading for the inverse-squared distance.

The second method (B) used to analyse the measurements was proposed by Tölli *et al* (2010) and is based on the following expression for the collection efficiency in a pulsed beam:

$$f = \frac{Q_c}{Q_0} = \frac{1}{u}\ln(1+u) \tag{3}$$

where $u = \frac{\alpha Q_0 h2}{eV\ (k_1+k_2\ )U}$, with α being the recombination coefficient, Q_0 the amount of charge

that escapes initial recombination, h the electrode separation, e the elementary charge, V the sensitive volume of the chamber, k_1 and k_2 the mobilities of the positive and negative charges, and U the applied voltage. For gas-filled chambers, the two-voltage method combines measurements at voltages U_1 and U_2 to obtain the value of u_1 numerically:

$$\frac{f(U_1)}{f(U_2)} = \frac{U_1}{U_2}\frac{ln(1+u_1)}{ln(1+\frac{U_1}{U_2}u_1)} \quad (4)$$

The collection efficiency is then calculated using (3). In a similar way, the two-dose rate method consists of taking the ratio of charges measured at dose per pulse d_1 and d_2:

$$\frac{Q_c(d_1)}{Q_c(d_2)} = \frac{ln(1+u_1)}{ln(1+\frac{Q_0(d_2)}{Q_0(d_1)}u_1)} \quad (5)$$

Given that initial recombination effects are independent of the dose rate, and that the ratio of charges initially created in the liquid must be the same as in the air-filled chamber after correcting for the general recombination, the equation becomes

$$\frac{Q_c(d_1)}{Q_c(d_2)} = \frac{ln(1+u_1)}{ln(1+\frac{Q_{aic}(d_2)}{Q_{aic}(d_1)}u_1)} \quad (6)$$

As in the two-voltage method, it is essential that the charge ratio should be large enough for the numerical resolution to be accurate. It is also worth noting that this formalism is valid as long as the charge collection from one pulse is completed before the arrival of the next one.

One advantage of this approach is that, unlike the first one, it provides absolute values of the collection efficiency f.

As an application of these results, the collection efficiency was used to apply a correction on percentage-depth doses (PDDs) acquired with the microLion detector. The dose per pulse was calculated for each measurement point using equation (2) and the attenuation of water. All values were then corrected with the efficiency f corresponding to the calculated dose per pulse at the distance and depth considered.

2.2. Modelling of the Cyberknife head

The Cyberknife® system (Accuray Inc., Sunnyvale, CA, USA) consists of a linac head that delivers a 6 MV beam mounted on a robot with six axes of rotation allowing a large number of treatment incidence angles. The beams have a circular shape and a size ranging from 5 to 60 mm at the isocentre. There are 12 fixed collimators that can be interchanged, and an Iris collimator consisting of two tungsten banks that allow us to vary the size of the beam during a treatment session. The geometry of the device is represented in figure 2.

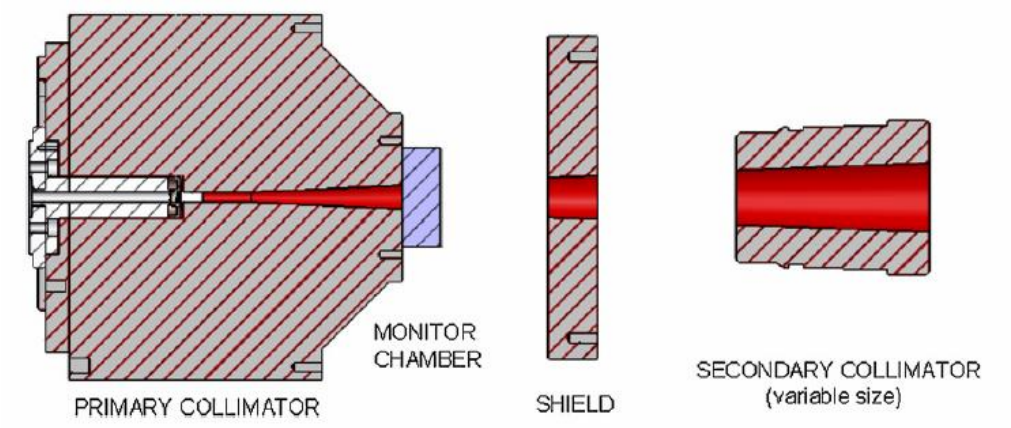

Figure 2. The Cyberknife geometry as defined in the BEAMnrc simulations.

The measurements (off-axis ratios, PDDs and output factors) on which the modelling was based were realized with a PTW60008 diode and a PTW31014 pinpoint chamber. The profiles were first measured without a secondary collimator mounted in order to verify the upstream part of the head (De Smedt *et al* 2005). The secondary collimators were then added in the simulation and compared with the measurements to fine-tune their dimensions individually, starting with the large 60 mm collimator. The simulations were run using 'BEAMnrc' (Rogers *et al* 1994) for the modelling of the linac head, and 'dosrznrc' (Rogers *et al* 2010) for the transport in the water phantom, considering the circular symmetry of the dose profiles. These are user codes from the EGSnrc Monte Carlo system (Kawrakow 2000). The threshold energies used were ECUT = 561 keV in the head and ECUT = 521 keV in the phantom, and PCUT = 10 keV. The geometry and materials were introduced based on the specifications provided by the manufacturer.

The output factors currently used in our centre are based on the method described by Francescon *et al* (2008), which consists of correcting the measured data with factors evaluated through measurements from different detectors (diode, pinpoint chamber, EBT films) and an indirect estimation of the beam spot size.

2.3. Detector modelling

Following the formalism described by Alfonso *et al* (2008), the absorbed dose to water at a reference point in a phantom for a clinical field f_{clin} of quality Q_{clin} is obtained from the dose delivered by the machine-specific reference field f_{msr}, and a field output factor $\Omega_{Q_{\text{clin}},Q_{\text{msr}}}^{f_{\text{clin}},f_{\text{msr}}}$:

$$D_{w,Q_{\text{clin}}}^{f_{\text{clin}}} = D_{w,Q_{\text{msr}}}^{f_{\text{msr}}} \Omega_{Q_{\text{clin}},Q_{\text{msr}}}^{f_{\text{clin}},f_{\text{msr}}} \tag{7}$$

As this output factor is a ratio of absorbed doses to water, it must be corrected when measured as the ratio of detector readings

$$\Omega_{Q_{\text{clin}},Q_{\text{msr}}}^{f_{\text{clin}},f_{\text{msr}}} = \frac{M_{Q_{\text{clin}}}^{f_{\text{clin}}}}{M_{Q_{\text{msr}}}^{f_{\text{msr}}}} k_{Q_{\text{clin}},Q_{\text{msr}}}^{f_{\text{clin}},f_{\text{msr}}} \tag{8}$$

where $M_{Q_{clin}}^{f_{clin}}$ and $M_{Q_{msr}}^{f_{msr}}$ are the dosimeter readings corrected for influence quantities in the

fields f_{clin} and f_{msr}. The correction factor $k_{Q_{clin},Q_{msr}}^{f_{clin},f_{msr}}$ is thus defined as

$$k_{Q_{clin},Q_{msr}}^{f_{clin},f_{msr}} = \frac{(D_{w,Q_{clin}}^{f_{clin}}/M_{Q_{clin}}^{f_{clin}})}{(D_{w,Q_{msr}}^{f_{msr}}/M_{Q_{msr}}^{f_{msr}})} \quad (9)$$

If we now assume that the reading of the detector is proportional to the absorbed dose in its sensitive volume, the correction factor can be obtained through Monte Carlo simulations:

$$k_{Q_{clin},Q_{msr}}^{f_{clin},f_{msr}} = \frac{(D_{w,Q_{clin}}^{f_{clin}}/D_{det,Q_{clin}}^{f_{clin}})}{(D_{w,Q_{msr}}^{f_{msr}}/D_{det,Q_{msr}}^{f_{msr}})} \quad (10)$$

The advantage of this approach is the possibility of isolating the different effects that influence the response and induce deviations from the ideal case of a water-equivalent and infinitely small detector. Once the geometry of a detector has been modelled, simulations allow us to replace a given component by water in order to isolate its effect on the calculated dose. The dose volume effect can also be evaluated by simulating a very small volume of water (in which the variation of the beam intensity profile is negligible) and comparing the results with the full detector model.

Simulations were realized using the EGSnrc code CSCavity, which makes use of the correlated sampling technique (Buckley *et al* 2004): particles that enter a correlated region are copied and re-transported through the correlated geometries. Five different geometries were introduced as depicted in figure 3: (1) the full chamber geometry, (2) the chamber with the graphite electrode replaced by water, (3) the same geometry with the polystyrene wall replaced by water, (4) the detector with all materials set to water including the iso-octane filled sensitive cavity and (5) a small disc of water with 0.2 mm radius. This procedure allows us to isolate the effect of each component of the LIC, the last step providing the evaluation of the volume effect. The correction factor $p_{eff}^{f_{clin}}$ associated with a specific effect and field size f_{clin} is simply given by the ratio of the absorbed dose in the sensitive volume in the modified geometry to the dose calculated from the previous geometry (see figure 3):

$$p_{el}^{f_{clin}} = \frac{D_{(2)}}{D_{(1)}} \quad p_{wall}^{f_{clin}} = \frac{D_{(3)}}{D_{(2)}} \quad p_{iso}^{f_{clin}} = \frac{D_{(4)}}{D_{(3)}} \quad p_{vol}^{f_{clin}} = \frac{D_{(5)}}{D_{(4)}} \quad (11)$$

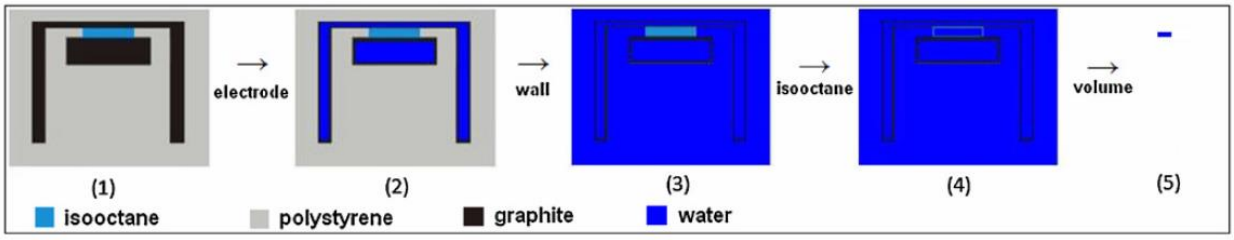

Figure 3. The five correlated geometries of the chamber.

The calculations were performed for four different collimators, namely 5, 10, 30 and 60 mm (which corresponds to the machine-specific reference field f_{msr}). An additional series of simulations was run after modifying the geometry by rotating the detector to orientate it perpendicularly to the beam direction, with its centre at 1.5 cm depth. The rest of the setup

remained unchanged. These calculations were performed in order to assess the influence of the orientation on the correction factors for the different components.

Finally, from the correction factors associated with each effect, the global corrections $k_{Q_{\mathrm{clin}},Q_{\mathrm{msr}}}^{f_{\mathrm{clin}},f_{\mathrm{msr}}}$ for the output factors were calculated for each collimator by taking the ratio of the products of $p_{\mathrm{eff}}^{f_{\mathrm{clin}}}$ for the collimator considered to the products of $p_{\mathrm{eff}}^{f_{\mathrm{msr}}}$:

$$k_{Q_{\mathrm{clin}},Q_{\mathrm{msr}}}^{f_{\mathrm{clin}},f_{\mathrm{msr}}} = \frac{p_{\mathrm{el}}^{f_{\mathrm{clin}}} p_{\mathrm{wall}}^{f_{\mathrm{clin}}} p_{\mathrm{iso}}^{f_{\mathrm{clin}}} p_{\mathrm{vol}}^{f_{\mathrm{clin}}}}{p_{\mathrm{el}}^{f_{\mathrm{msr}}} p_{\mathrm{wall}}^{f_{\mathrm{msr}}} p_{\mathrm{iso}}^{f_{\mathrm{msr}}} p_{\mathrm{vol}}^{f_{\mathrm{msr}}}} \tag{12}$$

These corrections were applied to the measurements in order to assess the correspondence with the reference values used in our centre.

Concerning the evaluation of uncertainties, several aspects must be accounted for. The type-A uncertainties on the p_{eff}^{f} and $k_{Q_{\mathrm{clin}},Q_{\mathrm{msr}}}^{f_{\mathrm{clin}},f_{\mathrm{msr}}}$ factors were calculated from the statistical uncertainties on the simulated dose ratios of the correlated geometries. The systematic (type-B) uncertainties, originating from cross-sectional variations, transport options and geometry variations, are not taken into account in our simulations. Regarding variations of the detector geometry and cross section uncertainties, we refer to the results of Francescon *et al* (2011, 2012) who studied the influence of modifying the sensitive volume diameter and the wall thickness and density of the microLion. They found the overall type-B uncertainty to be under 0.6%.

3. Results and discussion

3.1. Recombination effects

The results of method A are shown in figure 4. To relate the dose per pulse to the actual dose rate, one should keep in mind that a value of 0.89 mGy pulse^{-1} corresponds to 8 Gy min^{-1} (reference conditions of the device). As this method does not provide absolute values of efficiency, f was normalized to 1 for a dose rate of 0 mGy pulse^{-1}. The collection efficiency shows linear behaviour with respect to the dose rate, which is consistent with the results obtained by Stewart *et al* (2007). The collection efficiency drops to 0.977 for a dose rate of 1.58 mGy pulse^{-1} (58.5 cm SSD). Recombination is thus responsible for more than 2% loss in signal between 0 and 1.58 mGy pulse^{-1}. However, during routine clinical measurements, the range of dose rate usually spanned is more restricted.

Figure 4 illustrates that the uncertainties are quite important. The uncertainties from both signals (especially from the LIC) affect the uncertainty on the collection efficiency through the ratio. Moreover, there could be an influence between the two detectors as they are placed right next to each other.

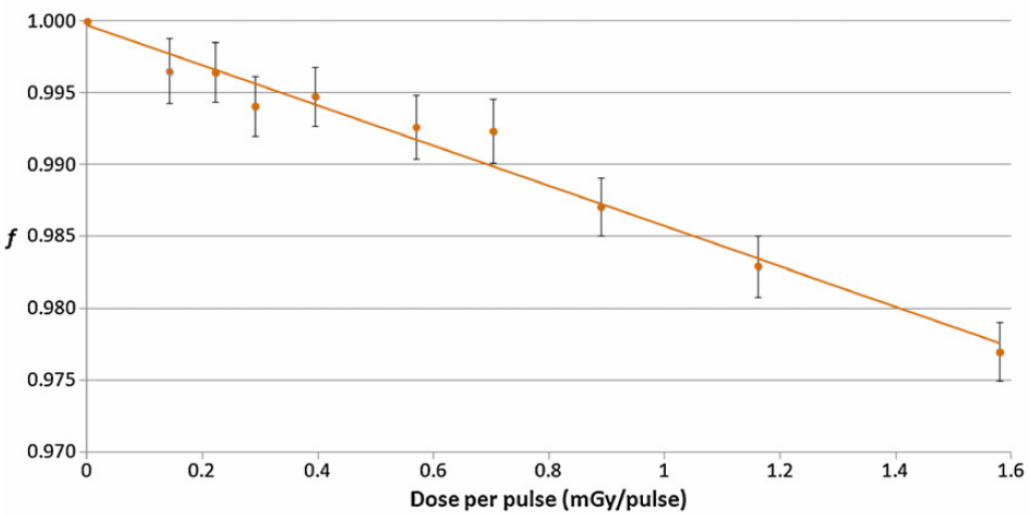

Figure 4. General collection efficiency calculated from method A.

An additional series of measurements was realized with the 0.125 cm^3 chamber in air with the build-up cap to verify the independence of the chamber response with respect to the dose per pulse. The values were corrected with an inverse-squared distance factor. The results show a slight increase at higher distances, meaning that there could be a small recombination effect. Between 78.5 and 158.5 cm SSD, there is a 0.2% variation of the collected charge. However, this value is comparable to the measurement uncertainty of the detector, and it was included in the uncertainty calculations.

The results for the second method (B) are shown in figure 5. The collection efficiency f ranges from 0.998 at 0.14 mGy $pulse^{-1}$ to 0.981 at 1.58 mGy $pulse^{-1}$. This represents a 1.9% loss in the range considered, slightly lower compared to the relative method. This method proves more accurate and has the advantage of providing absolute values of the collection efficiency.

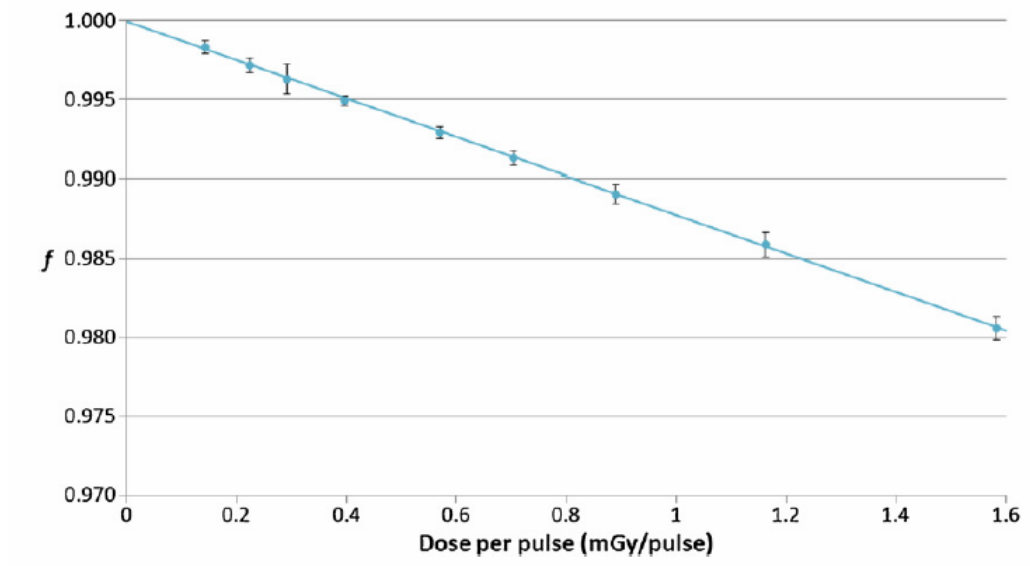

Figure 5. General collection efficiency calculated from method B (based on the Boag formula).

The application of the recombination correction is illustrated in figure 6 for the relative depth dose. When the curves measured with the diode and the LIC are normalized at large depth (where recombination is negligible), the values do not fit in the build-up region, the diode giving a slightly higher signal. As this is the area where the dose rate is the highest, the relative effect of recombination is not negligible between the build-up and the tail of the curve (at 240 mm depth), and the diode curve is 1% higher than that measured with the LIC. The third curve shows the values of the microLion corrected for the dose rate-dependent efficiency and fits much more closely to the diode curve that is not subject to recombination.

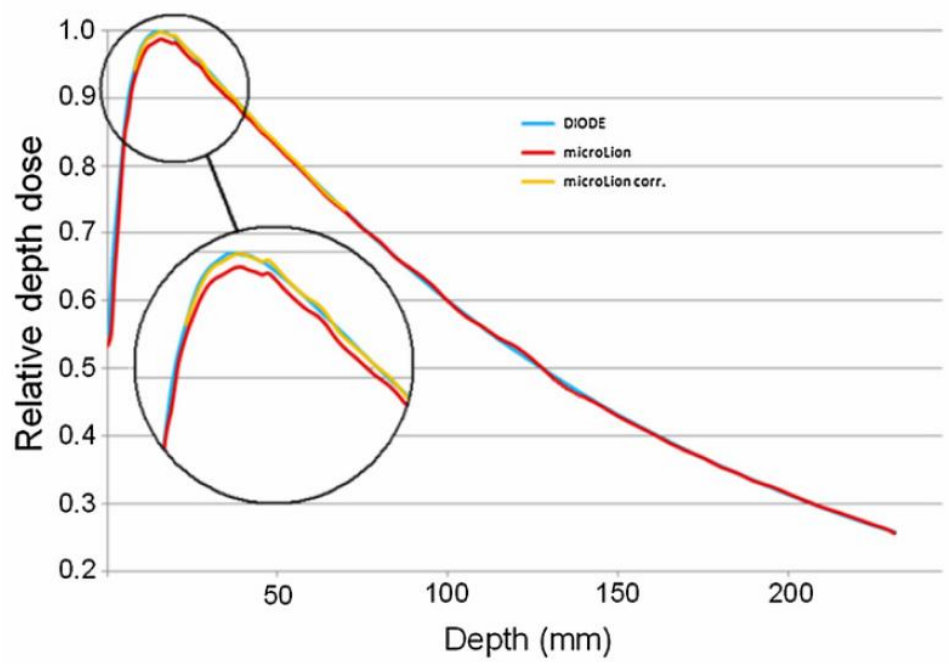

Figure 6. Illustration of the recombination correction on relative depth dose measurements. The blue curve corresponds to the measurements acquired with the diode, while the red and yellow curves represent the uncorrected and corrected data from the microLion, respectively.

The influence of recombination on the output factor measurements can also be calculated. As mentioned earlier, the dose per pulse under the reference conditions (60 mm collimator, 78.5 cm SSD, 15 mm depth) based on equation (2) is 0.889 mGy pulse^{-1}. The largest deviation is observed for the 5 mm collimator, where the dose per pulse drops to approximately 0.6 mGy pulse^{-1}. From the curve in figure 5, this implies an overestimation for the output factor of 0.35%.

3.2. Modelling of the Cyberknife head

The geometry used for the simulations is represented in figure 2. For the first calculations, the secondary collimator was replaced by air, and the profiles were compared to the measurements realized without any secondary collimator mounted. This was helpful in order to focus on fine-tuning the electron beam parameters (i.e. spot size and energy) without taking into account the effect of secondary collimators. Those were added afterwards and optimized individually.

The best fit to experimental results was found using a monoenergetic electron beam of 7 MeV with an FWHM of 1.93 mm. The comparison between measured and simulated data for the 5 and 60 mm diameters is shown in figure 7.

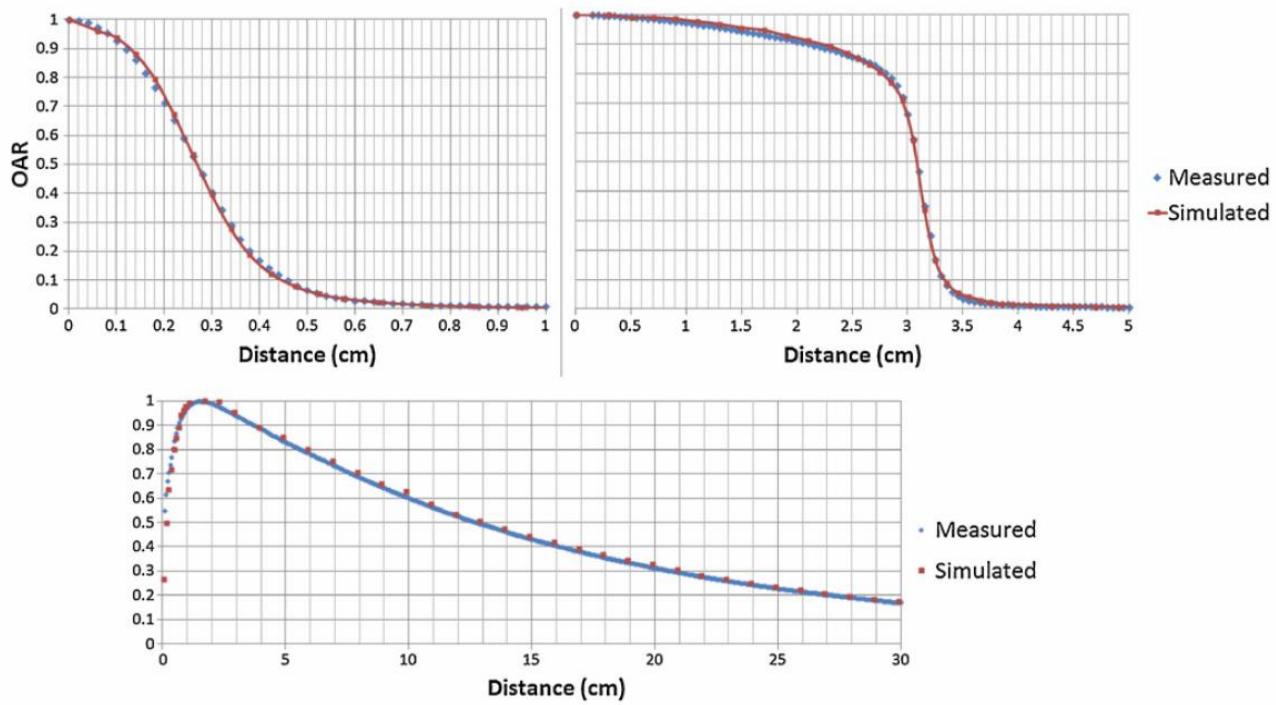

Figure 7. Comparison of measured and simulated data for the 5 and 60 mm collimators and of the PDDs for the 60 mm collimator.

3.3. Detector modelling

The simulations in 'CScavity' using the correlated geometries allowed an evaluation of each effect individually. The correction factors $p_{\text{eff}}^{f_{\text{clin}}}$ are presented in table 1.

Table 1. Correction factors $p_{\text{eff}}^{f_{\text{clin}}}$ to apply for each component (in the case of the vertically oriented chamber), for the 5, 10, 30 and 60 mm field sizes. The uncertainties correspond to one standard deviation.

	Field size (mm)			
Effect	5	10	30	60
Electrode	0.968	0.985	1.000	1.000
Wall	1.002	1.006	1.010	1.011
Iso-octane	0.950	0.945	0.937	0.941
Volume	1.049	1.004	1.000	0.997
Type-A uncertainty	0.1%	0.3%	0.4%	0.6%
Type-B uncertainty	0.6%	0.6%	0.6%	0.6%
Total factor	0.966	0.940	0.947	0.941
Total uncertainty	0.6%	0.7%	0.7%	0.8%

The electrode induces an overestimation of the dose for the smallest field sizes, which amounts to approximately 3% for the 5 mm collimator and 1.5% for the 10 mm collimator. The effect is negligible for the 30 and 60 mm collimators. It seems that the effect is large for beams having a size close to that of the electrode. For example, in the case of the 5 mm collimator, the central electrode (4.991 mm diameter) covers the whole transverse extension of the beam at 1.5 cm depth. This means that all the electrons produced by interactions beyond that depth are not created in water, but in graphite (or polystyrene). The high density of the graphite (1.85 g cm−3) then leads to a higher signal and thus an overestimation of the dose. As the size of the beam increases, the contribution from the graphite is reduced. The effect of the polystyrene wall is an underestimation of the dose, which is not very important for the small collimators, and becomes higher (1%) for the 30 and 60 mm collimators. The iso-octane leads to an overestimation of the absorbed dose, of 5 to 6% depending on the collimator. This is likely related to the stopping power ratio of water to iso-octane; as can be seen in figure 8, the ratio is close to 0.93 for an energy of 2 MeV. The dose volume effect induces a 5% underestimation of the dose for the 5 mm collimator. As expected, this correction is much lower for the 10 mm collimator and becomes negligible for the larger sizes.

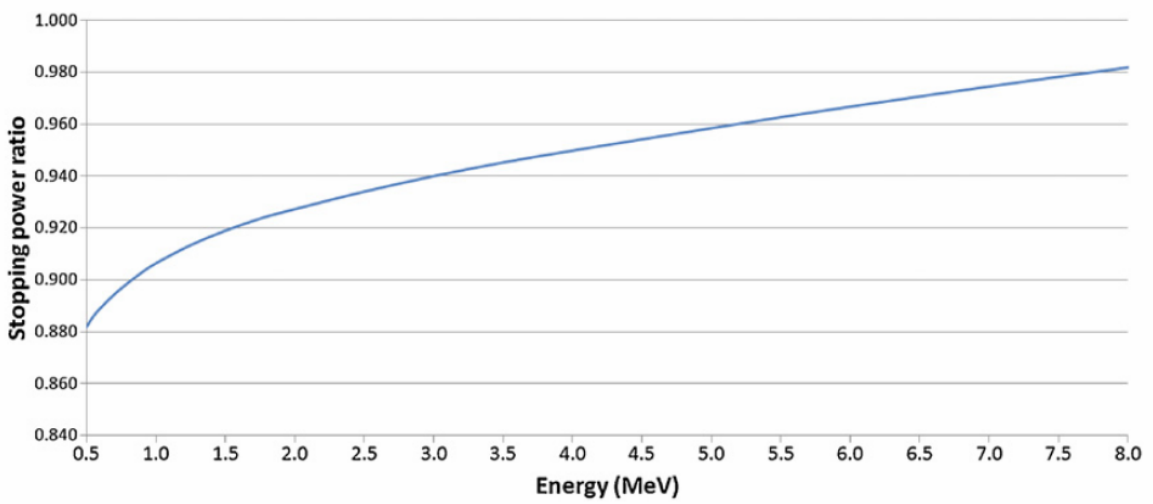

Figure 8. Stopping power ratio of water to iso-octane (data from the NIST http://www.nist.gov/pml/data/star/index.cfm).

Table 2. Correction factors $p_{\text{eff}}^{f_{\text{clin}}}$ to apply for each component (in the case of the horizontally oriented chamber), for the 5, 10, 30 and 60 mm field sizes. The uncertainties correspond to one standard deviation.

	Field size (mm)			
Effect	5	10	30	60
Electrode	0.943	0.978	0.995	0.998
Wall	0.993	0.997	1.002	1.003
Iso-octane	0.936	0.928	0.927	0.933
Volume	1.014	1.004	1.000	0.991
Type-A uncertainty	0.1%	0.2%	0.2%	0.3%
Type-B uncertainty	0.6%	0.6%	0.6%	0.6%
Total factor	0.889	0.909	0.924	0.925
Total uncertainty	0.6%	0.6%	0.6%	0.7%

To investigate the influence of the orientation on the correction factors, the LIC was rotated and placed horizontally. The results are shown in table 2, and both configurations are compared in figure 9.

The electrode overestimation effect is even more pronounced in this situation, reaching 6% for the 5 mm collimator. The wall correction, on the other hand, is reduced. The effect of the replacement of iso-octane with water is stronger with the horizontal setup (reaching 7% correction). This is due to the fact that the cylindrical cavity is oriented vertically after the 90◦ rotation, resulting in its longer dimension being parallel to the beam direction. This leads to a higher fraction of the electrons being created and detected in the cavity. Finally, the volume effect is substantially reduced. This was to be expected as the sensitive cavity has its smaller dimension facing the beam, increasing the spatial resolution in one of the transverse directions, whereas the volume effect acted on both directions in the original setup. It is worth noting that although the correction factor for the volume decreases, this situation is affected by the loss of symmetry that characterized the vertical situation, making it more sensitive to setup errors especially if the beam does not show perfect circular symmetry.

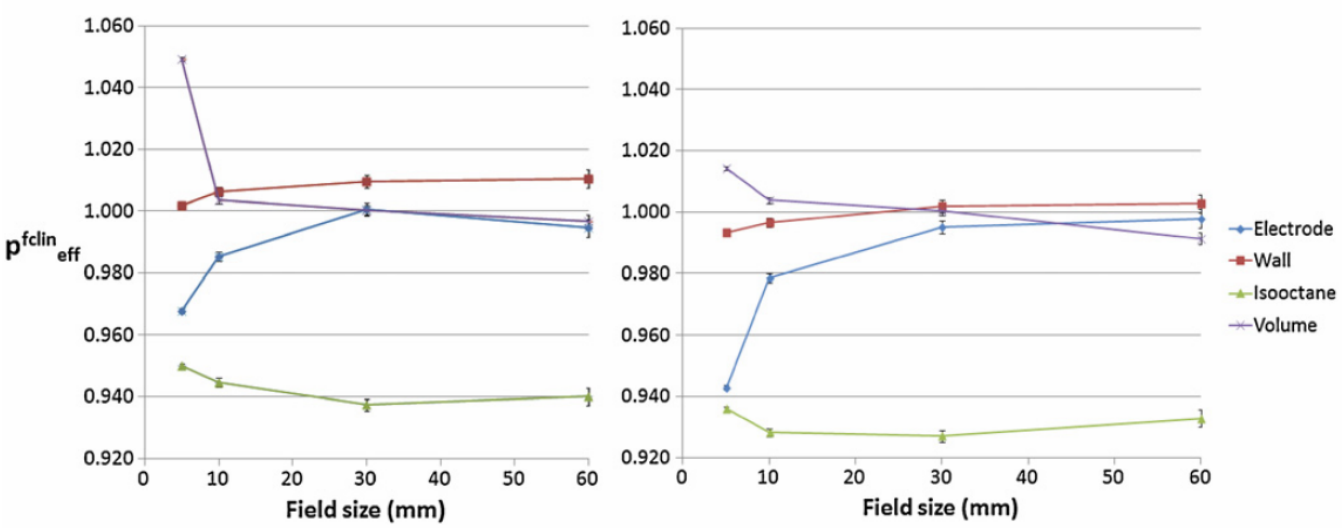

Figure 9. Comparison of the factors for the different perturbing effects ($p_{\mathrm{el}}^{f_{\mathrm{clin}}}$, $p_{\mathrm{wall}}^{f_{\mathrm{clin}}}$, $p_{\mathrm{iso}}^{f_{\mathrm{clin}}}$ and $p_{\mathrm{vol}}^{f_{\mathrm{clin}}}$) for the vertical LIC setup (left) and the horizontal setup (right).

Table 3. Correction factors $k_{Q_{\mathrm{clin}},Q_{\mathrm{msr}}}^{f_{\mathrm{clin}},f_{\mathrm{msr}}}$ to be applied to the output factor values for the 5, 10 and 30 mm collimators, for both the vertical and the horizontal setup. The uncertainties correspond to one standard deviation.

	Collimator (mm)		
	5	10	30
Vertical position			
of correction factor (without recombination)	1.027	0.999	1.006
of correction factor (with recombination)	1.024	0.997	1.006
Uncertainty	1.0%	1.1%	1.1%
Horizontal position			
of correction factor (without recombination)	0.961	0.982	0.999
of correction factor (with recombination)	0.958	0.980	0.999
Uncertainty	0.90%	0.90%	0.90%

From the corrections to the individual effects, it was possible to obtain global factors $k_{Q_{\mathrm{clin}},Q_{\mathrm{msr}}}^{f_{\mathrm{clin}},f_{\mathrm{msr}}}$ to apply to the measured output factors (see equation (12)). These are shown in table 3. The corrections for the recombination were added; as we mentioned earlier, these are rather small compared to the other effects involved. In the case of the vertically oriented detector, we can see that the factor decreases when switching from the 5 mm to the 10 mm field size and increases again for the 30 mm collimator. This is due to the strong decrease of the volume effect (4.5%) between the 5 and 10 mm field sizes, while it remains unchanged for the other collimators. On the other hand, the electrode effect continues to increase for the 30 mm collimator (see table 1).

The results show good agreement with the recent results of Francescon *et al* (2012), who obtained factors of 1.025 and 0.995 for the 5 and 10 mm collimators, respectively. However, one should keep in mind that these factors are dependent on the beam spot size and cannot be directly applied to different systems.

Figure 10 shows the output factors (relative to the machine-specific reference field of 60 mm diameter) before and after the corrections given in table 3, for the vertical and the horizontal setup. These corrected factors are calculated following equation (8). The reference output factors used in the treatment planning system (TPS) are also shown, based on measurements from different detectors.

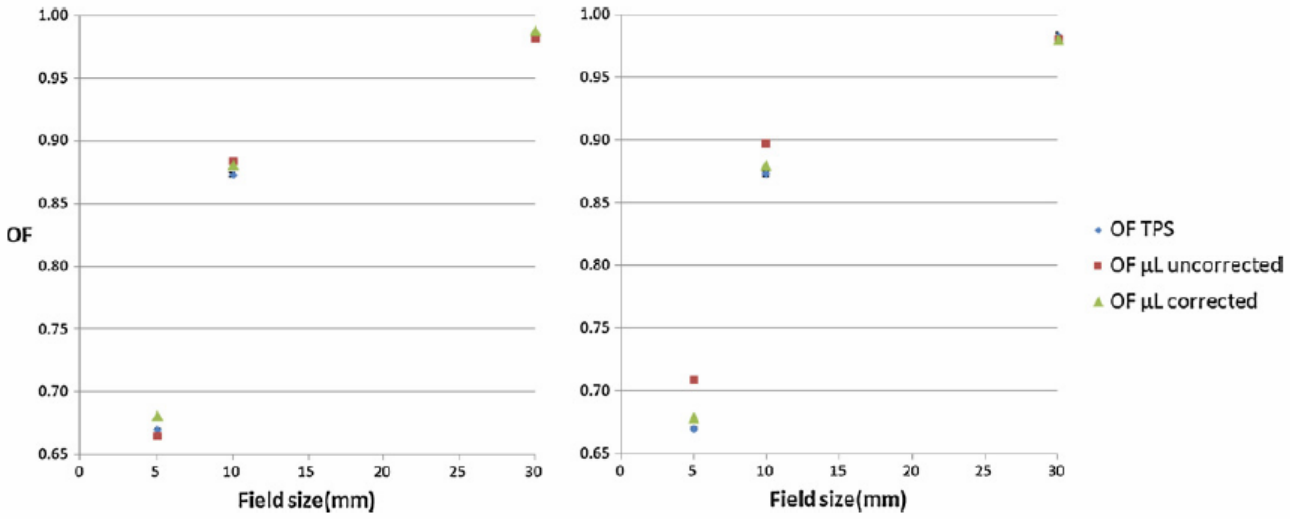

Figure 10. Output factors measured with the microLion before (OF μL) and after correction (OF μL corrected), for the vertical setup (left) and horizontal setup (right). The output factors used in the TPS are also represented.

We can see from these results that the corrected factors show good agreement with the reference values obtained from the other detectors. In the vertical setup, the output factor for the 5 mm collimator is slightly overcorrected, but remains within 2% of the reference value. The difference for the 10 mm collimator is under 1%. The effect of these corrections is more dramatic in the horizontal configuration where the gap between corrected and uncorrected values is much more pronounced. As an example, in the 5 mm case, the deviation between the reference value and the microLion measurements drops from 5.8% to 1.3%.

4. Conclusion

The aim of this work was to fully characterize a liquid ionization detector and its potential use in stereotactic radiotherapy dosimetry. The Cyberknife system was modelled using BEAMnrc. Good correspondence between measured and simulated data was obtained. Before applying this model to simulate the microLion, the effects of recombination in iso-octane were investigated. Results suggest that recombination effects have a low impact as long as the dose per pulse range remains restrained. The relative error on uncorrected output factors does not exceed 0.35%, but the effect becomes somewhat higher for a PDD measurement where the relative error reaches 1%.

The modelling of the LIC shows that the response of the chamber is more influenced by other factors, such as the volume effect or the electrode, and that the corrections depend on the orientation of the detector. These effects must imperatively be corrected for small collimator measurements; as an example, the relative error on the uncorrected output factor can reach 2.7% (5 mm field size, vertical LIC). While the corrected values show good correspondence with the reference values that are currently used on our device, these factors cannot be directly applied to other systems as they depend on the beam spot size. Concerning off-axis ratio measurements, the circular shape of the Cyberknife beam profiles does not allow us to eliminate the volume effect, which would be more difficult to correct for than in the static case of output factor measurement (the volume effect in a circular beam is not constant during a profile measurement where the chamber is moving along the transverse direction). Regarding the detector geometry, the volume effect would be less of a problem for profile measurements on fields having only one small dimension (such as Tomotherapy®) as the longitudinal resolution of the chamber is very high.

References

Alfonso R *et al* 2008 A new formalism for reference dosimetry of small and nonstandard fields *Med. Phys.* **35** 5179–86

Andersson J and Tölli H 2010 Application of the two-dose-rate method for general recombination correction for liquid ionization chambers in continuous beams *Phys. Med. Biol.* **56** 299–314

Araki F 2006 Monte Carlo study of a Cyberknife stereotactic radiosurgery system *Med. Phys.* **33** 2955–63

Boag JW 1950 Ionization measurements at very high intensities: part 1. Pulsed radiation beams *Br. J. Radiol.* **23** 601–11

Boag JW 1952 The saturation curve for ionization measurements in pulsed radiation beams *Br. J. Radiol.* **25** 649–50

Bouchard H, Seuntjens J, Carrier J and Kawrakow I 2009 Ionization chamber gradient effects in nonstandard beam configurations *Med. Phys.* **36** 4654–63
Buckley LA, Kawrakow I and Rogers DWO 2004 CSnrc: correlated sampling Monte Carlo calculations using EGSnrc *Med. Phys.* **31** 3425–35
Chung E, Soisson E and Seuntjens J 2011 Dose homogeneity specification for reference dosimetry of nonstandard fields *Med. Phys.* **39** 407–14
Crop F, Reynaert N, Pittomvils G, Paelinck L, De Wagter C, Vakaet L and Thierens H 2009 The influence of small field sizes, penumbra, spot size and measurement depth on perturbation factors for microionization chambers *Phys. Med. Biol.* **54** 2951–69
Das I J, Din G X and Ahnesjö A 2008 Small fields: non-equilibrium radiation dosimetry *Med. Phys.* **35** 206–15
De Smedt B, Reynaert N, Flachet F, Coghe M, Thompson M G, Paelinck L, Pittomvils G, De Wagter C, De Neve W and Thierens H 2005 Decoupling initial electron beam parameters for Monte Carlo photon beam modelling by removing beam-modifying filters from the beam path *Phys. Med. Biol.* **50** 5935–51
Francescon P, Cora S and Cavedon C 2008 Total scatter factors of small beams: a multidetector and Monte Carlo study *Med. Phys.* **35** 504–13
Francescon P, Cora S and Satariano N 2011 Calculation of $k_{Q_{\mathrm{clin}},Q_{\mathrm{msr}}}^{f_{\mathrm{clin}},f_{\mathrm{msr}}}$ for several small detectors and for two linear accelerators using Monte Carlo simulations *Med. Phys.* **38** 6513–27
Francescon P, Kilby W, Satariano N and Cora S 2012 Monte Carlo simulated correction factors for machine specific reference field dose calibration and output factormeasurement using fixed and iris collimators on the Cyberknife system *Phys. Med. Biol.* **57** 3741–58
Griessbach I, Lapp M, Bohsung J, Gademann G and Harder D 2005 Dosimetric characteristics of a new unshielded silicon diode and its application in clinical photon and electron beams *Med. Phys.* **32** 3750–54
Johansson B, Wickman G and Bahar-Gogani J 1997 General collection efficiency for liquid iso-octane and tetramethylsilane in pulsed radiation *Phys. Med. Biol.* **42** 1929–38
Kawrakow I 2000 Accurate condensed history Monte Carlo simulation of electron transport: part I. EGSnrc, the new EGS4 version *NRCC Report* PIRS-701
Rogers D W O, Faddegon B A, Ding G X, Ma C M, We J and Mackie T R 1994 BEAM: A Monte Carlo code to simulate radiotherapy treatment units *Med. Phys.* **22** 503–24
Rogers D W O, Kawrakow I, Seuntjens J P, Walters B R B and Mainegra-Hing E 2010 NRC user codes for EGSnrc *NRCC Report* PIRS-702(revB)
Stewart K J, Elliott A and Seuntjens J P 2007 Development of a guarded liquid ionization chamber for clinical dosimetry *Phys. Med. Biol.* **52** 3089–104
Tölli H, Sjgren R and Wendelsten M 2010 A two-dose-rate method for general recombination correction for liquid ionization chambers in pulsed beams *Phys. Med. Biol.* **55** 4247–60
Wickmann G and Nystrom H 1992 The use of liquids in ionization chambers for high precision radiotherapy dosimetry *Phys. Med. Biol.* **37** 1789–812
Wulff J, Heverhagen J T, Zink K and Kawrakow I 2010 Investigation of systematic uncertainties in Monte Carlo calculated beam quality correction factors *Phys. Med. Biol.* **55** 4481–93
Yin Z, Hugtenburg R P and Beddoe H 2004 Response corrections for solid-state detectors in megavoltage photon dosimetry *Phys. Med. Biol.* **49** 3691–702

3.3. Modelling of the iris collimator

The Monte Carlo modelling of the Cyberknife described in the article above was performed for the 12 fixed collimators. As mentioned in the article, the first simulations were run without integrating the secondary collimator. This allows comparing with measurements performed with that setup during the commissioning process of the Cyberknife [65]. When a good agreement is reached between these simulated profiles and PDDs, one should be able to keep changes to the primary part of the treatment head (primary collimator, shield, MU chamber, mirror) and electron beam parameters (energy, spot size) rather small during the next steps of the modelling. The smallest (5 mm) and largest (60 mm) collimators were optimized next, and finally the 10 remaining sizes were added.

This modelling was sufficient to validate the geometry and beam parameters selected, and to perform the study on the microLion detector. However, the vast majority of treatments on the Cyberknife are performed with the iris collimator due to its higher flexibility (only the 5 mm fixed collimator is sometimes used to treat very small targets, e.g. choroidal melanoma or spinal lesions). Indeed, the user can easily select up to 5 or 6 diameter sizes when planning with the iris, thus increasing the conformity and coverage to the target while maintaining a reasonable treatment time. As the fixed collimator can not vary its diameter from one beam to another, each diameter selected imposes to perform a new path around the patient; this results in much longer treatment times, even with a smaller number of collimator sizes.

Therefore, to be able to perform patient plan re-calculations, the modelling of the iris collimator had to be realised as well. Following the argument above, the primary part of the geometry and the electron beam were kept the same. The iris, on the other hand, required a completely different model. This is because although it produces a beam quite similar to the one of the fixed collimators, its design is very different, consisting of two superimposed banks of 6 prism-shaped tungsten segments each that open and close in the manner of a diaphragm (Figure 29). The two banks are tilted by 30° with respect to each other, so that the beam has a dodecagonal shape.

Figure 29. Left: the 12 fixed circular collimators, with their diameter at isocenter varying from 5 to 60 mm. Right: view from under the iris collimator, showing the two banks of tungsten segments rotated with respect to each other.

Hence, during the commissioning of an iris collimator size, two dose profiles are acquired: one horizontally and another at a 15° angle. These two directions correspond to the largest and smallest possible sizes of dose profiles (provided the treatment head has been rotated properly with respect to the water tank). This is represented in Figure 30. These two profiles are then averaged to a single one that is used as reference for dose calculations in the TPS.

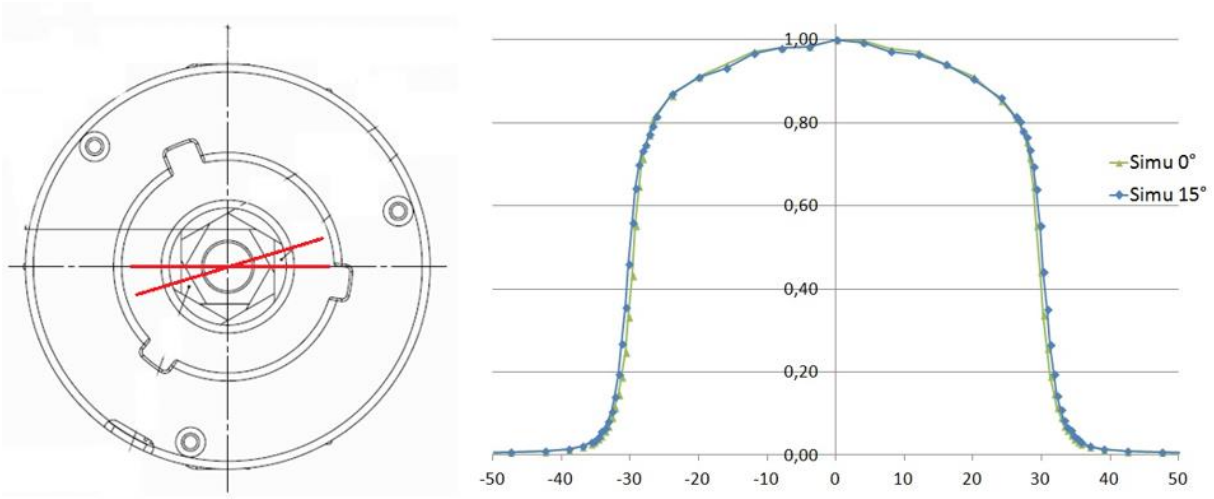

Figure 30. Left: view of the iris collimator from below, with the two directions of movement of the detector during the acquisition of dose profiles. Right: simulated dose profiles at 0° and 15°, showing the slight difference in profile size.

Although the profile size differences are small when projected at SAD, they are still measurable and should be taken into account in our Monte Carlo model. Unfortunately, no component module exists to account for such geometry in BEAMnrc, where only the "classical" shapes of a linac are integrated: cones, chamber, jaws, mirror, MLC, etc. For this reason, the choice was made to use a C++ package called egs++ [77], and to construct a "home-made" geometry describing the iris collimator. The iris thus becomes a C++ class defined as the intersection of planes, cylinders and prisms, with a variable size determined by the projected size of the beam at isocenter. The egs_view package allows to visualize the geometry in 3 dimensions to assist in optimizing the setup and dimensions (Figure 31).

To run a simulation with the iris collimator, particles are first transported through the primary part of the treatment head (modelled in the previous section) with BEAMnrc and a phase-space file is created at the bottom, which corresponds to the entrance plane of the iris geometry. This phase-space is then used as input to transport the particles through the iris geometry, and the dose is finally scored in the water phantom below the collimator.

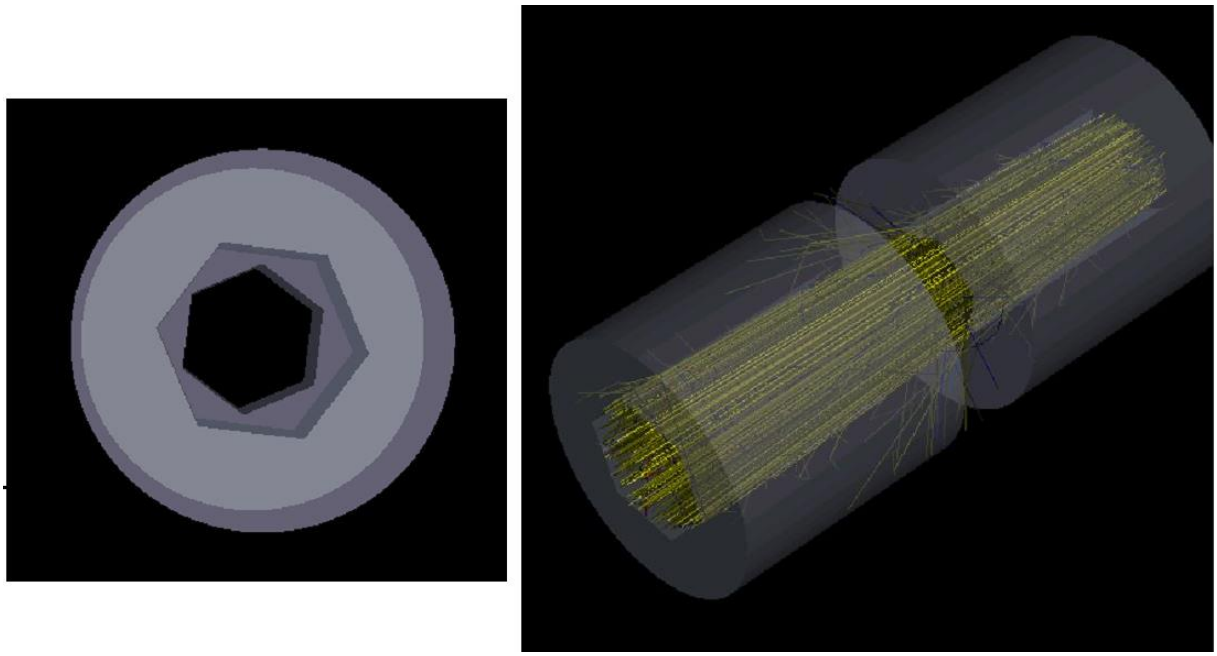

Figure 31. Left: egs++ iris geometry for the 60 mm collimator, visualized from the bottom (to be compared with the right part of Figure 29). Right: oblique view of the iris with 2000 particle tracks projected through the geometry. The photons are coming from the upper right side of the image. The two tungsten banks have a length of 6 cm each, with an air gap of 2 cm in between.

Similarly to the commissioning measurements, two dose profiles were simulated for each collimator by rotating the whole geometry by 15°, and then averaged and compared to the measurements. The results for the 5 and 60 mm apertures are shown in Figure 32. The PDDs are very similar to the results of the fixed collimators and were not included here.

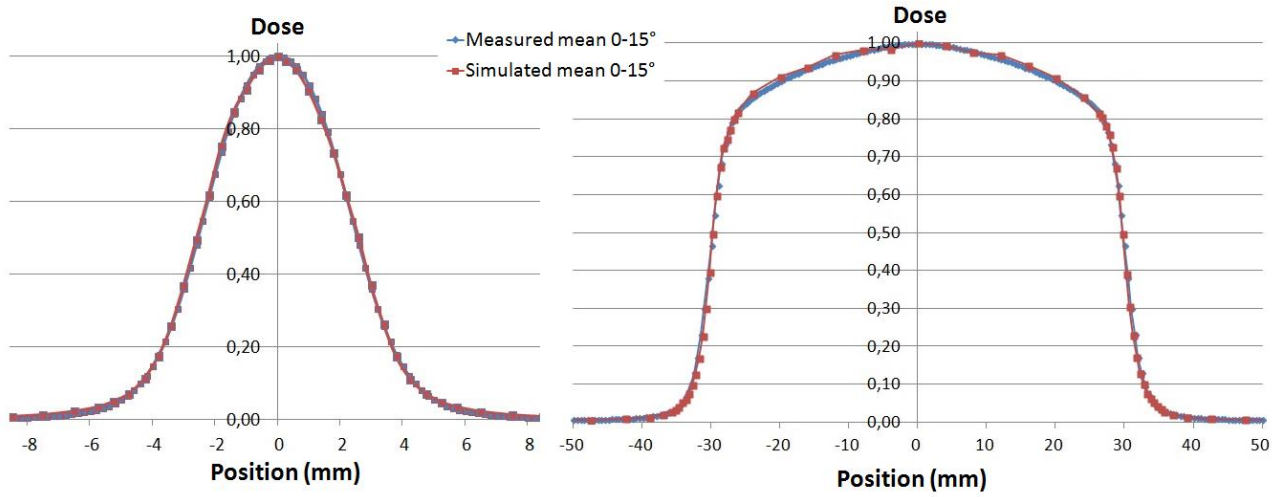

Figure 32. Measured and simulated profiles in water (after averaging between 0° and 15°) for the 5 mm and 60 mm apertures.

All 12 iris apertures were optimized until good correspondence was achieved. Only the diameter had to be adapted slightly for each beam, as small differences may exist between the nominal dimensions in the data provided by the manufacturer and the actual sizes of the device.

Once all dose profiles and PDDs were deemed comparable, the model could be used to re-calculate patient plans. This is performed by generating phase-space files and integrating them in the Moderato platform, as will be detailed in the next chapter.

4. The *Moderato* platform

4.1. Aim

In the first chapter of this thesis, we introduced the problems regarding the uncertainties in the delivered dose, and justified the motivation to design a platform that would enable recalculating and reconstructing the dose to the patient, as a first step towards a clinical decision support system (CDSS). This platform is currently being developed conjunctly at COL and IJB and is called *Moderato*.

Moderato is based on the MCDE system [78] developed in 2004 in Ghent. Entirely based on BEAMnrc/DOSXYZnrc, it was able to recalculate a complete patient plan from the machines present at Ghent hospital (IMRT and VMAT techniques). However it lacked the automation and user-friendliness necessary to generalize its use to the routine of a radiotherapy department. *Moderato* was then developed following this paradigm of a fast and easy to use system. The following features were integrated:

- a DICOM interface allowing to directly import data from the TPS, such as the patient CT images, the contours (RTstruct file), the plan (RTplan file) and the dose distribution (RTdose file)
- an independent dose calculation grid, allowing to change the resolution in order to speed up dose computation
- a stoichiometric calibration for the conversion of CT data into tissue parameters [79]
- a modular architecture allowing to easily add new machines to the database, including machines modelled with different Monte Carlo codes
- a Graphical User Interface (GUI) to provide accessibility to all users
- a dropbox automatically scanned by the platform to convert newly arrived data and launch simulations

In short, the objective of the system is to provide a fast, independent, automated and user-friendly interface for dose recalculation and reconstruction, which could be used in a radiotherapy department without adding any additional time-consuming tasks to the dosimetrists and physicists.

4.2. Description of the platform

A more detailed description of the system is given in Reynaert et al [80], and the article has been included in the appendix of this thesis (chapter 7). A diagram is shown in Figure 33. First, the geometry and BEAMnrc input files (RTplan or xml files) are initialized. Then a global "cylindrical" phase-space file is created all around the patient geometry, combining particles from all beams.

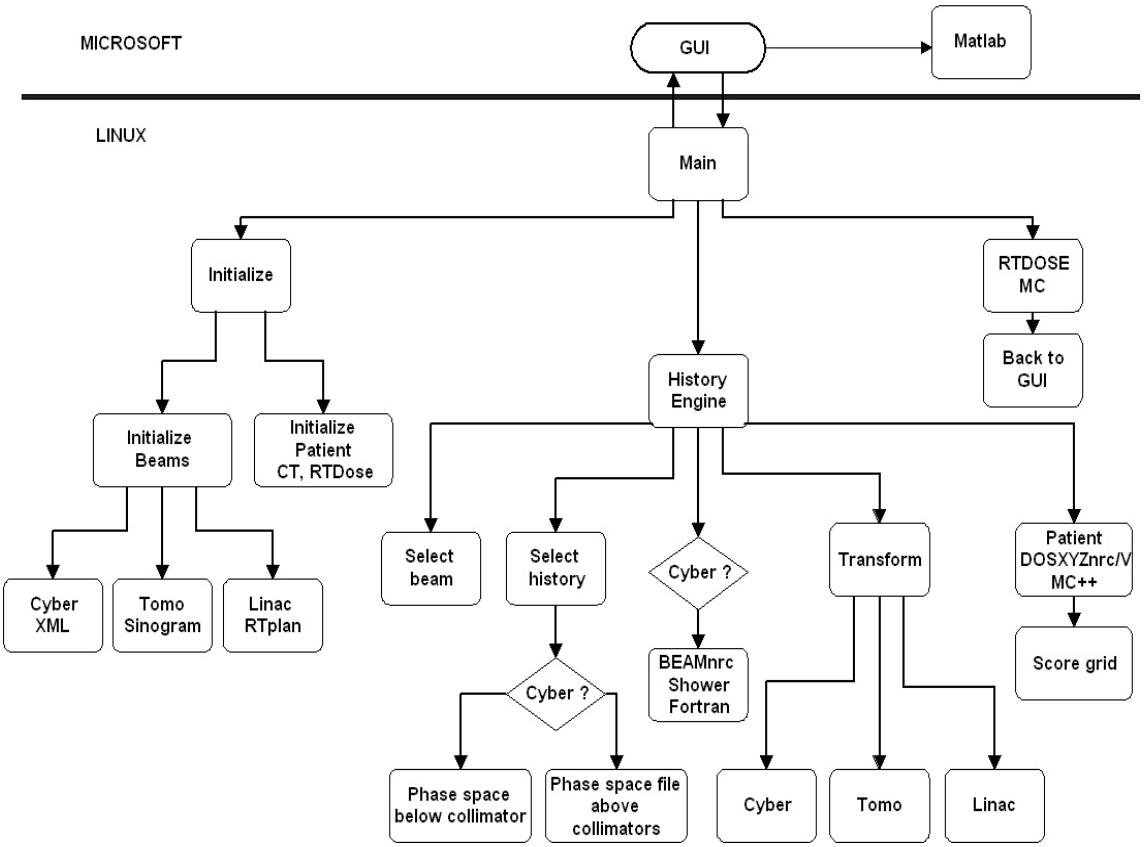

Figure 33. Diagram of the *Moderato* platform.

In the next step, the particles from the phase-space are projected inside the patient and the dose calculation is realized. This computation is parallelized to increase speed. Finally, all dose files are re-combined to provide the total dose in the patient, and the results are displayed in the GUI. This visual interface offers the possibility to visualize the dose distributions from both calculations (TPS and *Moderato*) next to each other, with both DVHs displayed below.
Additional options of dose constraints generation for OARs and visual warnings for constraints violations were added at a later stage. They will be detailed in the article of section 4.3.

4.2.i. Cyberknife

The Cyberknife accelerator was integrated in the platform using the modelling realized in chapter 3. Phase-space files were generated for each field size of the iris and fixed collimators (5, 7.5, 10, 12.5, 15, 20, 25, 30, 35, 40, 50 and 60 mm diameter at isocenter). These phase-space files are stored in the database. When a specific collimator is present in the RTplan file of a patient, the corresponding phase-space file is read and transformed to the position of the treatment head for that particular beam. The operation is repeated for every beam to create the global patient-specific phase-space file mentioned above. This allows reducing simulation time as no transport has to be re-performed inside the treatment head when starting a patient calculation.

The model was tested on several Cyberknife patients with different diseases, treated with the iris collimator. Two examples are given in Figure 34. Additional results can be found in the publication describing Moderato in chapter 7.

The M6 Cyberknife was modelled at a later stage, and details will be given in chapter 5.

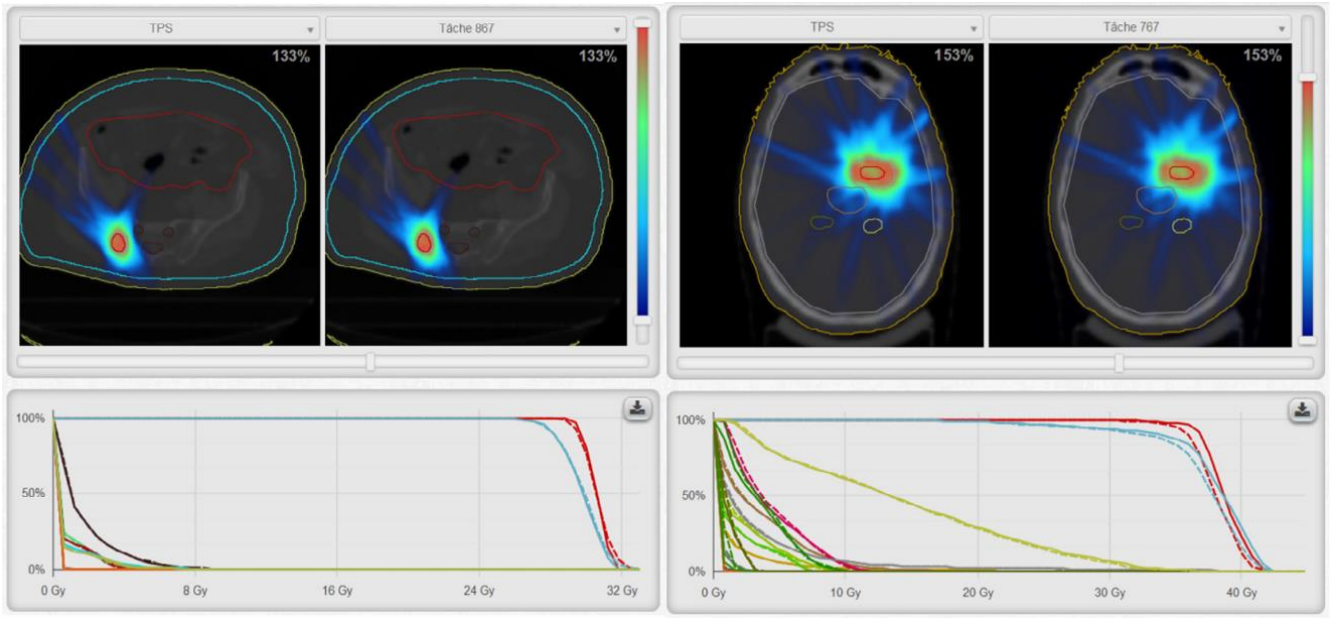

Figure 34. Recalculated doses for two Cyberknife treatments of a pelvic (left) and brain (right) lesion. The agreement in PTV doses is within 2% for both cases.

4.2.ii. Tomotherapy

The Tomotherapy system was modelled using a double Gaussian spot [81] and the diagrams provided by the vendor. An accelerated option was included for the transport through the binary MLC, using a Russian roulette process (photons have a probability of being discarded if they travel a large distance through tungsten, to avoid "wasting" time on less significant histories).

The model was validated based on water phantom measurements, integrated in *Moderato* and then tested on patients with various treatment sites [80].

4.3. Article

This article was published in *Physica Medica* (*European Journal of Medical Physics)* [82] and focuses on the introduction of a new evaluation (or "Prescription-validation") module in the platform, designed to generate and compare dose constraints to OARs as calculated by the TPS and by *Moderato*.

The references of the article were included directly at its end in *Physica Medica* format.

Use of an in-house Monte Carlo platform to assess the clinical impact of algorithm-related dose differences on DVH constraints

A. Wagner[1], F. Crop[1], X. Mirabel[2], C. Tailly, N. Reynaert[1]

1: Department of Medical physics, Centre Oscar Lambret and University Lille 1

2: Academic Department of Radiation Oncology, Centre Oscar Lambret, and University Lille 2

Abstract

Purpose: The aim of the present work is to evaluate a semi-automatic prescription and validation system of treatments plans for complex delivery techniques, integrated in a Monte Carlo platform, and to investigate the clinical impact of dose differences due to the calculation algorithms, by assessing the changes in DVH constraints.

Methods: A new prescription module was implemented into the *Moderato* system, an in-house Monte Carlo platform, with corresponding dose constraints generated depending on the anatomical region and fractionation scheme considered. The platform was tested on 83 cases treated with Cyberknife and tomotherapy machines, to assess whether dose variations between the re-calculated dose and the Treatment Planning System might impact the dose constraints on the sensitive structures.

Results: Dose differences were small (within 3 %) between calculation algorithms in most of the thoracic, pelvic and abdominal cases, both for the Cyberknife and Tomotherapy machines. On the other hand, spinal and head and neck treatments presented a few significant dose deviations for constraints on small volumes, such as the optic pathways and the spinal cord. These differences range from -11% to +6%, inducing constraint violations of up to 8% over the dose limit.

Conclusions: The *Moderato* platform offers an interesting tool for plan quality validation, with a prescription module highlighting crucial features in the structures list, and a Monte Carlo dose re-calculation for complex modern techniques. Due to the high number of warnings appearing in some situations, display optimization is required in practice.

Keywords: treatment planning, Monte Carlo, QA, dose constraints

Introduction

In radiotherapy, the treatment chain consists of several steps that can introduce errors, and workflow is an essential aspect in the quality management of a department. The number of different actors and the numerous steps in a patient course before treatment require very fast and flexible tools, and much effort has been put into the automation and optimization of the processes in our department, as introduced in [1]. An important step is the prescription performed by the physician. If it is not clear enough or lacks some elements when the patient file reaches the dosimetry step, additional interaction is needed between the physicist or dosimetrist and the physician, which inevitably slows down the process. Sometimes an unusual fractionation scheme is adopted, which requires new constraints to be calculated. The validation step of a treatment plan can also be very time-consuming, as it implies both the physicist and the physician reviewing the quality of the plan, including a number of regions-of-interest (ROI) to make sure these are all spared (or covered) adequately. This manual verification is one of the last checkpoints before a patient receives his or her first treatment session, and an error or oversight during this step might have serious consequences. All these aspects support the need for a system that would speed up the process while preserving its quality and safety aspects, as well as guaranteeing that no element is overlooked.

As introduced in [2], *Moderato* is an independent treatment QA platform that allows for dose re-calculation of complex radiation therapy techniques. It consists of a Monte Carlo (MC) based platform designed to be used in the daily clinical routine as most of the processes are automated: the Dicom files (images, structures and dose) are converted and simulations are launched without user interaction, and a graphical interface allows for a quick visual comparison of the dose distributions and Dose-Volume Histogram (DVH) data. The Cyberknife and Tomotherapy machines were modeled [4] and validated based on dose profiles, depth-dose curves and simple phantom geometries. It is generally recognized that Monte Carlo algorithms provide a higher precision for dose distributions calculated in complex geometries, where many material interfaces are involved [5]. The main drawback of the use of Monte Carlo codes in routine has been their computation time, but this issue has been addressed in *Moderato*. This allows to use it on a much larger scale and to systematically re-calculate all patient plans.

The aim of the present work is to implement a semi-automated Prescription/Validation module into our existing *Moderato* platform, allowing for an improvement of the process in terms of speed and safety. As doses are re-calculated using a high-precision MC engine, our second objective is to evaluate the clinical impact of the calculation algorithms on the dose constraints for the different anatomical structures considered.

Materials and Methods

The *Moderato* platform, which is originally based on MCDE [6] is introduced in detail in Reynaert et al [2]. Calculations for the patients considered in this study were based on BEAMnrc [7] and DOSXYZnrc [8] (other codes are available). The modeling of the Tomotherapy is partly based on Chen et al [3], whereas the Cyberknife modeling was validated earlier in our center [4]. Standard MC calculation parameters are defined in the

system and can be modified if necessary. The number of histories was set to result in an uncertainty of 2% in 95% of the Planning Target Volume (PTV). This corresponds to approximate calculation times between 15 and 45 minutes. The image value to density table and tissue composition are based on a stoichiometric calibration method [9,10].

A new *Prescription* module was implemented into the system, consisting of a graphical interface where the physician first selects a "model", which corresponds to an indication (e.g. head and neck, thoracic, pelvis), the desired dose level and number of fractions. All OAR constraints are automatically displayed based on the anatomical region and the fractionation scheme. The physician can add or remove structures from the list and modify the dose constraints if necessary, depending on the clinical specificity of the patient considered (priority between target coverage and close OAR, re-irradiation case, etc.)

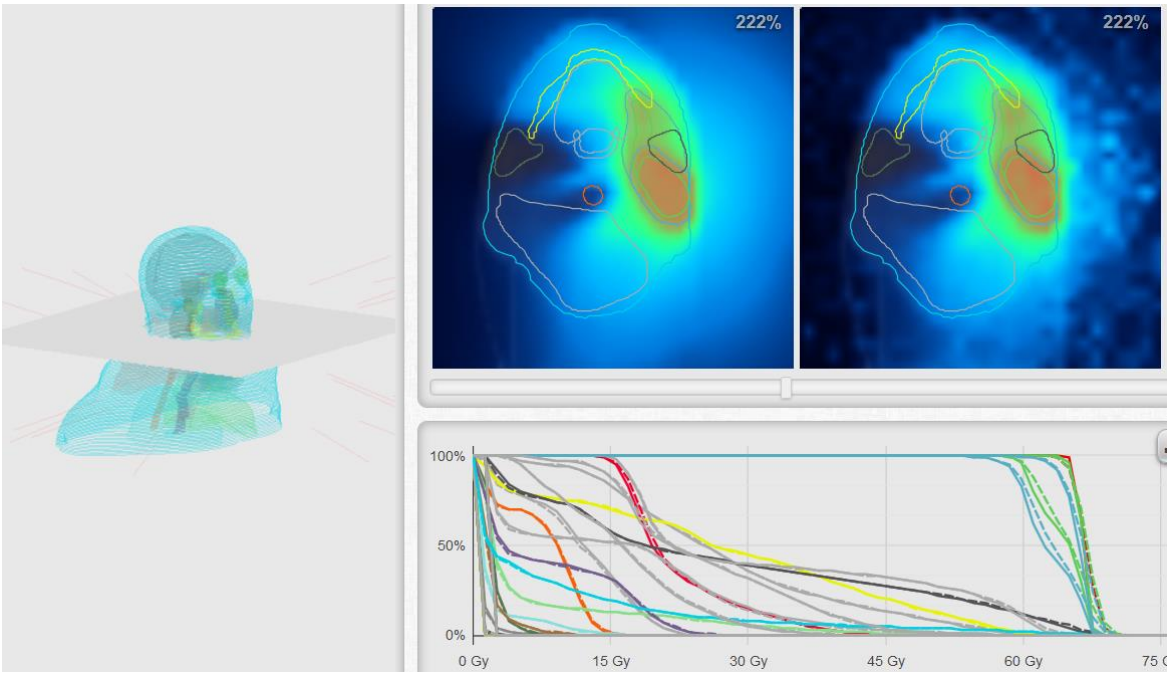

Figure 1. The DVH and isodose visualization of *Moderato*.

Treatment planning is realized using the dedicated commercial Treatment Planning System (TPS). Upon completion, the dose is re-calculated in *Moderato* with standard simulation parameters (which can be modified if necessary), and a tag is activated in the patient flow system [1] to indicate the plan is ready for validation. The system displays the isodoses and the Dose-Volume Histograms in a manner similar to a conventional TPS (figure 1). In addition, the system creates a table containing all the DVH points of interest (corresponding to dose constraints), both according to the TPS and to the MC calculation. The first structures shown are those where constraints are violated, either in the TPS calculation, the Monte Carlo calculation, or both. Three different color codes are associated with the magnitude of the deviation (0 – 3 %, 3 – 5 %, > 5 %). Next, structures fulfilling all constraints are displayed. Finally the table shows the structures usually associated to the selected model, but that could not be found in the structures list. This allows the physician to verify whether some structure was omitted during the contouring phase.

Table 1. The constraints table as displayed in the evaluation interface, for the case in figure 1. Doses from the TPS are shown in the left column, and those calculated with Monte Carlo on the right. Here the oral cavity presents two dose warnings.

	tps	task1786
Cavité buccale		
V15 < 80%	15.8 Gy	16.0 Gy
V30 < 50%	25.0 Gy	25.3 Gy
V45 < 25%	35.0 Gy	35.5 Gy
V50 < 2%	57.0 Gy	58.0 Gy

	tps	task1786
Chiasma		
V54 < 0.003cm³	0.7 Gy	0.8 Gy

	tps	task1786
Encéphale irradiation partielle		
V60 < 10cm³	9.6 Gy	9.6 Gy

	tps	task1786
Hypophyse		
V50 < 0.035cm³	0.9 Gy	0.9 Gy

	tps	task1786
Larynx		
V30 < 60%	18.6 Gy	19.0 Gy
V45 < 50%	19.6 Gy	20.0 Gy
V65 < 2%	41.0 Gy	41.0 Gy

	tps	task1786
Moëlle épinière		
V45 < 10%	12.6 Gy	12.8 Gy
V50 < 0.003cm³	15.7 Gy	16.1 Gy

	tps	task1786
Oesophage		
V45 < 40%	9.0 Gy	8.5 Gy
V55 < 30%	15.7 Gy	15.7 Gy

	tps	task1786
Thyroïde		
V50 < 50%	21.5 Gy	21.8 Gy

	tps	task1786
Tronc cérébral		
V54 < 0.003cm³	11.1 Gy	11.6 Gy

	tps	task1786
Articulation temporo-mandibulaire droite		
V55 < 2%	???	???

	tps	task1786
Articulation temporo-mandibulaire gauche		
V55 < 2%	???	???

	tps	task1786
Conduit auditif, oreille moyenne		
V6 < 2%	???	???

The structure display is illustrated in table 1. Here the first constraint on the oral cavity, V15 Gy < 80%, is violated. The table shows the dose actually delivered to 80 % of the organ, and highlights it as it deviates by approximately 7% from the limit. Although this display might seem less intuitive than showing directly the volume percentage, it is more logical as the comparison focuses on the dose calculation from both algorithms, and not the volume. The choice was made not to modify the constraints list as the form Vx < Y % is most common in the literature and is the one used by the physicians in our department.

Twenty-seven Cyberknife (CK) patients and fifty-six Helical Tomotherapy (HT) patients were included in this work. The CK cases consisted of 8 head and neck, 5 thoracic, 6 spine, 3 liver, and 5 pelvic treatments. The distribution of patients treated with HT was 20 head and neck, 5 thoracic, 14 breast, 4 abdominal, and 13 pelvic cases. No selection criteria were used and the relative proportions of indications simply reflect the database of each machine at the time of the study. All OARs were reviewed to look for constraint violations, and these were analyzed in order to assess their relevance within the context of plan validation: indeed, this step implies a fine balance between too many “false positives” generated from constraints that would be too severe, and the risk of missing actual errors by setting too large tolerances on deviations. Most of these constraint violations resulted from informed decisions at the time of the patient treatment.

Results

Cyberknife

Among the thoracic cases, constraint violations were detected for one patient with two lesions close to the ribs (Table 2). The *Moderato* calculation presents a significant dose reduction for the second rib.

Table 2. Constraint violations on the ribs for a lung Cyberknife treatment.

	tps	task1789
Côte 1		
V29 < 1cm³	39.7 Gy	40.2 Gy
V37 < 0.035cm³	48.9 Gy	49.1 Gy

	tps	task1789
Côte 3		
V29 < 1cm³	40.0 Gy	37.0 Gy
V37 < 0.035cm³	51.7 Gy	50.4 Gy

No constraints were violated in all five pelvic cases, and no deviations were found between the dose algorithms. Dose constraints were also met for the liver cases (Table 3), but some deviations were detected in the dose distributions for targets in the upper part of the liver, which is due to the proximity of the lung (for most liver cases TPS calculations are performed with a type *A* Raytracing algorithm).

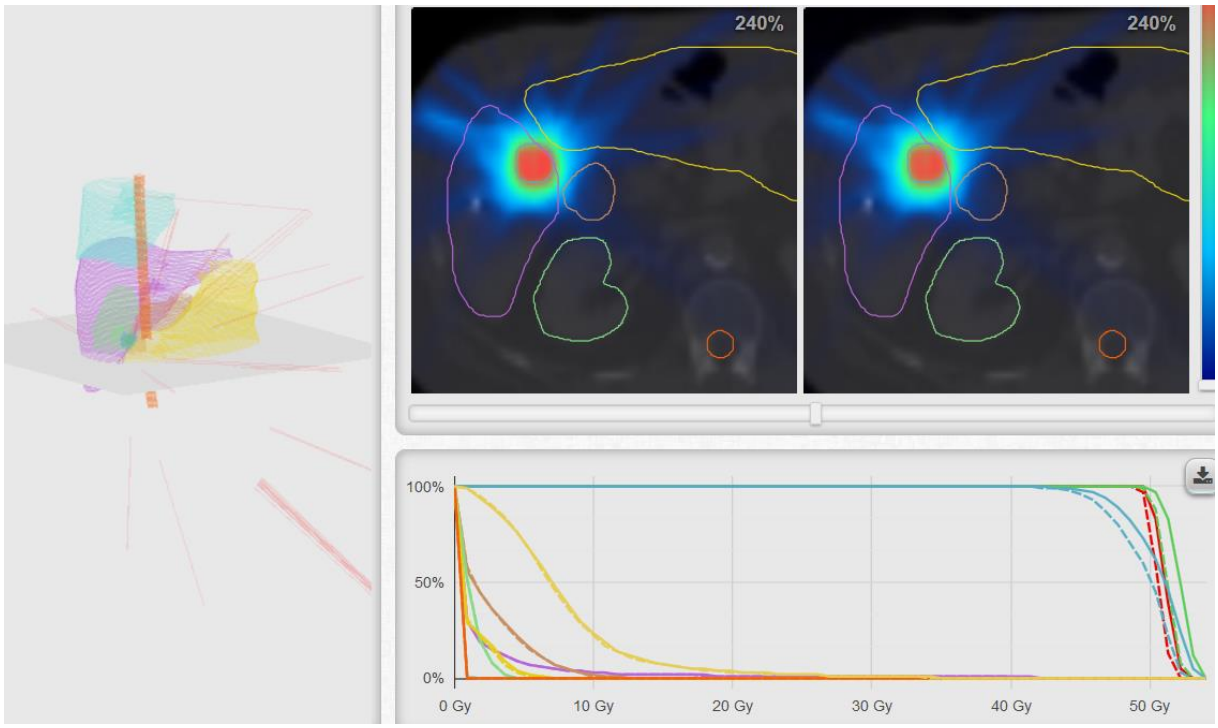

Figure 2. Example of a liver CK case, with a target surrounded by the duodenum and the small intestine.

Table 3. Constraints table for the CK liver case presented in figure 2, showing no warnings despite the proximity with the OARs. Displayed OARs include the colon, duodenum, liver, small intestine and spinal cord.

	tps	task1860
Colon		
V20 < 20cm³	8.7 Gy	8.6 Gy
V30 < 1cm³	26.4 Gy	26.4 Gy

	tps	task1860
Duodénum		
V15 < 5cm³	8.9 Gy	8.9 Gy
V24 < 0.5cm³	12.1 Gy	11.9 Gy

	tps	task1860
Foie irradiation partielle		
V15 < 50%	0.7 Gy	0.7 Gy
V21 < 33%	0.9 Gy	0.9 Gy
Vtotal - V17 > 700cm³	1744 cm³	1744 cm³

	tps	task1860
Intestin grêle		
V16 < 5cm³	6.9 Gy	6.8 Gy
V27 < 0.5cm³	6.9 Gy	6.8 Gy

	tps	task1860
Moëlle épinière		
V16 < 1.2cm³	0.7 Gy	0.6 Gy
V18 < 0.25cm³	0.7 Gy	0.7 Gy
V22 < 0.003cm³	0.7 Gy	0.7 Gy

	tps	task1860
Coeur		
V24 < 15cm³	???	???
V30 < 2%	???	???

Among the eight head and neck patients, three presented with constraint violations on one or both optic nerves. The *Moderato* re-calculated dose appeared to be lower than that from the TPS, inducing a change of the warning level, as illustrated in Table 4.

Table 4. Re-calculation causing a change of the warning intervals for the right optic nerve and left optic nerve in two Cyberknife head cases.

	tps	task1972
Chiasma		
V21.5 < 0.2cm³	13.8 Gy	13.8 Gy
V27 < 0.035cm³	27.4 Gy	25.9 Gy

	tps	task1972
Nerf optique droit		
V21.5 < 0.2cm³	14.0 Gy	13.9 Gy
V27 < 0cm³	28.9 Gy	27.9 Gy

	tps	task1972
Nerf optique gauche		
V21.5 < 0cm³	27.2 Gy	24.9 Gy
V27 < 0.003cm³	27.2 Gy	24.9 Gy

	tps	task1869
Nerf optique gauche		
V21.5 < 0.2cm³	5.9 Gy	5.9 Gy
V27 < 0.003cm³	30.8 Gy	27.3 Gy

	tps	task1869
Chiasma		
V21.5 < 0.2cm³	11.5 Gy	11.4 Gy
V27 < 0.035cm³	16.8 Gy	16.7 Gy

	tps	task1869
Cristallin droit		
V6.5 < 0.003cm³	0.2 Gy	0.7 Gy

Spinal cases showed the highest numbers of constraint violations, with five out of six patients causing dose warnings. However dose differences between the TPS and *Moderato* were within 2 % except for one case, illustrated in Table 5, where the dose went from 5 % to 8 % above the limit.

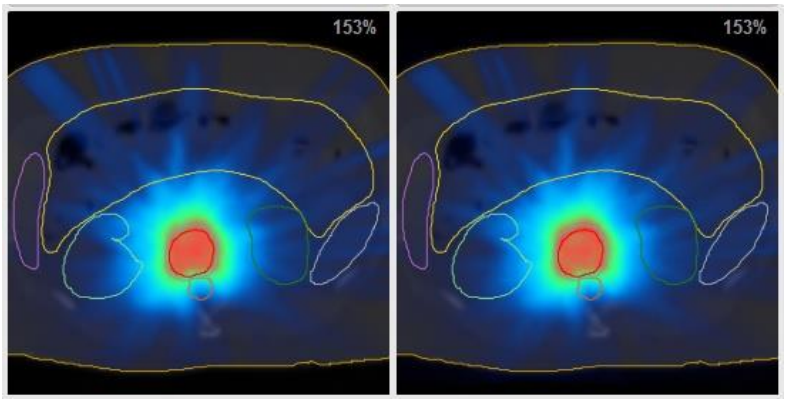

Figure 3. Example of a spine case treated with the Cyberknife.

Table 5. Constraints table for the CK case in figure 3, showing a higher level of warning for the spinal cord for the MC calculated dose.

	tps	task1823
Moëlle épinière		
V16 < 1.2cm³	15.6 Gy	15.6 Gy
V18 < 0.25cm³	18.9 Gy	19.5 Gy
V22 < 0.003cm³	18.9 Gy	19.5 Gy

Tomotherapy

Two of the five thoracic cases exceeded the V50 < 15cc constraint on the heart, with one minor warning (< 5 %) arising with the dose difference.

Only one of the four abdominal treatments showed dose warnings (table 6), but all of these were consistent between both algorithms.

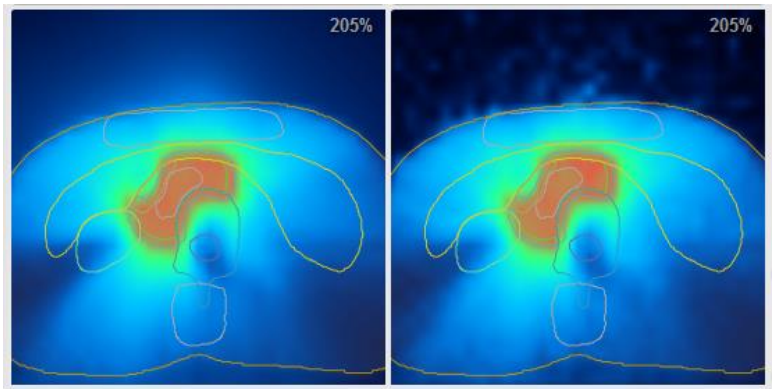

Figure 4. Abdominal HT case with a target surrounded by the small intestine.

Table 6. Dose constraints table for the abdominal HT case in figure 4, for the duodenum and the small intestine, showing a consistent level of warning between algorithms.

	tps	task1797
Duodénum		
V45 < 10cm³	48.4 Gy	48.4 Gy
V50 < 5cm³	50.5 Gy	50.5 Gy
V64 < 0.5cm³	51.9 Gy	52.4 Gy

	tps	task1797
Intestin grêle		
V40 < 200cm³	27.3 Gy	27.3 Gy
V50 < 35cm³	49.1 Gy	50.1 Gy

Among the thirteen pelvic treatments, four presented small violations of the V40 < 200cm^3 on the intestine, but again no deviations emerged between calculation algorithms.

Among the 14 breast patients considered, 6 presented dose deviations on the maximum dose for the spinal cord, D_{max} = 15 Gy. All other OARs were within dose limits and showed dose deviations under 3 %.

The head and neck cases presented by far the highest number of constraint violations (Table 7), but deviations between algorithms were small. Of the 20 patients evaluated, 5 presented dose deviations on the oral cavity, larynx or parotids, but none of these modifying the warning level.

Table 7. Head-and-neck HT case generating a high number of warnings on organs-at-risk.

	tps	task1924
Articulation temporo-mandibulaire droite		
V55 < 2%	71.1 Gy	70.3 Gy

	tps	task1924
Articulation temporo-mandibulaire gauche		
V55 < 2%	67.5 Gy	65.7 Gy

	tps	task1924
Cavité buccale		
V15 < 80%	33.0 Gy	31.7 Gy
V30 < 50%	52.3 Gy	50.7 Gy
V45 < 25%	60.5 Gy	58.0 Gy
V50 < 2%	72.1 Gy	70.0 Gy

	tps	task1924
Encéphale irradiation partielle		
V60 < 10cm³	60.4 Gy	59.9 Gy

	tps	task1924
Hypophyse		
V50 < 0.035cm³	65.4 Gy	64.9 Gy

	tps	task1924
Larynx		
V30 < 60%	46.0 Gy	45.2 Gy
V45 < 50%	47.8 Gy	47.2 Gy
V65 < 2%	60.0 Gy	70.0 Gy

	tps	task1924
Mandibule		
V35 < 50%	46.0 Gy	44.0 Gy

	tps	task1924
Nerf optique gauche		
V54 < 0.003cm³	54.7 Gy	53.8 Gy

	tps	task1924
Oreille interne droite		
V45 < 50%	45.3 Gy	44.7 Gy
V50 < 2%	58.9 Gy	57.7 Gy

	tps	task1924
Oreille interne gauche		
V45 < 50%	51.3 Gy	49.3 Gy
V50 < 2%	63.1 Gy	62.5 Gy

	tps	task1924
Parotide droite		
V15 < 65%	56.3 Gy	54.7 Gy
V25 < 50%	60.0 Gy	58.5 Gy
V30 < 45%	60.8 Gy	59.3 Gy

	tps	task1924
Parotide gauche		
V15 < 65%	53.5 Gy	51.7 Gy
V25 < 50%	58.2 Gy	56.5 Gy
V30 < 45%	59.2 Gy	57.8 Gy

	tps	task1924
Thyroide		
V50 < 50%	56.7 Gy	55.2 Gy

	tps	task1924
Chiasma		
V54 < 0.003cm³	42.8 Gy	43.1 Gy

	tps	task1924
Cristallin droit		
V6 < 0.003cm³	4.1 Gy	3.9 Gy

	tps	task1924
Cristallin gauche		
V6 < 0.003cm³	4.0 Gy	3.7 Gy

	tps	task1924
Moëlle épinière		
V45 < 10%	34.5 Gy	33.0 Gy
V50 < 0.003cm³	45.4 Gy	44.5 Gy

	tps	task1924
Nerf optique droit		
V54 < 0.003cm³	52.9 Gy	52.9 Gy

	tps	task1924
Oeil droit		
V35 < 50%	7.5 Gy	7.0 Gy

	tps	task1924
Oeil gauche		
V35 < 50%	7.4 Gy	6.9 Gy

	tps	task1924
Oesophage		
V45 < 40%	1.8 Gy	1.7 Gy
V55 < 30%	3.3 Gy	2.7 Gy

	tps	task1924
Trachée, grosses bronches		
V80 < 2%	55.0 Gy	54.0 Gy

	tps	task1924
Tronc cérébral		
V54 < 0.003cm³	51.8 Gy	51.1 Gy

	tps	task1924
Conduit auditif, oreille moyenne		
V6 < 2%	???	???

In one complicated case with a target embedded in the optic pathways (figure 5), the dose rose from 55.9 to 57.9 Gy on the left optic nerve, reaching more than 7 % above the limit of 54 Gy.

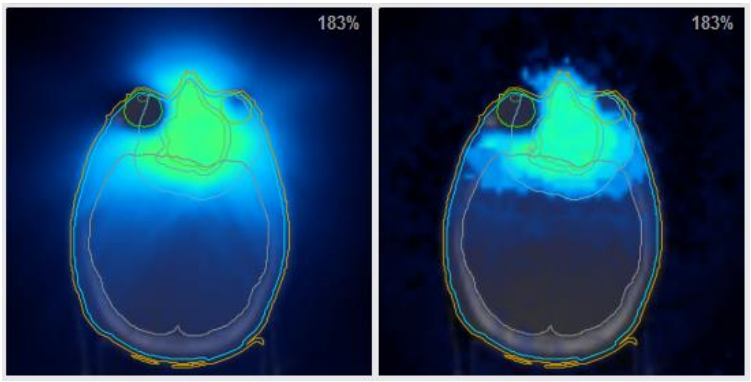

Figure 5. Head-and-neck treated with HT, with a target close to the optic pathways.

Table 8. Constraints on the optic chiasm and optic nerves for the HT case shown in figure 5.

	tps	task1798
Chiasma		
V54 < 0.003cm³	54.7 Gy	55.9 Gy

	tps	task1798
Nerf optique gauche		
V54 < 0.003cm³	55.9 Gy	57.9 Gy

	tps	task1798
Nerf optique droit		
V54 < 0.035cm³	55.9 Gy	56.6 Gy

Discussion

In the present study a new module of prescription and validation was implemented in the *Moderato* Monte Carlo platform, and tested on 83 patients treated with stereotactic radiotherapy and helical tomotherapy. Results are summarized in Tables 9 and 10, and show that the overall accuracy of both TPSs (Cyberknife *MultiPlan*, and Tomotherapy Planning Station) is reliable.

Concerning the thoracic CK cases, it is worth noting that differences remain small as the lung cases are calculated with a Monte Carlo algorithm available in the TPS. These differences are mainly due to a lower electron energy cutoff. However, doses calculated for moving structures should be considered with precaution if no 4D calculation is performed. Dose reconstruction in 4D is currently being implemented in the system, and dose warnings will be considered more reliable for such indications once this is achieved. The same holds for the liver cases, although first results suggest a small impact of motion [2], probably due to the use of a treatment belt.

Pelvic CK cases showed good agreement between dose distributions, and the warning level did not change with the Monte Carlo calculation. This is also true for most pelvic HT treatments, where the highest deviation between algorithms was 2.5 % on the V40 < 200cm^3 for the intestine, raising the dose to 5 % above the limit. This constraint is often difficult to meet for the large abdominal volumes treated with rotational therapy as the structure is surrounding the target.

The abdominal and breast HT cases showed a good correlation in dose warnings between algorithms. The irradiation of breast and lymph nodes involves large complex volumes for which rotational therapy is an interesting choice given its high modulation capabilities. However as these patients are conventionally treated with tangential fields delivering practically no dose to the distant OARs, and have a longer life expectancy as compared to other typical HT indications, it is essential that distant OARs are well-spared and low-dose spillage is reduced as much as possible. Thus a conservative approach is applied in our department, and dose constraints on the spinal cord for example are stronger (D_{max} = 15 Gy) than those applied in the treatment of other localizations.

Table 9. Summary of the results for the Cyberknife patients. For each indication, the table shows the total number of patients, the number of patients where dose deviations over 3 % were detected, the structures involved, the number of constraints with dose deviations and their range, and the number of constraints subject to a change of warning level.

Indication	# patients	Patients with deviation > 3%	Structures	# deviations	Range of deviations	# changes in warning level
Thoracic	5	1	Rib	1	-7.5%	0
Pelvis	5	0	-	-	-	-
Abdomen	3	0	-	-	-	-
Head & Neck	8	3	Optic pathways	5	-3 to -11%	3
Spine	6	1	Spinal cord	1	+3.2%	1

Table 10. Summary of the results for the Tomotherapy patients. For each indication, the table shows the total number of patients, the number of patients where dose deviations over 3 % were detected, the structures involved, the number of constraints with dose deviations and their range, and the number of constraints subject to a change of warning level.

Indication	# patients	Patients with deviation > 3%	Structures	# deviations	Range of deviations	# changes in warning level
Thoracic	5	0	-	-	-	-
Pelvis	13	0	-	-	-	-
Abdomen	4	0	-	-	-	-
Breast	14	6	Spinal cord	6	+3 to +6%	0
Head & Neck	20	5	Optic pathways	1	+4%	1
			Parotids, oral cavity, larynx	11	-4 to+4%	0

Head and neck cases treated with CK presented differences for maximum dose constraints on small OARs close to the target volume (optic pathways). Interestingly, the calculated doses showed a decrease with *Moderato*, sufficient to induce a change of the warning level.

On the other hand, one spinal case showed an increase reaching 8 % above the limit. These cases involve complex targets located close to the spinal cord, where dose limits were knowingly exceeded in the hope of achieving local control of the tumor. These are difficult cases where no therapeutic alternative was available, and the medical team chose to favor tumor coverage while informing the patient of the potential risks.

For these structures it should be noted that the uncertainty of the Monte Carlo calculated dose is higher as it involves a few voxels, and one should consider increasing the number of histories for these specific situations. Nevertheless, it can be seen that depending on the situation, differences can affect the dose either by raising it above the threshold, or lowering it to an acceptable level. This illustrates the importance of such a verification tool for those cases where the plans are fine-tuned until reaching a subtle compromise between coverage and OAR protection.

Among the 20 head and neck HT patients evaluated, only 3 generated a fully "green" result. Indeed, in order to achieve sufficient target coverage, limits were frequently exceeded for the oral cavity, the larynx, the thyroid, etc. As a consequence, the system generates too many warnings because it includes OARs that are partly or entirely intersecting the targets. The difficulty thus resides in finding a way to select and discard those structures that cannot be spared to alleviate the display. In one specific case, dose re-calculation triggered dose increase and warnings for the optic pathways, unlike the CK situation where a decrease was noticed, once again stressing the importance of re-calculation for difficult cases.

A commercial solution offering tridimensional dose distribution verification was recently introduced (M3D) [11]. However it is based on a collapsed cone convolution/superposition algorithm, which is used in many TPSs such as Tomotherapy planning station, and some significant differences were detected in stereotactic body radiation therapy plans between M3D and EGSnrc doses [12].

The use of a verification system raises an important question: at which point should one consider a dose difference as a major deviation, and what action should be undertaken? The warning levels of 3 – 5 % adopted here are based on generally accepted thresholds [13], but it is clear that the amount of warnings generated is highly variable and should be adapted according to the indication, the technique and the importance of the structure considered. This is an ongoing work in our department by progressively optimizing the displayed data with the corresponding physicians. The concept of warning itself depends on the situation considered: a dose deviation might appear too large for the physicist seeking to achieve a high accuracy even in complex techniques and geometries, whereas the physician would consider it clinically irrelevant. In the latter case it is probably not necessary to consider plan revision, which would introduce a delay in the start of the treatment that might be harmful.

Determining a threshold from which a dose deviation would potentially impact clinical outcome is a very difficult problem that implies biological concepts in addition to the purely physical aspect of dose. It would be interesting to be able to determine those situations where deviations are most likely to occur, so that similar cases can be detected early on in the future and treatment planning can be realized more robustly with respect to dose calculation, rather than adapted *a posteriori*. Such results require a large number of patients, included in multi-institutional studies evaluating clinical outcome in relation to delivered dose. These data are tainted by the dosimetric deviations between different centers and techniques [14]. The larger the spread caused by dosimetric uncertainties, the more patients need to be included in a trial in order to detect small variations between different experimental schemes. This aspect could be improved by the use of a single system to re-calculate dose distributions, offering more coherence between all the combined data, and *Moderato* offers great potential in this prospect.

Other new features are being currently implemented into the system, such as robustness evaluation and dose reconstruction. The first allows for dose re-calculation with the introduction of positioning uncertainties, and their impact on the DVH points of interest, while the latter consists of computing the actually delivered dose in a specific treatment session using logs generated by the machine and 4D patient data. This feature will bring new information on intra-fraction motion for lung and abdominal cases as mentioned above, but it is also likely to identify an impact from the anatomical changes that occur between treatment sessions, for pelvic, abdominal and head and neck cases. This is an essential point in the quest

for high-quality data to be related to patient outcome [15], and the introduction of these factors is likely to produce substantial modifications of the dose distribution and hence generate warnings of higher magnitude or on structures for which no deviations were detected, or conversely lead to the elimination of some others. This would improve the quality and reliability of the database, and constitute an important step towards the development of a clinical decision support system [16] in radiation therapy.

Conclusions

The *Moderato* platform constitutes a promising tool for plan validation based on Monte Carlo based dose calculations, with the inclusion of a Prescription/Validation module performing semi-automated evaluation of plan quality. This study has focused on the clinical impact of dose differences arising from the calculation algorithms, showing that the results depend on the region and constraints considered. Once the warning system is optimized, the patient workflow could be greatly improved by increasing the safety and speed of the process. In parallel to this, dose re-calculation can be performed for complex techniques for which no commercial system is currently available.

References

[1] F. Crop, T. Lacornerie, X. Mirabel and E. Lartigau, “Workflow optimization for robotic stereotactic radiotherapy treatments: Application of Constant Work In Progress workflow,” *Operations Research for Health Care,* vol. 6, pp. 18-22, 2015.

[2] N. Reynaert, B. Demol, M. Charoy, S. Bouchoucha, F. Crop, A. Wagner, T. Lacornerie, F. Dubus, E. Rault, P. Comte, R. Cayez, C. Boydev, D. Pasquier, X. Mirabel, E. Lartigau and T. Sarrazin, “Clinical implementation of a Monte Carlo based treatment plan QA platform for validation of Cyberknife and Tomotherapy treatments,” *Phys Med,* pp. S1120-1797, 2016.

[3] Q. Chen, Y. Chen, M. Chen, E. Chao, E. Sterpin and W. Lu, “A slit method to determine the focal spot size and shape of TomoTherapy system,” *Med Phys,* vol. 38, no. 6, pp. 2841-9, 2011.

[4] A. Wagner, F. Crop, T. Lacornerie, F. Vandevelde and N. Reynaert, "Use of a liquid ionization chamber for stereotactic radiotherapy dosimetry," *Phys Med Biol,* vol. 58, no. 8, pp. 2445-59, 2013.

[5] N. Reynaert, S. Van der Marck, D. Schaart, W. Van der Zee, C. Van Vliet-Vroegindeweij, M. Tomsej, J. Jansen, B. Heijmen, M. Coghe and C. De Wagter, “Monte Carlo treatment planning for photon and electron beams (Topical Review),” *Rad Phys Chem,* vol. 76, no. 4, pp. 643-686, 2007.

[6] N. Reynaert, B. De Smedt, M. Coghe, L. Paelinck, B. Van Duyse, D. G. W, C. De Wagter, W. De Neve and H. Thierens, “MCDE : a new Monte Carlo dose engine for IMRT,” *Phys Med Biol,* vol. 49, no. 14, pp. N235-41, 2004.

[7] D. Rogers, B. Walters and I. Kawrakow, “BEAMnrc users manual,” *NRC report PIRS 509(a)revI,* 2005.

[8] B. Walters, I. Kawrakow and D. Rogers, “DOSXYZnrc Users Manual,” *NRC report PIRS 794(rev B),* 2005.

[9] B. Demol, R. Viard and N. Reynaert, “Monte Carlo calculation based on hydrogen composition of the tissue for MV photon radiotherapy,” *J Appl Clin Med Phys,* vol. 16, no. 5, p. 5586, 2015.

[10] B. Vanderstraeten, P. Chin, M. Fix, A. Leal, G. Mora, N. Reynaert, J. Seco, M. Soukup, E. Spezi, W. De Neve and H. Thierens, “Conversion of CT numbers into tissue parameters for Monte Carlo dose calculations : a multi-centre study,” *Phys Med Biol,* vol. 52, no. 3, pp. 539-62, 2007.

[11] J. Fontenot, “Evaluation of a novel secondary check tool for intensity-modulated radiotherapy treatment planning,” *J Appl Clin Med Phys,* vol. 15, no. 5, p. 4990, 2014.

[12] N. Hardcastle, B. Oborn and A. Haworth, “On the use of a convolution-superposition algorithm for plan checking in lung stereotactic body radiation therapy,” *J Appl Clin Med Phys,* vol. 17, no. 5, p. 6186, 2016.

[13] D. Thwaites, “Accuracy required and achievable in radiotherapy dosimetry: have modern technology and techniques changed our views?,” *Journal of Physics: Conference Series,* vol. 444, no. 1, 2013.

[14] M. Pettersen, E. Aird and D. Olsen, “Quality assurance of dosimetry and the impact on sample size in randomized clinical trials,” *Radiotherapy and Oncology,* vol. 86, pp. 195-199, 2008.

[15] J. D, P. Lindsay, K. Brock, J. Deasy and W. Tomé, “Accurate accumulation of dose for improved understanding of radiation effects in normal tissue,” *Int J Radiation Oncology Biol Phys,* vol. 76, no. 3, pp. S135-S139, 2010.

[16] P. Lambin, E. Roelofs, B. Reymen, E. Velazquez, J. Buijsen, C. Zegers, S. Carvalho and al, “Rapid learning health care in oncology - an approach towards decision support systems enabling customised radiotherapy,” *Radiother Oncol,* vol. 109, no. 1, pp. 159-64, 2013.

4.4. Discussion

The previous article constitutes the first test of a clinical use of our Monte Carlo platform. Although significant differences were noted between algorithms in some specific cases, these remained rare considering the large number of patients considered and the many organs-at-risk in each of these. After some optimization of the display, this module could be used as a clinical tool that would cover the legal need for dose recalculation (that is not yet commercially available for such techniques), but that would also offer the physician and physicist an easy and unique tool for fast plan validation.

The few deviations observed for small structures are difficult to analyze as there exists no ground truth on which to base conclusions. Measurements should be performed to be able to determine which algorithm delivers the results closest to reality. These are however quite hard to set up, especially if one is to include heterogeneities: they would require very small detectors in an anthropomorphic phantom, posing challenges of positioning accuracy, materials cost, tissue equivalency, etc.
Measurements in a homogeneous medium are simpler to realize, although more limited in terms of algorithm testing. Films can easily be used with slabs and have the advantage of offering a very high spatial resolution. In the next chapter, we will introduce some film-based evaluation of the algorithms present in the Accuray TPS and in Moderato, after modelling the latest M6 Cyberknife device.

In the case of a radiotherapy department where systematic dose recalculation is not feasible, Moderato could be used as an initial quality control platform before or immediately after a new technique has been implemented, to perform dose verification on the first patients until it is no longer deemed necessary. This approach would allow detecting significant systematic errors via a fully independent calculation, preventing these from impacting all subsequent treatments. This control could be repeated with a certain frequency, or even be realized as an external audit in a department where the machines are already running.

As an example to illustrate this potential, the first clinical tests of Moderato [80] allowed us to detect a problem with the Tomotherapy TPS. After finding a dose difference of 4 % between the Accuray TPS (Precision) and Moderato for a breast case, the deviation was attributed to a ring artifact present only on large reconstruction diameters on our CT-scanner, resulting to an overestimation of the attenuation of the beam. This effect could be corrected by modifying the IVDT (image value to density table) in the TPS (see the results section of the appendix for more details).

However, using the platform as an initial or periodic verification system for other departments would require modelling new accelerators in a fast and simple way. Modelling an entirely new device inevitably takes a considerable amount of time: the geometry has to be constructed from schematics (when these are available) and the beam parameters (energy spectrum, spatial distribution) need to be optimized. This process might have to be repeated several times if simulated results do not match with measurements.

On the other hand, the modelling of an accelerator for which a Monte Carlo model has already been built in another department could be simplified: if the geometry is assumed to be the same, only the electron beam parameters are left to be determined. With some additional assumptions on the form and range of values of these parameters, a correlation could be established between those and the dose measurements performed in a commissioning procedure. This is the subject of the next chapter: assuming the geometry of an accelerator is known, a machine learning method will be introduced to predict electron beam parameters based on dose measurements.

After validation of such a method, it would be possible to quickly integrate a new accelerator model in the platform, validate it from dose curve measurements and simple phantom geometries, and start performing plan recalculations on the patients treated in that specific department.

5. Integration of the M6 Cyberknife in the *Moderato* Monte Carlo platform and prediction of beam parameters using machine learning

5.1. Aim

As introduced in section 2.3, the M6 Cyberknife system was installed at Centre Oscar Lambret in 2017. Its main novelty is the addition of a third treatment head equipped with an MLC (the *Incise2*) allowing to treat larger targets than the fixed and iris collimators.

A new Monte Carlo model thus had to be built in EGSnrc (the primary part of the treatment head was modified from the VSI version modelled in chapter 3). This modelling constitutes the first part of the article introduced in the next section: the process is similar as previously described for the fixed and iris collimator, except a component module of the type MLCE is used, and five selected rectangular beam sizes are simulated in order to validate the model (the number of possible beam sizes and shapes being infinite).

After being validated from the dose curves correspondence, the M6 model is integrated in Moderato in the second part of the paper, and patient plans are re-calculated for different indications. Delivered doses to targets and OARs are compared to assess the agreement between dose algorithms. Film measurements are also performed on complex-shaped beams. This allows validating the MC model as well as evaluating the accuracy of the two algorithms available in the TPS (FSPB and AMC).

Finally, the third part of the article introduces a new machine learning method to predict electron beam parameters from measured dose curves for an accelerator for which the geometry is already known. This feature is of particular interest for the development of Moderato, which design is focused on easily integrating new machines. As two instances of the same accelerator may have significantly different beam energies and spot sizes, considerable time gain could be obtained by predicting these parameters from measured dose profiles and PDDs (as these data are available from the commissioning of the device).

As machine learning has a very broad range of applications that fall outside of the scope of the present study, the choice was made to exclude it from the description of the tools realised in chapter 2. However, in order to provide better understanding of the method

used in the following article, we give a brief description of the concept of machine learning in the next section.

5.2. Machine learning : principle

Machine learning is a subdomain of artificial intelligence, where an algorithm is "trained" to perform predictions from specific input data. Many different types of machine learning exist, and we will limit ourselves here to briefly describing the principle of regression algorithms, which are part of the supervised learning methods.

Supervised learning refers to the methods where the algorithm is trained on examples of input/output pairs, and then asked to predict output resulting from new input data. The goal of a *regression* algorithm is to predict a continuous number (as opposed to *classification* algorithms that aim to label data according to a defined list of classes). More specifically, in the article below we use a linear regression model called the *Ridge* regression.

Linear regression follows the general prediction formula [88]:

$$\hat{y} = w[0] * x[0] + w[1] * x[1] + \cdots + w[p] * x[p] + b$$

where $x[i]$ denote the features, $w[i]$ and b are model parameters (that will need to be optimised), and $\hat{y}$ is the prediction of the model. Intuitively, this equation indicates that the predicted outcome $\hat{y}$ is a weighted sum (with weights $w[i]$) of the input features $x[i]$ and offset b.

In the simplest form of linear regression (also called ordinary least squares) the algorithm searches for the $w[i]$ and b that minimize the mean squared error between the prediction $\hat{y}$ and the actual output values y from the training set.

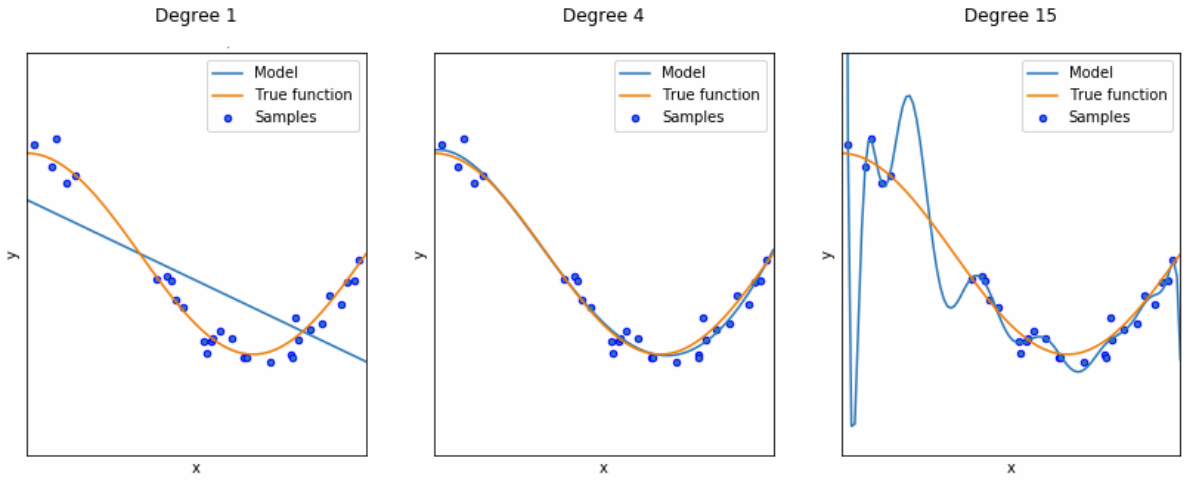

Figure 35. Illustration of the concept of under- and overfitting for a regression algorithm. Experimental samples following a cosine function (denoted "true function" on the graph) are fitted with different polynomial models. The degree 1 (left) corresponds to a simple linear regression which fits poorly with the true function, showing an example of *underfitting*. On the other hand, the degree 15 model *overfits* the data, building a function that is strongly influenced by the noise in the samples (right). The degree 4 model appears as the best choice in this particular case (example from *scikit-learn.org*).

The Ridge regression algorithm is a linear regression where the coefficients $w[i]$ are constrained to be as small as possible. This regularization process is introduced to avoid overfitting, which means building a model that closely fits the training set, but generalizes poorly to new input data (see Figure 35). An additional parameter called alpha is introduced to control the constraint applied to the coefficients $w[i]$: the higher the alpha, the more the coefficients are constrained toward zero, and vice versa.

5.3. Article

This work has been accepted for publication in *Physica Medica* (*European Journal of Medical Physics)* in January 2020.

Integration of the M6 Cyberknife in the *Moderato* Monte Carlo platform and prediction of beam parameters using machine learning

A. Wagner[1,2], K. Brou Boni[1], E. Rault[1], F. Crop[1], T. Lacornerie[1], D. Van Gestel[2,3], N. Reynaert[1,2,4]

1: Department of Medical Physics, Centre Oscar Lambret, Lille, France

2: Faculty of Biomedical Sciences, University of Brussels ULB, Belgium

3: Department of Radiation Therapy, Institut Jules Bordet, Brussels, Belgium

4: Department of Medical Physics, Institut Jules Bordet, Brussels, Belgium

Abstract

Purpose: This work describes the integration of the M6 Cyberknife in the *Moderato* Monte Carlo platform, and introduces a machine learning method to accelerate the modelling of a linac.

Methods: The MLC-equipped M6 Cyberknife was modelled and integrated in *Moderat*o, our in-house platform offering independent verification of radiotherapy dose distributions. The model was validated by comparing TPS dose distributions with *Moderato* and by film measurements. Using this model, a machine learning algorithm was trained to find electron beam parameters for other M6 devices, by simulating dose curves with varying spot size and energy. The algorithm was optimised using cross-validation and tested with measurements from other institutions equipped with a M6 Cyberknife.

Results: Optimal agreement in the Monte Carlo model was reached for a monoenergetic electron beam of 6.75 MeV with Gaussian spatial distribution of 2.4 mm FWHM. Clinical plan dose distributions from Moderato agreed within 2% with the TPS, and film measurements confirmed the accuracy of the model. Cross-validation of the prediction algorithm produced mean absolute errors of 0.1 MeV and 0.3 mm for beam energy and spot size respectively. Prediction-based simulated dose curves for other centres agreed within 3% with measurements, except for one device where differences up to 6% were detected.

Conclusions: The M6 Cyberknife was integrated in *Moderato* and validated through dose re-calculations and film measurements. The prediction algorithm was successfully applied to obtain electron beam parameters for other M6 devices. This method would prove useful to speed up modelling of new machines in Monte Carlo systems.

Keywords: Cyberknife, treatment planning, Monte Carlo, machine learning

Introduction

Cancer treatment and radiation therapy in particular are evolving towards individualization. Delivery techniques have become more diverse and complex over the years, and stereotactic radiotherapy now plays a major role among the therapeutic options. In this context, the essential aspect of dose verification is becoming increasingly critical, as delivered dose is more difficult to measure for these techniques, whereas uncertainties and errors present a higher risk in hypofractionated schemes. Besides patient safety and treatment quality, the accuracy of delivered dose assessment is also essential in the development of rapid learning and clinical-decision support systems (CDSS) [1]. The aim of such systems is to continuously learn and adapt therapeutic strategies based on a variety of patient data, among which the dose to the tumor and normal tissues. In this prospect, assuming the delivered dose is equal to the dose calculated by the Treatment Planning Station (TPS), regardless of the numerous sources of uncertainty that might affect its value, would likely degrade the conclusions and introduce bias that could not be detected [2].

The Moderato platform was introduced in a previous publication [3]. It is an independent treatment QA platform offering dose re-calculation for complex radiotherapy delivery techniques with Monte Carlo. The system is currently in an early commercialization phase. An effort has been put into the automation and ease-of-use of the platform: the necessary files coming from the TPS are automatically imported and converted to be used in the Monte Carlo code, and results can be visualized in a Graphical User Interface (GUI) in the form of dose distributions and Dose-Volume Histograms (DVH). An evaluation module introduced in [4] was also implemented, and allows generating dose constraints to the organs-at-risk (OAR) based on the literature and the fractionation scheme selected for a specific patient. The user evaluates the plan using visual warnings with a color code that highlights dose constraints violations to the organs, either in the TPS-planned dose or in Monte Carlo calculated distribution of Moderato. The Tomotherapy (Accuray) and the VSI Cyberknife (Accuray, earlier model released before the M6) installed at our institution were modelled and integrated in the platform. The Monte Carlo code selected for these devices was BEAMnrc/DOSXYZnrc [5,6] (although other codes can be used in Moderato). The use of phase-space files and approximation techniques allowed to speed up the simulations substantially, down to a re-calculation time between 15 and 45 minutes.

The latest version of the Cyberknife, the M6, includes a multi-leaf collimator (MLC) besides the 12 circular collimators (5 to 60 mm) integrated in the previous version [7]. The MLC is mounted on the robot as an interchangeable accessory, thus making all targeting and tracking options identical to circular collimators, while increasing the maximum field size to 115x100 mm and allowing to treat larger targets and reduce treatment time.

Two distinct dose calculation algorithms are available in the TPS provided by the manufacturer (Precision, Accuray). The Finite-Size Pencil Beam (FSPB) [8] utilizes stored pencil kernels formed from the difference of two exponential functions. Lateral scatter correction can be included as an option. The second algorithm is simply called “Monte Carlo” in the TPS, and will be named AMC (Accuray Monte Carlo) throughout this paper to avoid confusion. It is based on the MCDOSE algorithm [9] and relies on a virtual source model generated during commissioning of the accelerator [10].

The first objective of this study is the Monte Carlo modelling of the MLC of the M6 Cyberknife device, and its validation through patient plan recalculations and film measurements.

One of the purposes of the Moderato platform is the integration of many medical accelerators from different institutions. This requires modelling several devices of the same model, e.g. the M6 Cyberknife machines installed in different centres. The process of optimizing a Monte Carlo model may require a significant amount of time. The search for the optimal electron beam spot size and energy involves repetitive actions based on the knowledge of the qualitative impact of these parameters on the dose curves, which can take a variable amount of time depending on the amount of information available to the user from the constructor, the simulation time, and the experience.

Several studies have been performed on the determination of electron beam parameters in Monte Carlo models for conventional linacs. Pena et al. [11] used cost functions to compare simulated and measured lateral profiles and depth dose curves in an iterative process. Conneely et al. [12] also used simulated data to search for the optimal beam parameters by comparing wide field profiles and output factors.

In the last part of this paper, a method is devised with the aim of accelerating and simplifying this step to avoid the necessity of an "expert" having to optimize the Monte Carlo model for each different centre involved. The method was created from the M6 model and tested on other M6 devices, and is based on simple dose measurements (performed during the commissioning of the accelerator) and a machine learning algorithm.

Materials and methods

M6 Monte Carlo modelling

The M6 Cyberknife (Accuray, Sunnyvale, CA) is a stereotactic radiotherapy device composed of a flattening filter-free 6 MV treatment head mounted on a robot with 6 axes of rotation. Three different heads can be attached to the robot, namely the fixed, iris and MLC head. There are 12 circular collimators for the fixed and iris heads, ranging from 5 to 60 mm diameter at isocentre. Fixed collimators are rarely used as they do not allow variable field size during the treatment session, resulting in significantly longer fraction times. However the fixed 60 mm beam remains the reference field in relation to which all output factors are calculated.

The Incise2 MLC [7] constitutes one of the novelties introduced in the M6 model. It consists of two banks of 26 leaves with 3.85 mm width at 800 mm source-axis distance, 90 mm height and a maximum treatment field size of 115 x 100 mm. The leaves are focused to the direction of the target, after which the whole bank is tilted by 0.5° to reduce interleaf leakage.

The modelling was based on values of off-axis ratios (at source-skin distance SSD = 80 cm and 1.5 cm depth), PDDs and output factors measured in a water phantom during the commissioning of the device with a 60008 diode and a PTW 31014 pinpoint chamber (PTW, Freiburg). The linac was modelled with BEAMnrc [13] and the transport in the water phantom with DOSXYZnrc [14]. As the design of the primary part of the treatment head was modified compared to the previous Cyberknife modelled in [15], this part was first modelled

using measurements from the smallest (5 mm) and largest (60 mm) fixed collimators. The MLC was then added as an additional component module (CM) of the type MLCE. Energy thresholds were set at ECUT = 561 keV and PCUT = 10 keV. Finetuning was performed until a satisfactory correspondence was reached between measured and simulated off-axis ratios, PDDs and output factors for five field sizes (115 x 100 mm, 69.3 x 69.2 mm, 30.8 x 30.8 mm, 15.4 x 15.4 mm and 7.6 x 7.7 mm).

Integration of the M6 model in Moderato

To include the accelerator in the Moderato platform, the BEAMnrc model is integrated as a library and particles exiting the collimator are read and transformed to the patient-specific phase-space file [3]. The positions of the nodes, target coordinates and MUs of all beams from a patient plan are retrieved from an xml file (as well as the collimator rotation for the MLC), whereas CT images, structures and doses are imported in Dicom format using the Moderato interface. The CT Hounsfield units (HU) are converted into densities and material composition using CTcreate (BEAMnrc) and an image value to density table (IVDT) obtained with a stoichiometric calibration [16,17]. Absolute calibration was obtained from the Monte Carlo dose for the 60 mm reference field (Gy/primary history), to provide a calibration factor to be multiplied with the number of MUs in the plan.

After integration, the model was tested on patient plans. Dose distributions from both algorithms included in the TPS (Finite-Size Pencil Beam *FSPB* and Accuray Monte Carlo *AMC*) and from *Moderato* were compared for four tumour sites as introduced in Table 1. The AMC algorithm is routinely used for lung Cyberknife treatments in our department, whereas FSPB calculation is performed for all other indications. Calculations were performed with a spatial resolution of 2 mm.

Table 1. Indications, doses, number of beams, and calculation algorithms for the 4 patients evaluated using Moderato.

Indication	Prescribed dose (Gy)	Number of beams	TPS algorithm
Brain	50.4	31	FSPB
Pelvis	20	52	FSPB
Liver (2 targets)	45	45	FSPB
Lung	54	59	AMC

The Precision TPS offers the possibility of creating *peripheral* fields, which consist of narrow beams designed to cover the edges of the target. This particular shape makes it an interesting candidate to test the accuracy of the algorithms using film measurements.

A batch of radiochromic films (Gafchromic EBT3) was calibrated in dose response using red and blue channels [18]. Calibration films were irradiated at doses ranging from 0.25 Gy to 8 Gy. Exposed films were scanned 24 hours after irradiation at 72 dpi in 48bits-RGB transmission mode using an Epson Expression 12000XL. In order to reduce noise in measured

dose distributions, all radiochromic films were scanned 6 times and the median image was computed using the last five scans.

A plan with a single peripheral beam setup was manually created in the Precision TPS (Figure 1) on a phantom consisting of 13 water equivalent plates (PTW RW3, 1 cm thickness) imaged on an Aquilion LB (Toshiba) CT scanner. Dose distributions were calculated using the FSPB and AMC algorithms, with a spatial resolution of 2 mm. The plan was delivered and a planar dose was measured at 4 cm depth using the radiochromic film. Manual matching was performed between the film and the dose planes (applying the same registration to all three dose algorithms). The four 2D dose distributions (FSPB, AMC, Moderato, film) were then evaluated using Verisoft (version 7.2, PTW Freiburg), performing gamma analysis (1%/1 mm and 2%/2mm, local dose) and visual dose profiles comparison.

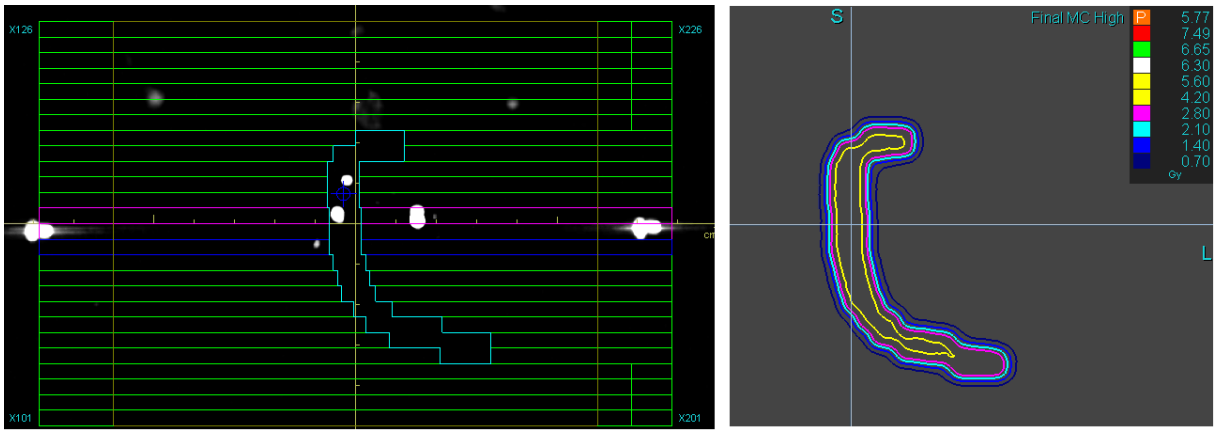

Figure 1. The leaf setup of the MLC field used for dose measurements is displayed on the left, and the resulting isodoses at the measurement plane on the right (calculated with the AMC algorithm).

Electron beam parameters prediction

The principle of the prediction method is based on the following assumption: by feeding a machine learning algorithm with a number of simulated dose data and corresponding electron beam spot sizes and energies of a given accelerator model, one should be able to predict those parameters when being presented with measured data from a new machine of the same model.

To generate the data necessary for the training of the algorithm, a series of 30 simulated dose distributions were obtained for the MLC 115 x 100 mm and fixed 5 mm beams, while varying beam spot size from 1 to 4 mm and energy from 4 to 8 MeV (Table 2), and leaving the geometry unchanged. These values were chosen to span a sufficient range around the "nominal" value of the accelerator: the energy of 6 MeV comes from the vendor specifications, whereas the spot size range was selected based on the value of 1.95 mm for the previously modelled VSI Cyberknife [15] (no spot size value is specified by the manufacturer).

Table 2. Values of electron beam energy and spot size used in the simulations generated for the training step.

Parameter	Energy (MeV)	Spot size (mm)
Values	4.0	1.0
	5.0	2.0
	6.0	2.4
	6.75	3.0
	7.25	4.0
	8.0	

Data preprocessing and the prediction algorithm are performed using the Scikit-learn library [19]. The simulated dose profiles are linearly interpolated and arranged in the form of a list of *N* dose points. Only half the profile in x (leaf travel direction) is used. The PDD at 20 cm depth and the dose ratio at the centre between the fixed 5 mm and the MLC 115 x 100 mm are also used as features (the latter can be viewed as an output factor, with the exception that the 115 x 100 mm beam is used as reference instead of the fixed 60 mm to avoid additional simulations). If $p_{i,j}$ denotes the j-th dose point of the *i*-th dose profile, the input features become:

$$\begin{pmatrix} p_{1,1} & \cdots & p_{1,N} & PDD_1 & OF_1 \\ \vdots & p_{i,j} & \vdots & \vdots & \vdots \\ p_{30,1} & \cdots & p_{30,N} & PDD_{30} & OF_{30} \end{pmatrix}$$

Standardization is applied by centering and scaling independently on each column after computing the relevant statistics on the samples. Every row is associated with one pair, the spot size and energy used in the simulation. A Ridge regression model is fitted with the input features, and once training is completed, the model can be asked to predict a spot size and energy from one dose profile, one PDD_{20cm} and an output factor.

The general principle of the algorithm is represented in Figure 2.

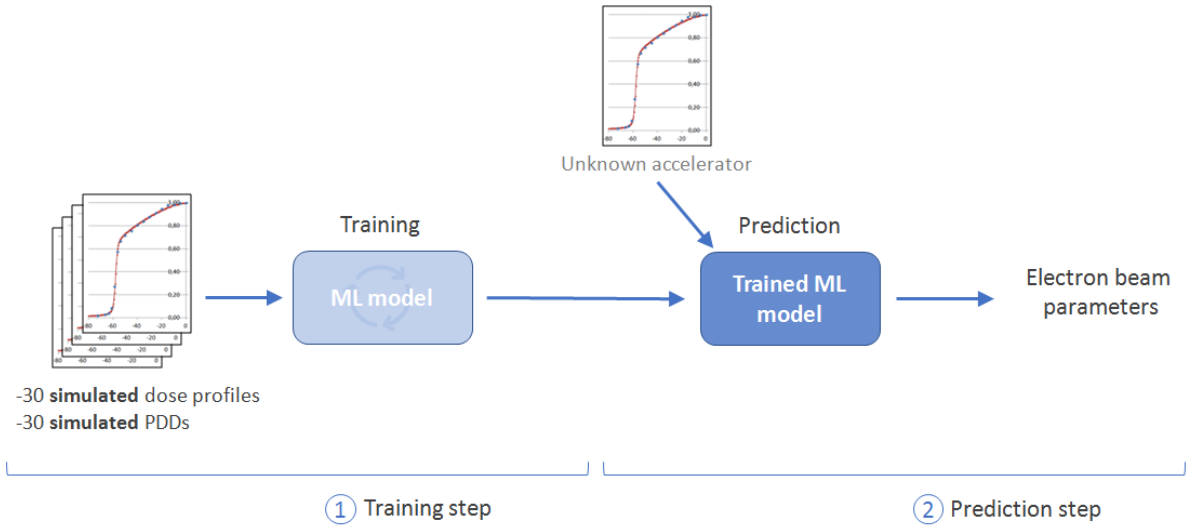

Figure 2. Principle of the ML algorithm designed to predict the electron beam parameters of the MC model.

Before testing the prediction capability of the model on real measured data, the model performance was evaluated using a random permutations cross-validation. Five splits and a

validation size of 0.2 are chosen since it allows a finer control of the proportion of the sample on each side of the train and validation sets. The alpha regularization parameter was optimised over a large range of values. Successive trainings were repeated and the accuracy was assessed using the mean absolute error (MAE) between the predictions and the actual values.

After this evaluation, a new model is trained with all dose curves in order to be tested with the measured profiles and PDDs from five other institutions (named centre #1, 2, 3, 4 and 5 in the rest of this paper) equipped with a M6 Cyberknife. These measured profiles are displayed in Figure 3 for the 115 x 100 mm beam. The data points were preprocessed in the same way as the input training features, applying the same standardization to the dose points (profiles, PDDs and output factors).

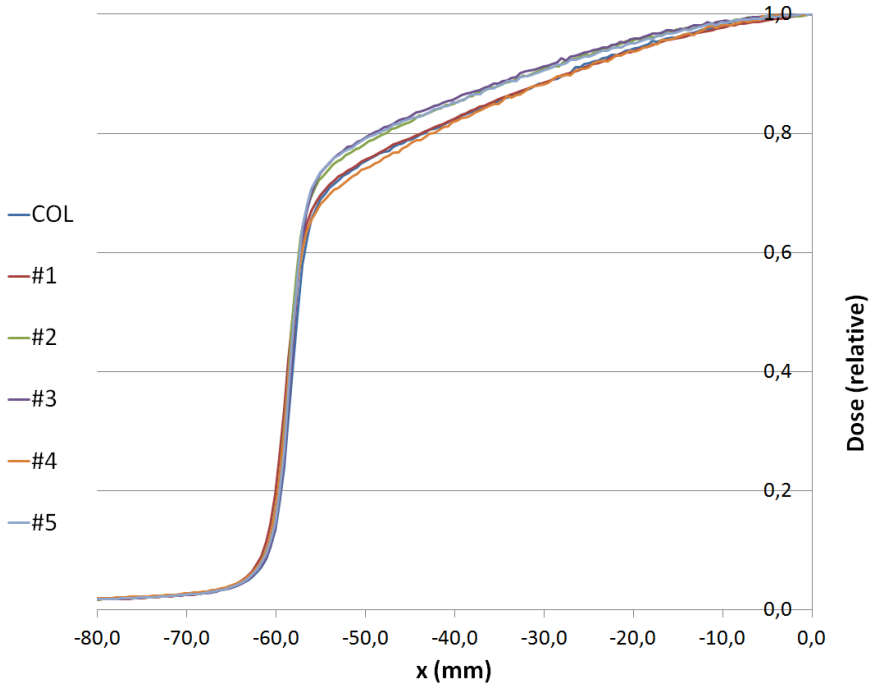

Figure 3. Measured 115x100 mm half profiles from the five M6-equipped departments, after SSD correction for centres #1, 2, 3, and 4.

The spot sizes and energies predicted by the algorithm were then used to create a BEAMnrc model for each of these unknown devices, without any modification to the geometry of the head. Simulations were run for the 115 x 100 mm MLC and the fixed 5 mm beam, and resulting dose profiles were compared with measurements to assess the quality of the predictions. For the fixed 5 mm beam, the diameter of the secondary collimator in the BEAMnrc input file was allowed to be adapted according to this first comparison as its very small size may vary from one model to another due to machining differences.

Results

M6 Monte Carlo modelling

Best agreement was reached using a gaussian monoenergetic electron beam with a spot size of 2.4 mm FWHM, and energy of 6.75 MeV (using a conventional iterative method based on dose curves comparison). Dose profiles (off-axis ratios) and percentage depth doses (PDDs) were compared for 5 different MLC field sizes, and are shown in Figure 4 and Figure 5 for the largest (115x100 mm) and smallest (7.6x7.7 mm) commissioned MLC beams.

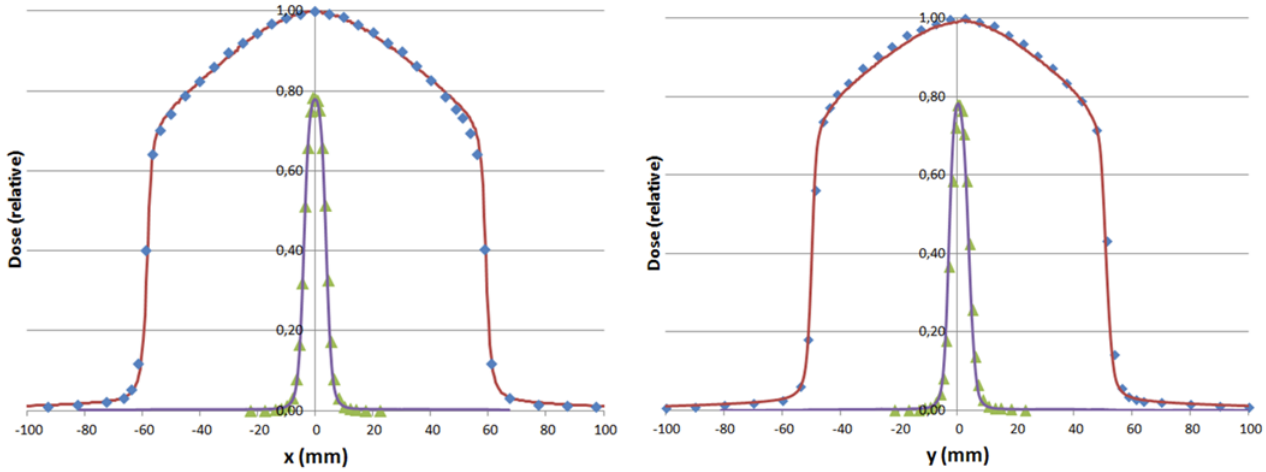

Figure 4. Measured (solid curves) and simulated (symbols) dose profiles for the 115x100 mm and 7.6x7.7 mm field size. The *x* axis corresponds to the leaf travel direction.

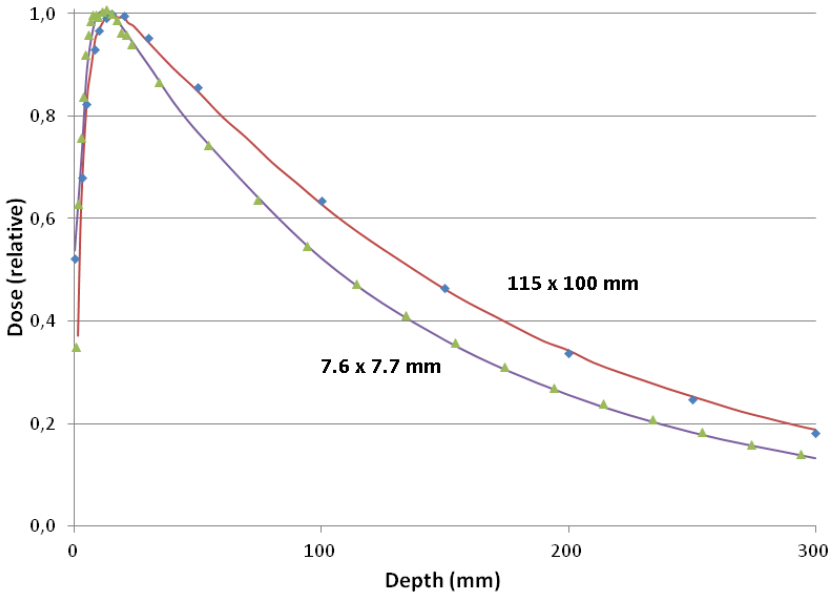

Figure 5. Measured (solid curves) and simulated (symbols) percentage depth dose curves for the 115 x 100 mm and 7.6 x 7.7 mm field sizes.

Simulated output factors were calculated as the ratios of the doses accumulated in a small voxel (which size depended on the beam size) at the centre of the profiles. Measured and simulated output factors were all within 1 % agreement, as shown in Table 3.

Table 3. Measured and simulated output factors for the 60 and 5 mm fixed collimators, and five MLC beam sizes. All OF values are relative to the 60 mm fixed beam, and percentages of deviation are given with respect to the measured values.

Field size	Measured	Simulated	Deviation (%)
Fixed 60 mm	1	1	-
Fixed 5 mm	0.653	0.654	0.15
MLC 115 x 100 mm	1.028	1.023	-0.49
MLC 69.2 x 69.3 mm	1.013	1.017	0.39
MLC 30.8 x 30.8 mm	0.986	0.984	-0.20
MLC 15.4 x 15.4 mm	0.986	0.987	0.10
MLC 7.6 x 7.7 mm	0.803	0.804	0.12

Integration of the M6 model in Moderato

Re-calculation of patient plans showed excellent agreement between algorithms. Table 4 displays the deviations in terms of median, near maximum and near minimum doses to the targets (GTV, CTV, PTV) for each of the four plans.

Table 4. Dose differences between algorithms after re-calculation in Moderato. Deviations are given in percentages as ($1-D_{TPS}/D_{Mod}$) where D_{Mod} and D_{TPS} are the median doses ($D_{50\%}$), dose near-max ($D_{2\%}$) and dose near-min ($D_{98\%}$) obtained in Moderato and the TPS (FSPB or AMC).

Indication	GTV (%)			CTV (%)			PTV (%)			TPS algorithm
	$D_{50\%}$	$D_{2\%}$	$D_{98\%}$	$D_{50\%}$	$D_{2\%}$	$D_{98\%}$	$D_{50\%}$	$D_{2\%}$	$D_{98\%}$	
Brain	-0.6	0.8	0	0	2.2	0	0.4	2.2	0	FSPB
Pelvis				-1.5	2.2	-0.5	-1.4	1.8	-1.0	FSPB
Liver (1st target)	0.4	0.6	0.2	0.4	0.8	0	0.8	0.8	-1.2	FSPB
Liver (2nd target)	-1.0	-1.1	-2.1	-1.2	-1.0	-1.3	-1.4	-1.1	-1.6	FSPB
Lung	0.7	-1.6	2.1				1.1	0.4	0.4	AMC

The dose results from the Moderato interface for the liver and lung cases are given in Figure 6 and Figure 7.

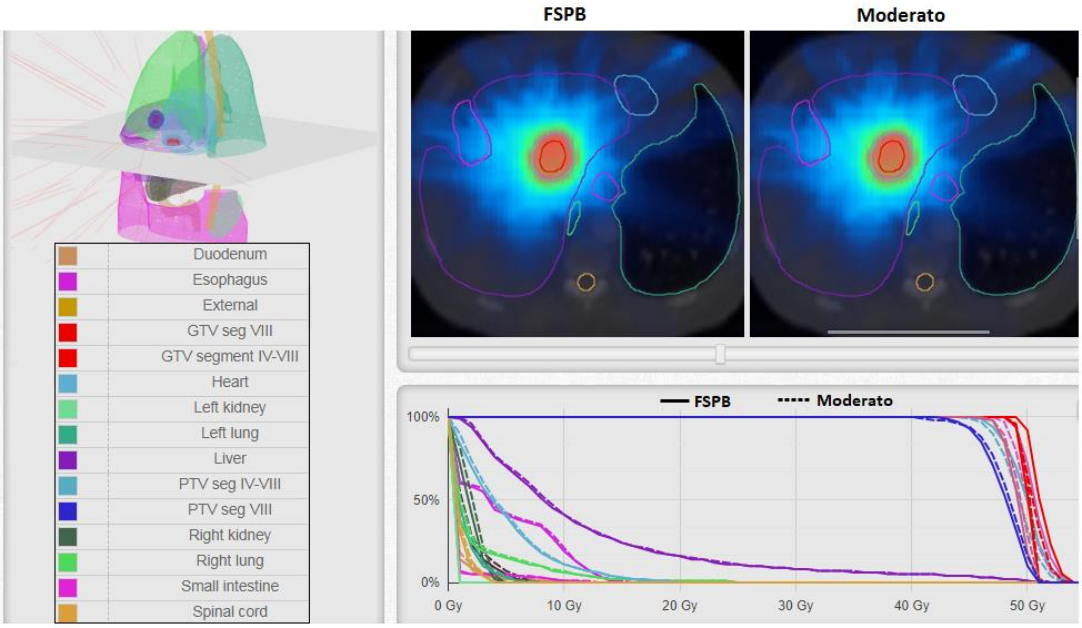

Figure 6. Dose volume histograms for the liver case re-calculated in Moderato, showing good correspondence between the FSPB algorithm (solid line) and Moderato (dashed line).

A very close correspondence was found for all organs-at-risk. Regarding the targets, the PTV in segment IV-VIII of the liver showed a slightly higher difference (-1.4 %, see Table 4), likely due to its location close to the lung and the inherent limitations of the FSPB algorithm for such interfaces. It is worth noting that all cases planned with FSPB are routinely re-calculated using AMC algorithm for comparison purposes.

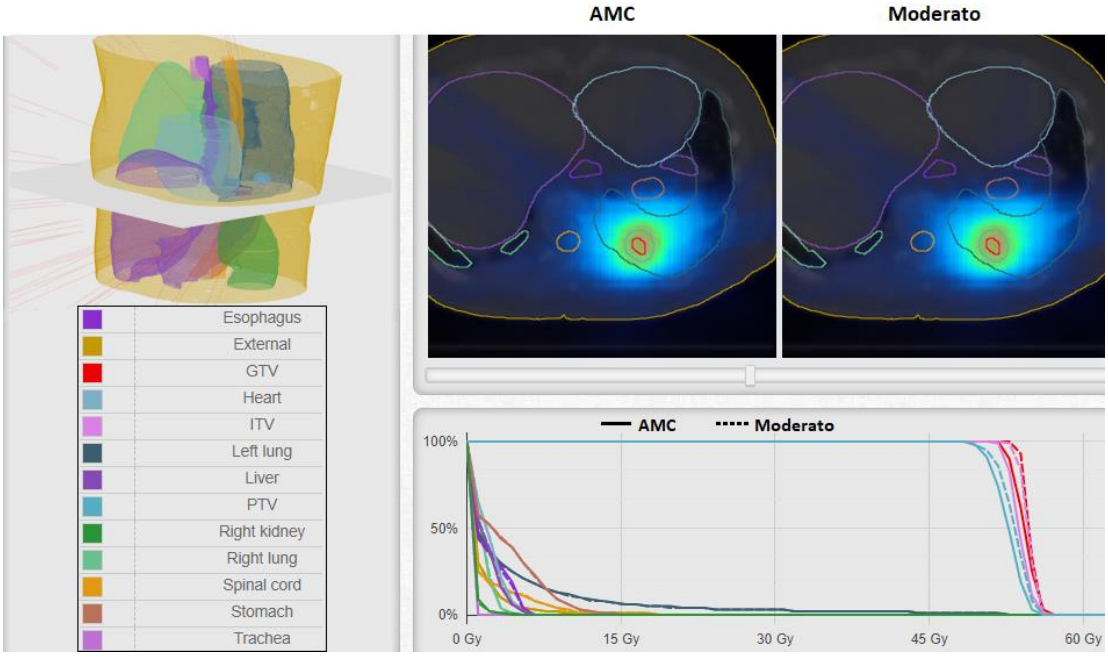

Figure 7. Dose volume histograms for the lung case re-calculated in Moderato, showing good correspondence between the AMC algorithm (solid line) and Moderato (dashed line).

The lung case results are characterized by less than 1 % deviation to the GTV median doses. A slightly higher difference was noted for the PTV (1.13 %), while remaining largely acceptable.

Gamma analysis for the single beam film measurements described in the methods section is shown in Table 5. Dose points under 10 % of the maximum dose were excluded (this threshold is routinely used for plan quality assurance in our department). Thresholds of 1%/1mm and 2%/2mm were applied. The FSPB algorithm exhibits a lower passing rate than the Monte Carlo methods. The AMC is slightly superior to Moderato, with both algorithms showing passing rates of 94 % or more.

Table 5. 3D gamma analysis of the planar measured dose with respect to the three algorithms, with thresholds of 1%/1mm and 2%/2mm. Dose points under 10 % of the maximum dose were excluded.

Algorithm	3D Gamma 1%/1mm	3D Gamma 2%/2mm
FSPB	88.1	92.2
AMC	97.4	99.9
Moderato	94.6	99.4

Dose profiles were taken for visual evaluation of the differences between the algorithms and the measurements, and are shown in Figure 8 and Figure 9. A similar trend as the one suggested by the gamma analysis can be observed, with the two Monte Carlo algorithms significantly outperforming the FSPB, and a slightly better correspondence for the AMC over Moderato.

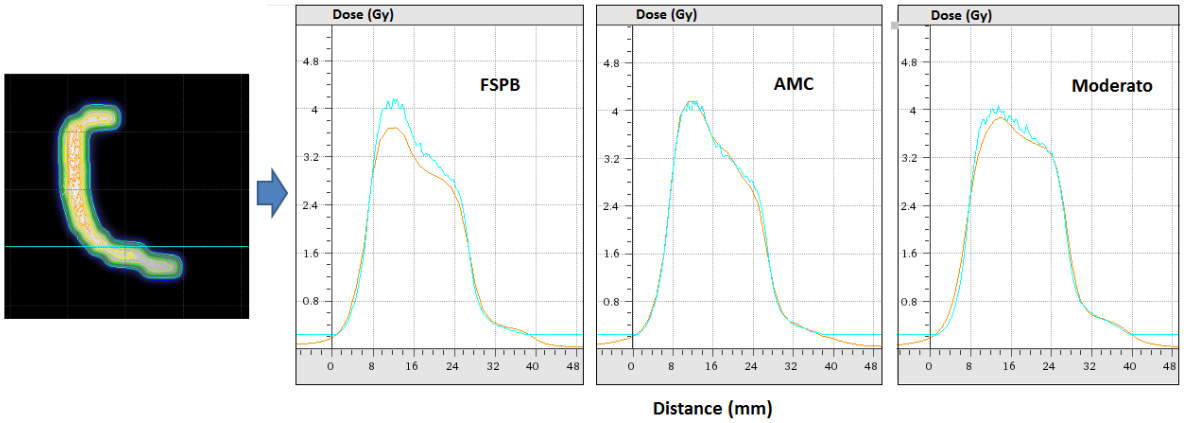

Figure 8. Dose profile in the leaf travel direction (x) : the film dose is shown in blue, and the dose calculated with each of the three algorithms in orange.

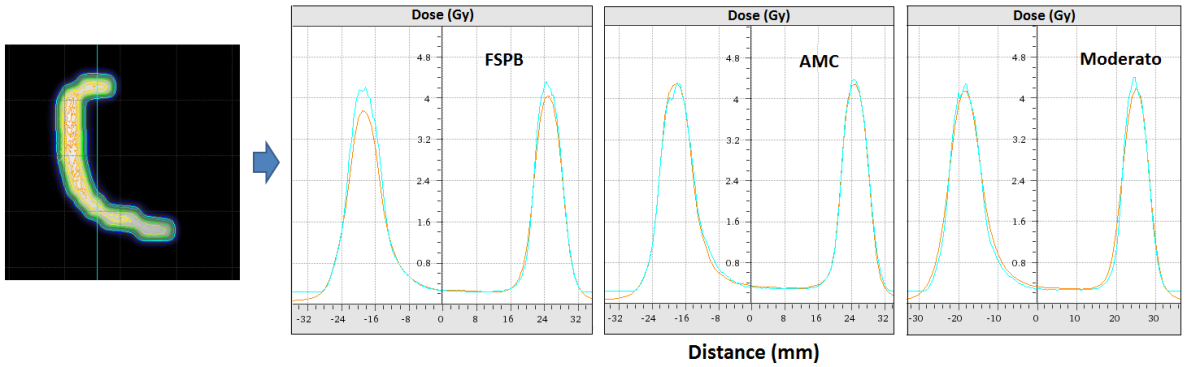

Figure 9. Dose profile in the direction perpendicular to the leaf travel direction (y) : the film dose is shown in blue, and the dose calculated with each of the three algorithms in orange.

Electron beam parameters prediction

The portion of the 115 x 100 mm dose profile included in the training appeared to have a strong influence on the results: the optimal choice was a range of -50 mm to the origin, thus excluding the penumbra area (Figure 10, right). One dose point was included every 0.5 mm. The optimal alpha parameter is found at each iteration by use of the RidgeCV method (Ridge regression with built-in cross-validation).

```
-------------------Exp. 4------------------

Test set = [4. 8. 6.]
Solutions = [3.8847319  7.79797874 6.075976  ]

 alpha =  0.17911536074332265

 R2 score :  0.9925160405874605
 MAE of E :  0.13108845206896058
```

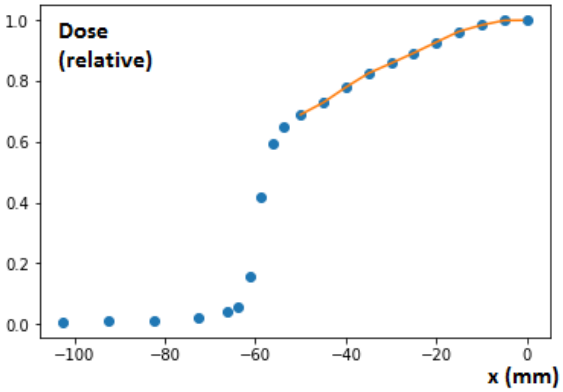

Figure 10. Left: Illustration of the optimization of the machine learning algorithm. Three energy values are sampled as the test set (4, 8 and 6 MeV), and the other values are used as the training set. The solutions are displayed on the lines below, as well as the alpha parameters, the R2 score and the MAE of the energy.

Right: Portion of the 115 x 100 mm crossplane profile included in the training algorithm (orange line).

The optimization through 5 splits (see example on the left of Figure 10) allowed bringing the MAE of the spot size and energy down to 0.3 mm and 0.1 MeV respectively. These values were deemed small enough to test the algorithm on real measured data.

The prediction results from the measurements of the five other M6-equipped institutions are displayed in Table 6. The algorithm execution takes less than 30 seconds to complete (including the training and prediction on the unknown series).

Table 6. Predicted electron beam spot sizes and energies for the five "unknown" M6 devices.

Institution	Predicted spot size (mm)	Predicted energy (MeV)
#1	2.6	7.2
#2	1.8	6.8
#3	2.1	6.5
#4	2.7	6.7
#5	2.0	6.5

The results from the 115 x 100 mm BEAMnrc simulations using the predicted parameters can be found in Figure 11. All devices show deviations of less than 3 % between measured and prediction-simulated profiles, except for centre #1 where the match is somewhat less accurate (up to 6 % in the "shoulder" region). This will be discussed in the next section.

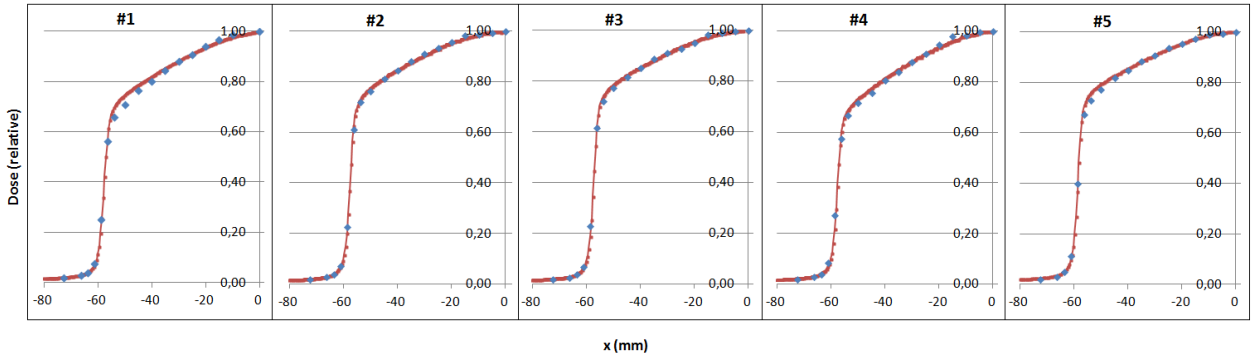

Figure 11. Comparison between 115 x 100 mm measured (red lines) and simulated profiles generated from predicted electron beam parameters (blue dots).

The results for the 5 mm fixed collimator are shown in Figure 12. The simulations for centres #1, 3 and 4 were restarted after correcting the size of the secondary collimator in the BEAMnrc geometry (to account for small machining differences), while for centres #2 and 5 no changes had to be made.

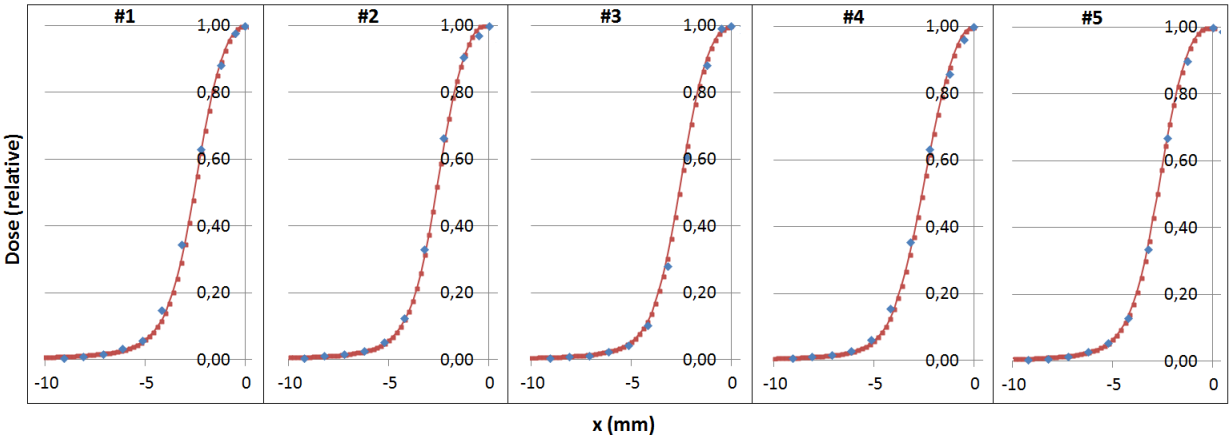

Figure 12. Comparison between fixed 5 mm measured (red lines) and simulated profiles generated from predicted electron beam parameters (blue dots).

Similar results were found for the inplane dose profiles for the 115 x 100 mm and the PDD curves for both fields (not shown).

Discussion

In the first part of this study, a model was built using BEAMnrc/DOSXYZnrc for the *Incise2* MLC of the M6 Cyberknife. Good agreement was obtained in terms of dose profiles, PDDs and output factors (within 1 % for all simulated MLC field sizes). The value of the energy in our model (6.75 MeV) is significantly higher than its nominal value of 6 MeV, but remains lower than the 7 MeV of our previous electron beam model for the VSI version of the Cyberknife [15]. This is also consistent with the results of Mackeprang et al. [20] who obtained an energy of 6.8 MeV for their M6 model. Regarding the spot size, the same authors obtained a value of 3.0 mm FWHM, to be compared with 2.4 mm for our model. This difference between devices of the same model highlights the potential interest of the beam parameters optimization method developed in the last part of the present study.

Four patient plans were re-calculated in Moderato to test the typical indications treated with the M6 Cyberknife. The results suggest that Moderato can now be used as a dose verification system for the Cyberknife M6 plans, in view of the good dose agreement for targets and organs-at-risk.

Before starting the treatment of a patient with the M6 Cyberknife, a Delivery Quality Assurance (DQA) is realized, consisting in delivering the beams to a phantom with a measurement device, usually films or a 2D array of ionization chambers. This provides an end-to-end test of the whole treatment. However, such procedures tend to hide small algorithm-related dose differences due to the superposition of a great number of beams. Besides, 2D arrays are sensitive to the angle of incidence of the beams, introducing another source of error that further increases the difficulty in detecting small deviations. For these reasons, the choice was made to focus on a single beam setup and on film measurements in the present study, while trying to create a challenging shape for the dose algorithm. The results show that for such complex beams, a simple algorithm such as FSPB might exhibit significant differences compared to more accurate methods, even in simple homogeneous geometries. This suggests that the use of the AMC algorithm should be encouraged when preparing MLC plans with the M6. The algorithm was tested and validated by several other groups: Heidorn et al. [21] performed radiochromic film measurements in a heterogeneous slab phantom, and Mackeprang et al. [22] benchmarked AMC against their Monte Carlo model introduced in [20].

Both AMC and Moderato demonstrated excellent agreement with the film measurements, with AMC performing slightly better than Moderato. These small differences are however unlikely to have a strong impact on patient plans, where beam superposition would tend to smooth them out, and where inhomogeneities might constitute a greater source of differences.

The machine learning method introduced in the last section of this work allowed generating predictions of electron beam parameters based on simple dose curves measurements. The first step of the method (the generation of a number of simulated profiles with varying electron beam characteristics) is a long process, but does not require extensive user interaction. The training and prediction steps are then completed in a few seconds. This method has the advantage of reducing the optimization time for a new device to a minimum (as well as the necessity of an expert), at the cost of a large number of simulations at the stage of the first modelling.

Provided the geometry of the accelerator is known, the algorithm was able to determine energy and spot size, which accuracy was verified by running new simulations based on the predicted values. Indeed, while significant differences are present in the 115 x 100 mm dose profiles for the five sites (Figure 3), the results from Figure 11 demonstrate that the algorithm was able to fit those profiles nonetheless.

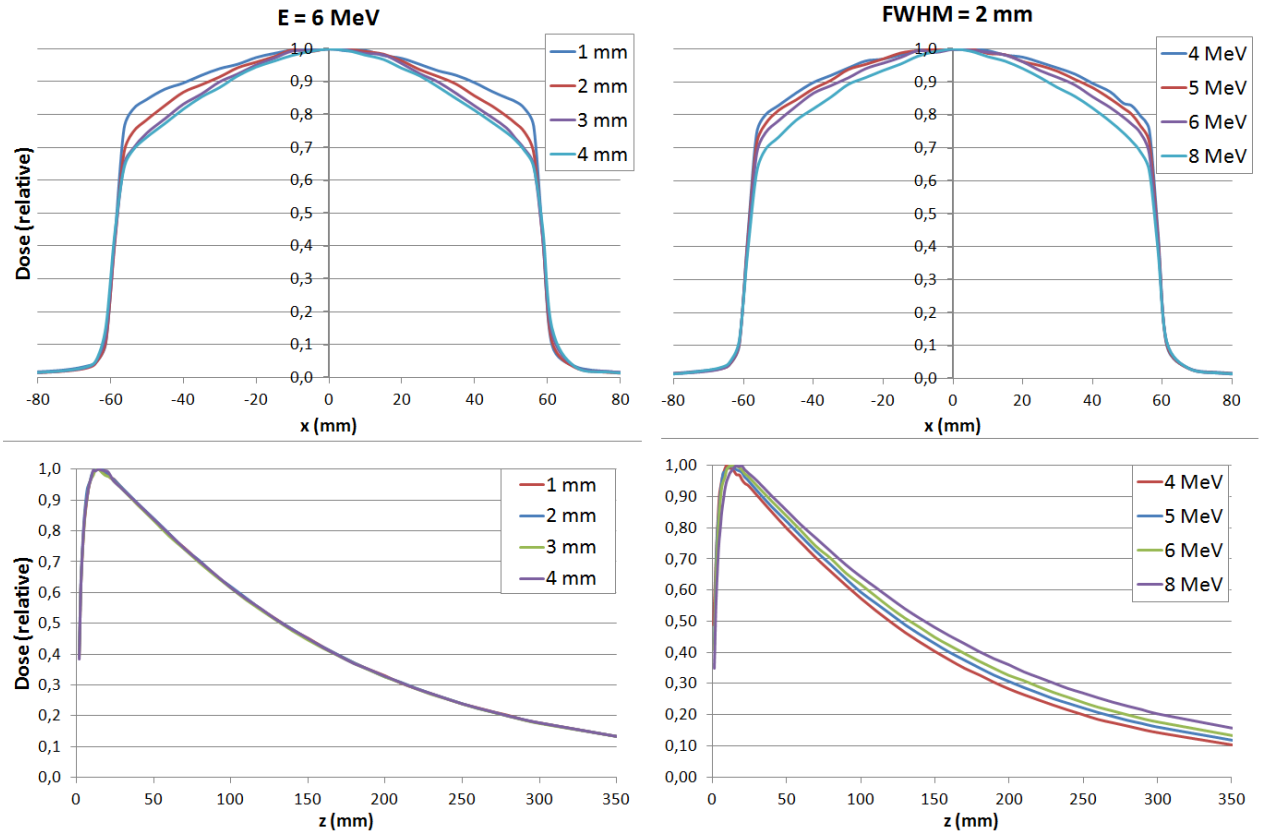

Figure 13. Dose profiles and PDDs simulated for the 115x100 mm beam, for a fixed energy of 6 MeV and a variable spot size (left), and a fixed spot size of 2 mm with a variable energy (right), illustrating the influence of the electron beam parameters on the simulated dose curves.

To further illustrate the relevance of this prediction, simulated dose profiles and PDDs are included in Figure 13 for the 115 x 100 mm beam, for a fixed energy and variable spot size, and vice versa. Both spot size and energy have a significant effect on the shape of the dose profiles, which can not be separated by any simple method. These variations show the sensitivity of the dose curves to the beam parameters, reflecting the value of their prediction from measurements.

The energy and spot size values used in the simulations were simply chosen to span a range around the "standard" values obtained in linac models, and more specifically in our two Cyberknife models (E = 7 MeV and FWHM = 1.95 mm for the VSI [15]; E = 6.75 MeV and FWHM = 2.4 mm for the M6). It is likely that adding more values inside and outside that range would provide more accurate results. During the cross-validation step, it appeared that test values close to the end of the range were predicted with less accuracy, as is illustrated in Figure 14.

```
-------------------Exp. 3------------------

Test set = [20. 40.]
Solutions = [20.9129749  32.40644472]

 alpha =  1.1686088553466496

 R2 score :  0.7075219750070794
 MAE of sp :  4.253265091347004
```

Figure 14. Example of a test set consisting of two spot sizes of 2.0 and 4.0 mm (values were entered as tenths of mm in the algorithm). The predictions are in the "Solutions" line below: the 2.0 mm spot size is predicted with an error below 0.1 mm, whereas a much larger error is associated with the 4.0 mm spot size, thus increasing the MAE significantly (last line).

The mean absolute error was significantly increased by these "outliers" during cross-validation. This however did not seem to degrade the predictions on real measured data, as these were farther from the end of the ranges.

As briefly mentioned in the results section, the prediction-based simulated curves for the 115 x 100 mm beam (Figure 11) presented a slightly poorer agreement in the case of centre #1, with differences up to 6 % between measured and simulated dose profiles. This was investigated and might be due to the fact that the full 115 x 100 mm profile presents a pronounced asymmetry, as can be seen from Figure 15.

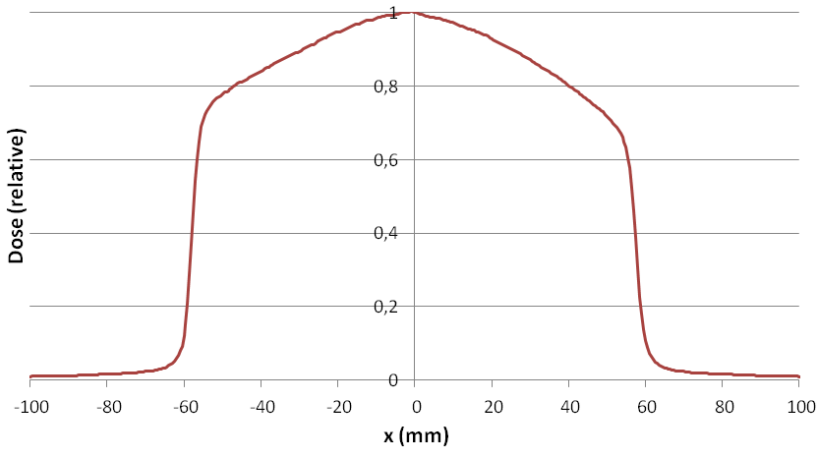

Figure 15. Off-axis ratio measurements in the leaf travel direction (x) for the M6 Cyberknife of centre #1, where an asymmetry can be observed.

The method presented above takes a half profile as input, which is in this case was an average of the negative and positives parts of the curve (this is also the standard procedure to generate beam data at commissioning stage for the Cyberknife). Our approach thus assumes that dose profiles are close to symmetric. Modelling asymmetry would require modifying characteristics of the source not included in our method, i.e. introducing an angle of incidence for the electron beam.

This proof of concept opens interesting perspectives in the modelling of linear accelerators, especially for the development of Monte Carlo dose verification platforms such as Moderato. The ability to quickly obtain values for the electron beam characteristics would allow significant time gain and spare the necessity of an experienced used when adding new

machines in the system. Investigations are currently underway to transfer this method to other devices.

Conclusions

In summary, the MLC-based M6 Cyberknife was successfully modelled in BEAMnrc and integrated in the *Moderato* platform. Patient plans were re-calculated for different indications and dose algorithms, showing excellent agreement with the results from the TPS. Film measurements confirmed the accuracy of Moderato and AMC for a complex field shape, where the FSPB algorithm proved somewhat less accurate, suggesting AMC should be used when calculating MLC plans, at least as a verification tool. The ML algorithm was developed using cross-validation and applied on a test set to validate the concept of predicting electron beam parameters from profile data. The measurements from other M6 devices could be matched using Monte Carlo simulations generated with predicted spot sizes and energies from the algorithm. This would allow to significantly speed up the integration of new accelerators in Monte Carlo-based verification platforms.

Acknowledgements

The authors wish to thank the colleagues who kindly agreed to share their data in order to test the prediction model: Sebastian Klüter, Raphaël Moeckli, Christoph Fürweger, Mahmoud Touleimat, Pascal François, Sonia Sobczak and Vincent Marchesi.

Second author is funded by Interreg 2 Seas 2014-2020 program co-financed by the European Development Fund under grant contract n° 2S04-022.

References

[1] Lambin P, Roelofs E, Reymen B, Velazquez ER, Buijsen J, Zegers CML, et al. “Rapid Learning health care in oncology” - An approach towards decision support systems enabling customised radiotherapy. Radiother Oncol 2013;109(1):159–64.

[2] Jaffray DA, Lindsay PE, Brock KK, Deasy JO, Tomé WA. Accurate Accumulation of Dose for Improved Understanding of Radiation Effects in Normal Tissue. Int J Radiat Oncol Biol Phys 2010;76(3 SUPPL.):135–9.

[3] Reynaert N, Demol B, Charoy M, Bouchoucha S, Crop F, Wagner A, et al. Clinical implementation of a Monte Carlo based treatment plan QA platform for validation of Cyberknife and Tomotherapy treatments. Phys Medica 2016;32(10).

[4] Wagner A, Crop F, Mirabel X, Tailly C, Reynaert N. Use of an in-house Monte Carlo platform to assess the clinical impact of algorithm-related dose differences on DVH constraints. Phys Medica 2017.

[5] Kawrakow I. Accurate condensed history Monte Carlo simulation of electron transport. I. EGSnrc, the new EGS4 version. Med Phys 2000;27(3):485–98.

[6] Rogers DWO, Faddegon BA, Ding GX, Ma CM, We J, Mackie TR. BEAM: a Monte Carlo code to simulate radiotherapy treatment units. Med Phys 1995;22(5):503–24.

[7] Asmerom G, Bourne D, Chappelow J, Goggin LM, Heitz R, Jordan P, et al. The design and physical characterization of a multileaf collimator for robotic radiosurgery The

design and physical characterization of a multileaf collimator for robotic radiosurgery. Biomed Phys Eng Express 2016;2.
[8] Jelen U, Söhn M, Alber M. A finite size pencil beam for IMRT dose optimization. Phys Med Biol 2005;50:1747–66.
[9] Ma CM, Li JS, Pawlicki T, Jiang SB, Deng J, Lee MC, et al. A Monte Carlo dose calculation tool for radiotherapy treatment planning. Phys Med Biol 2002;47(10):1671–89.
[10] Ma C, Li J, Deng J. Implementation of Monte Carlo Dose calculation for CyberKnife treatment planning. J Phys Conf Ser 2008;102.
[11] Pena J, González-castaño DM, Gómez F, Sánchez-doblado F. Automatic determination of primary electron beam parameters in Monte Carlo simulation n.d.
[12] Conneely E, Alexander A, Stroian G, Seuntjens J, Foley MJ. An investigation into the use of MMCTP to tune accelerator source parameters and testing its clinical application 2013;14(2):3–14.
[13] Rogers DWO, Walters B, Kawrakow I. BEAMnrc Users Manual. Source 2011;509:1–260.
[14] Walters B, Kawrakow I, Rogers DWO. DOSXYZnrc Users Manual. NRCC Rep PIRS-0794 2016(April):1–125.
[15] Wagner A, Crop F, Lacornerie T, Vandevelde F, Reynaert N. Use of a liquid ionization chamber for stereotactic radiotherapy dosimetry. Phys Med Biol 2013;58(8).
[16] Demol B, Viard R, Reynaert N. Monte carlo calculation based on hydrogen composition of the tissue for MV photon radiotherapy. J Appl Clin Med Phys 2015;16(5):117–30.
[17] Vanderstraeten B, Chin PW, Fix M, Leal A, Mora G, Reynaert N, et al. Conversion of CT numbers into tissue parameters for Monte Carlo dose calculations: a multi-centre study. Phys Med Biol 2007;52(3):539.
[18] Micke A, Lewis DF, Yu X. Multichannel film dosimetry with nonuniformity correction. Med Phys 2011;38(5):2523–34.
[19] Pedregosa F, Weiss R, Brucher M. Scikit-learn : Machine Learning in Python. J Mach Learn Res 2011;12:2825–30.
[20] Mackeprang P, Vuong D, Volken W, Henzen D, Schmidhalter D, Malthaner M, et al. Independent Monte-Carlo dose calculation for MLC based CyberKnife radiotherapy. Phys Med Biol 2018;63.
[21] Heidorn S, Kilby W, Fürweger C. Novel Monte Carlo dose calculation algorithm for robotic radiosurgery with multi leaf collimator : Dosimetric evaluation. Phys Medica 2019;55(October 2018):25–32.
[22] Mackeprang P, Vuong D, Volken W, Henzen D, Schmidhalter D, Malthaner M, et al. Benchmarking Monte-Carlo dose calculation for MLC CyberKnife treatments. Radiat Oncol 2019;14:1–11.

6. General conclusion

Objectives

The continuous individualization of radiation therapy is associated with a progressive shift in the clinical research paradigm: presented as an alternative to the time-consuming randomized trials, the concept of rapid learning consists in the fast exploitation of clinical data to continuously adapt treatment strategies, thus developing a Clinical-Decision Support System (CDSS). As mentioned briefly in the introduction, implementing such a tool requires a considerable effort on the standardization of the outcome and on the quality of the data to avoid introducing uncertainties and errors that would bias the conclusions.

For the medical physicist working in radiation therapy, one of the first steps towards this objective is the accurate reconstruction of the dose delivered to the patient during the course of the treatment, considering the numerous uncertainties that might impact its value, such as accelerator output variations, commissioning uncertainties, dose computation errors, patient and organ movement, etc. In particular, dose deformation and accumulation represent considerable challenges in the quest for an accurate dose reconstruction, as major physical problems appear when considering deformed dose matrices.

The Monte Carlo verification platform *Moderato* is being developed at Centre Oscar Lambret to provide re-calculation of Tomotherapy and Cyberknife treatment plans. The objective of this thesis was to perform the clinical implementation of this platform, with a focus on the Cyberknife device.

Original contributions

The first contribution of this work is the integration of the VSI Cyberknife into Moderato. In order to do this, the device was first modelled using the EGSnrc code and the BEAMnrc/DOSRZnrc suite, based on water phantom measurements performed in our department. The accelerator geometry, electron beam energy and spot size were optimized until reaching an agreement between simulated and measured dose curves. This modelling was first performed for the fixed collimators only, using the component modules available in BEAMnrc. Then, using the egs++ package, we developed a new geometry to model the iris collimator and its two superimposed banks of tungsten

leaves. The VSI Cyberknife model was then integrated into the Moderato system to allow patient plan re-calculations.

Another study concerning the corrections factors to apply to the readings of a liquid ionization chamber was also included. While falling somewhat outside the scope of the Moderato platform, this work however constitutes a contribution to the field of small beam dosimetry, which is a critical aspect of the uncertainties associated with most modern radiation therapy devices. A Monte Carlo model was built for the PTW microLion chamber using the EGS code CScavity, and perturbation factors were calculated for each component of the detector, using the VSI Cyberknife model introduced in the previous paragraph. An experimental study of the recombination effects was also conducted using the two dose rate method. In summary, this study provided a full characterization of this liquid ionization detector, allowing its use for small field measurements.

The next step consisted in the first clinical evaluation of our platform, through the re-calculation of a number of patient plans treated with Cyberknife and Tomotherapy. A prescription module was integrated in Moderato, which automatically provides constraints on organs-at-risk based on the fractionation prescribed and the anatomical region considered. A visual warning system in then displayed below the isodoses and Dose-Volume Histograms, allowing to quickly evaluate constraint violations and discrepancies between TPS algorithms and Monte Carlo.
This study represents a validation of our accelerator models incorporated in Moderato, as well as a first glance at the potential of such a system in the clinical routine and research. Although no ground truth is available when faced with significant dose deviations between algorithms, these differences stress the fact that a high accuracy is necessary to guarantee the quality of the data fed to a rapid learning / CDSS system.

In the final part of our work, the M6 Cyberknife system was also integrated in Moderato. The EGSnrc model had to be optimized once again due to its sensibly different geometry, and the new multi-leaf collimator. After the accelerator was incorporated in the platform, the model was verified using film measurements on complex small beams, as well as patient plans re-calculations.
A new machine learning algorithm was then introduced to predict the electron beam parameters based on simple dose measurements. The creation of this method was motivated by the fact that Moderato is destined to integrate a number of accelerators that might differ in terms of Monte Carlo modelling.
The accuracy of this algorithm was verified on real data provided by other M6-equipped institutions, confirming its potential use for adding new devices to the system.

Perspectives

The integration of the Cyberknife models in Moderato would allow performing systematic re-calculation of patient plans at Centre Oscar Lambret. Considering the very

large amount of data involved, this is pending some intervention of an IT engineer that will be hired in the upcoming months to ensure the full automation and maintenance of the system, as this falls somewhat outside the missions and field of expertise of the medical physicists. This would also allow working on the optimization of the display in the prescription-validation module together with the medical staff to evolve towards a system suitable for routine clinical use.

Moderato allows easily adding new accelerators in its supported models. With the machine learning prediction method, it would be possible to model a device from another department using commissioning measurements, without significant time and input from a Monte Carlo expert. This approach offers interesting perspectives for departments seeking a quick validation of a new technique, or periodic independent dose verification as a quality control.

As introduced in [80] (article in appendix), Moderato already offers the possibility of performing a 4D dose calculation for Cyberknife liver treatments, using the log files containing the positions of the robot and of the external markers and internal fiducials. This is realized by a Monte Carlo calculation on each phase of the 4DCT. After applying dose deformation and accumulation, the delivered dose is displayed on the original planning CT. Although small deviations were detected between planned dose and delivered dose (as liver motion is constrained by an abdominal belt during dose delivery), this constitutes a first step towards delivered dose reconstruction.

Regarding the Tomotherapy machines, a project of dose deformation and accumulation is also under construction. These machines are more suitable for such studies as they demand longer treatment times to deliver the full treatment (generally around 5 to 8 weeks), and anatomical modifications are more likely to occur and impact the delivered dose.
Moderato appears as a suitable tool to perform such evaluation. After importing the MVCT of a delivered fraction in the system, the dose can be re-calculated from the planned sinogram (the programmed leaf openings contained in the RT plan file) or the actual leaf openings from the log files generated during irradiation. Based on a deformable registration (DVFs) between the MVCT image and the planning kVCT, dose can then be deformed and accumulated on the original kVCT.

7. Appendix: description of *Moderato*

Clinical implementation of a Monte Carlo based treatment plan QA platform for validation of Cyberknife and Tomotherapy treatments

N. Reynaert[1], B. Demol[1], M. Charoy[1], S. Bouchoucha[1], F. Crop[1], A. Wagner[1], T. Lacornerie[1], F. Dubus[1], E. Rault[1], P. Comte[1], R. Cayez[1], C. Boydev[1], D. Pasquier[2], X. Mirabel[2], E. Lartigau[2], T. Sarrazin[1]

[1] *Department of medical physics, Centre Oscar Lambret, Lille, France*

[2] *Academic Department of Radiation Oncology, Centre Oscar Lambret, and university Lille 2*

Physica Medica, 2016, 32(10), 1225-1237

Abstract. *Purpose:* The main focus of current paper is the clinical implementation of a Monte Carlo based platform for treatment plan validation for Tomotherapy and Cyberknife, without adding additional tasks to the dosimetry department.

Methods: The Monte Carlo platform consists of C++ classes for the actual functionality and a web based GUI that allows accessing the system using a web browser. Calculations are based on BEAMnrc/DOSXYZnrc and/or GATE and are performed automatically after exporting the dicom data from the treatment planning system. For Cyberknife treatments of moving targets, the log files saved during the treatment (position of robot, internal fiducials and external markers) can be used in combination with the 4D planning CT to reconstruct the actually delivered dose. The Monte Carlo platform is also used for calculation on MRI images, using pseudo-CT conversion.

Results: For Tomotherapy treatments we obtain an excellent agreement (within 2 %) for almost all cases. However, we have been able to detect a problem regarding the CT Hounsfield units definition of the Toshiba Large Bore CT when using a large reconstruction diameter. For Cyberknife treatments we obtain an excellent agreement with the Monte Carlo algorithm of the treatment planning system. For some extreme cases, when treating small lung lesions in low density lung tissue, small differences are obtained due to the different cut-off energy of the secondary electrons.

Conclusions: A Monte Carlo based treatment plan validation tool has successfully been implemented in clinical routine and is used to systematically validate all Cyberknife and Tomotherapy plans.

Keywords. Monte Carlo, QA, treatment planning, delivered dose

Introduction

Currently, radiotherapy treatment plans are often validated using independent monitor unit calculation algorithms [1-4]. In France e.g., there is a legal obligation to apply this QA technique for all treatments when such a calculation is "technically feasible". This leads to a systematic validation of conformal treatments, using a limited number of beams, while the more complicated techniques, such as IMRT, VMAT and SBRT, are not often validated systematically. This is because few commercial tools are available for these techniques, or because the precision of these systems is limited. Furthermore, most monitor unit validation tools only recalculate dose at the isocenter, while for the advanced techniques a more detailed 3D dose distribution is needed, not only focusing on the PTV, but also paying attention to the organs at risk (OARs). Although there are a couple of commercial tools available, providing 3D plan validations, these do not provide a solution for Tomotherapy and Cyberknife.

During the last decades, Monte Carlo codes have become easily available and have been developed for quality control of radiotherapy treatment plans [5-8]. Furthermore, in the last decade, an increasing number of treatment planning systems are using Monte Carlo based algorithms [9,10]. As these algorithms are by nature relatively slow, a number of approximations are applied, sometimes leading to hybrid systems. Especially the beam model is often largely approximated [10]. This is unfortunate as the ability of modeling the beam in detail is the main advantage of a Monte Carlo algorithm, when comparing e.g. to collapsed cone algorithms that already provide an adequate precision for dose calculation within the patient geometry. Because of these approximations it remains important to validate treatment planning systems, with e.g. independent Monte Carlo algorithms using an accurate beam model [11]. The main challenge is not the implementation of such an algorithm but rather the introduction of such a tool in clinical routine. The Monte Carlo platform used in our department is based on our in-house Monte Carlo based dose calculation software MCDE [12]. This system was used at the University of Ghent to validate IMRT plans in different radiotherapy departments [13-15]. In MCDE the program DOSXYZnrc [16] was reprogrammed as a component module for BEAMnrc [17] and a dicom interface was added to translate the RTPlan file to a BEAMnrc input file (all beams were handled in one single input file). This demanded a reprogramming of certain parts of BEAMnrc/DOSXYZnrc. The RTStruct and RTDose files exported from the TPS were also imported in MCDE to allow the application of a statistics-based stop taking into account the statistical noise in all organs of interest [18]. A denoising algorithm was developed [19] and an independent scoring grid was introduced [20] to increase efficiency. The system was used to validate a large number of H&N treatments and was compared to Pinnacle, Helax, AAA and Peregrine [11,13-15]. The main problem of MCDE was that all QA specific modifications were applied inside BEAMnrc/DOSXYZnrc. This lack of flexibility led to the decision to reprogram the program completely, focusing on user-friendliness, flexibility and quality. This recently lead to a new system (Moderato) that allows an easy handling of new treatment units and even switching between different Monte Carlo engines. But the main focus of current paper is to describe how such a system was introduced in clinical routine in a smooth way that didn't add additional tasks to the dosimetrists.

Methods and Materials

Description of the Monte Carlo platform

As current Monte Carlo platform is based on MCDE it was originally constructed around BEAMnrc/DOSXYZnrc while focusing on flexibility. The main flow of a Monte Carlo plan validation is illustrated in figure 1.

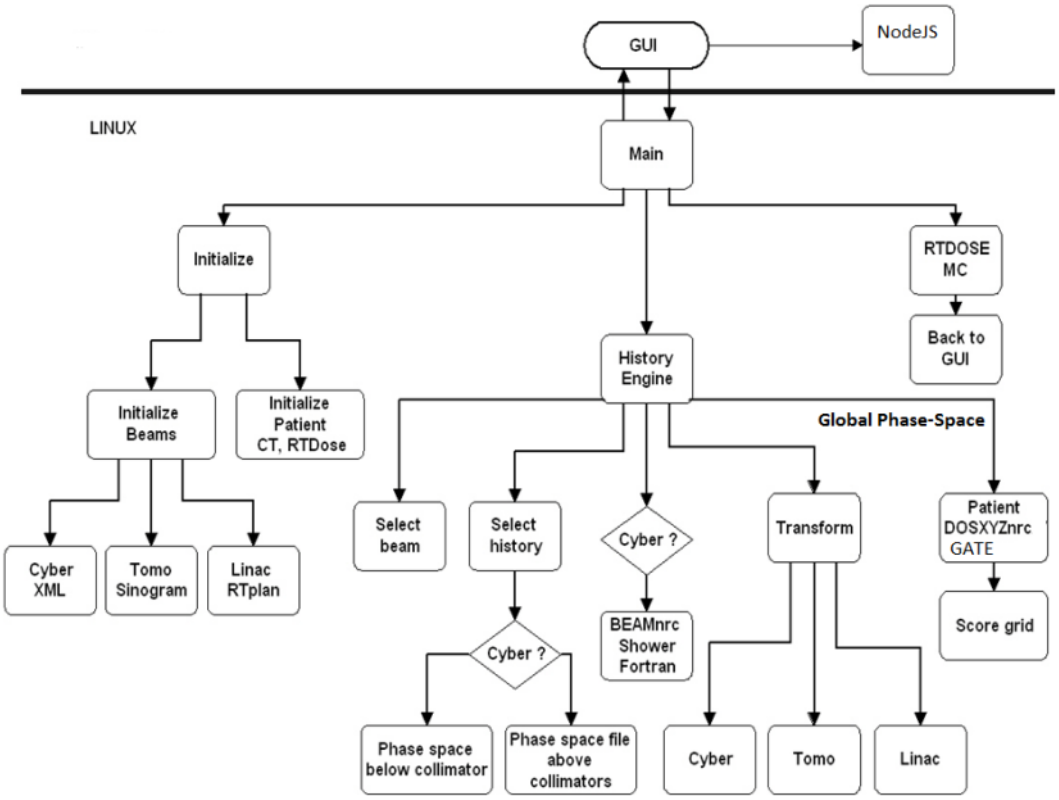

Figure 1. Flow chart of Moderato. The GUI is accessible via a web browser and allows uploading patient data, launching calculations, visualizing the isodoses and the DVHs, and printing a report. The main functionality is programmed in C++. The history engine is centralized in Moderato allowing easy switching between different Monte Carlo codes. For Cyberknife phase-space files can be pre-calculated for the two sets (fixed and Iris) of 12 collimators, consequently the BEAMnrc calculation step is replaced by simply reading these files. The initialization of Tomotherapy treatments is possible using the binary sinogram but also via the RTPlan file. The transformation depends on the degrees of freedom (rotation angles, table movement) of each modality. The patient calculation can be performed using DOSXYZnrc or GATE.

The process can be summarized as follows:

- Initializing geometry and BEAMnrc input files using the dicom/xml files exported from the TPS
- Generating a global phase-space file at the exit plane of the treatment head that combines particles from all beams (can be considered as a cylindrical phase-space surrounding the patient)
- Performing the dose calculation in the patient geometry for each sub-task (MC calculation is ran in parallel on several CPU cores)
- Combining and converting the obtained dose files for all sub-tasks and make the results available in the GUI (the web browser)

The first and the last tasks are handled by a master process (that is also providing the Javascript GUI). The middle part is handled by a number of slave processes and parallelized

over multiple CPU cores. Currently 3 servers, each having 64 CPU cores are combined to parallelize the Monte Carlo calculations. Each slave sub-process runs on a single core and generates phase-space by launching for example a BEAMnrc calculation; transforms this phase-space in dicom coordinates using the beam parameter information, and performs the patient calculation. In such a way each process simulates the complete treatment and the obtained dose files are merged by the master process. As Moderato is simply launching the Monte Carlo calculations by using default commands, one can easily switch between different Monte Carlo engines, by generating the specific input files. No modifications were applied to the Monte Carlo engines. Currently BEAMnrc/DOSXYZnrc and GATE [21] are implemented in Moderato. This allows for example to generate the phase-space using BEAMnrc, while calculating the patient dose distribution, using Gate. The IAEA phase-space format is used to ensure compatibility between the different codes. Ctcreate (BEAMnrc) is used to convert the CT Hounsfield units to a voxelized geometry (density and material composition). The image value to density table (IVDT) is obtained using the stoichiometric calibration method as described in [22, 23]. But other, e.g. TPS and CT specific, IVDT curves are available as well and are selected in the GUI when launching the calculation.

Modeling of the different treatment modalities

1. Cyberknife

The Cyberknife® (Accuray, Sunnyvale, CA, USA) was modeled by Wagner et al. [24]. Both the Iris and fixed collimators were modeled and phase-space files for the two sets of 12 collimators were pre-calculated and stored for utilization in Moderato, i.e. for these calculations the phase-space generation step is replaced by simply reading these phase-space files while saving the transformed particles to the global patient specific phase-space file as described above. Calibration was performed by linking the Monte Carlo calculation for the 6.0 cm field at SAD= 80 cm (1.5 cm depth) with the actual calibration in the water phantom. During the treatment plan calculation, absolute dose is obtained by multiplying the Monte Carlo dose (Gy/primary history) with the obtained calibration factor and the total number of monitor units in the plan. The Cyberknife M6^{TM} (including the Incise^{TM} MLC) was modeled as well. The Cyberknife M6 has a modified (pyramid shape) primary collimator allowing the maximal fieldsize (11.5 cm x 10 cm) when using the MLC. To model the MLC the diagrams provided by Accuray were used. The MLC data are also available in the plan xml file.

2. Tomotherapy

The Tomotherapy® unit (Accuray, Sunnyvale, CA, USA) was modeled using the drawings provided by Accuracy. A double Gaussian spot as described in [25] was needed to obtain agreement between measurements and MC calculations for all jaw openings (1.0, 2.5 and 5.0 cm). Recent treatment options such as the dynamic jaws and TomoDirect were included. The transport through the MLC can be performed using full Monte Carlo transport or by a more efficient ray-tracing technique. The ray tracing considers the detailed geometry (i.e. the tongue and groove, and the leaf bank tilt) of the leafs. The total distance travelled through tungsten is used to calculate an exponential attenuation factor used in a russian roulette process. This method, which is in principle less accurate as scatter in the MLC is completely neglected, is much faster than the full Monte Carlo option and is the default option when recalculating a patient plan in clinical routine. The modeling of the MLC (geometry and

position of the leafs) was based on measurements in the water phantom and treatment planning system calculations of individual beams traversing heterogeneous phantoms. The position of the leaf sides was read from the machine archive file for the individual machines (in our center, 3 Tomotherapy units are used in clinical routine). Afterwards, the commissioning of the global model of the linac head in Moderato was performed on 25 patients of different clinical indications to include treatments with different field sizes, modulation factors and pitch. For this commissioning the agreement with the TPS was considered as the metric. As the Tomotherapy TPS is using an accurate dose calculation algorithm (collapsed cone) and as the accuracy of the TPS has been validated by a large number of DQA measurements, we consider that on average, the TPS will provide accurate results. So we determined a distribution of differences between TPS and Moderato and verified if, on average both systems are in agreement. At the same time outliers could be investigated in detail.

For absolute calibration, the same method as described for the Cyberknife was applied, while replacing the number of monitor units by the treatment time.

Calculation Statistics and voxel sizes

Calculation time can be determined by simply defining the number of primary histories to be simulated, or by applying a statistic stop as described in [18]. When using this last option, the user defines the required uncertainty level and the normalization dose for each region of interest. For example, one can ask for 2 % of the prescription dose in the PTV and for 3 % of 40 Gy in the spinal cord. In a first iteration the Monte Carlo code will determine the uncertainty for 1e5 primary histories and then estimates the number of histories to be added to obtain the required uncertainty level and launches a second iteration. The code runs until all uncertainty levels are met in 95 % of the voxels in each region of interest included in the statistic stop. As this procedure is not efficient, it was only run for a couple of cases for each treatment modality, or for very specific cases. In clinical routine, the number of histories is defined and is only depending on the treatment modality. For Cyberknife 10^8 primary histories are simulated, while for Tomotherapy 10^7 are adequate. This leads to typical uncertainties of 2 % in 95 % of the voxels in the PTV. The number of particles in the phase-space file, just before entering the patient geometry, varies between treatment modalities and even large variations are possible when comparing different Cyberknife treatment plans, as this is largely depending on the collimator sizes used. Typically, the number of particles in these phase-space files is half of the number of primary histories. Moderato allows the user to select the number of times these particles need to be recycled in the patient calculation (on the order of 10). Calculation times on 40 CPU cores are about 15 minutes for the Cyberknife (using pre-calculated phase-space) and 45 minutes for Tomotherapy. For the Cyberknife M6 with MLC, phase-space cannot be pre-calculated and calculation time becomes comparable to Tomotherapy calculations. The dose is scored in the CT voxels. The resolution of the CT dataset can be lowered in the GUI. For Tomotherapy calculations the voxel size of the CT data exported from the Tomotherapy TPS (the CT data containing the treatment couch) is maintained (1.5x1.5x2 mm^3). For Cyberknife, depending on the number of CT slices the original resolution is maintained or divided by 2 in all directions. The slices are always 1 mm and the in-plane resolution is always 1 mm or even below 1 mm (for the head e.g.). For the Cyberknife simulation, the skin contour is used to delimit the number of voxels to be kept in

memory. In the visualization GUI the dose can be recalculated in larger spherical voxels, which comes down to smoothing. This process is only used when the results are really influenced by noise (large PTV tail e.g.).

Delivered dose reconstruction

During a Cyberknife treatment using the Synchrony^{TM} tracking mode for liver or lung tumors, several log files are written. These files contain the actual robot position and the position of the external markers and internal fiducials. For liver treatments the center of mass of the fiducials will serve as a surrogate for the tumor motion (most liver lesions are not visible on the two orthogonal x-ray images). The position of external markers and robot are measured at a frequency of 25 Hz (data were extracted at 10 Hz). The link between external markers and internal fiducials is updated at a frequency chosen by the therapists. The actual contents of the log files have not been validated, as it seems complicated to determine the actual robot position and angles independently. One can imagine that the errors will be very limited as these Kuka robots are known to be extremely precise, as they have been used for several decades in the car industry. In any case, we believe that the usage of these log files will give us a closer approximation of the actually delivered dose, even if these files would contain small errors.

Moderato is able to reconstruct the dose for these moving geometries in an automated way. From the moment the 4D CT (consisting of 5 or 10 phases) of the patient is uploaded into the system, Moderato automatically performs a 4D calculation. When the log files are available as well they are automatically used. If not, the complete treatment plan is applied on every phase of the 4D CT and the dose is warped and summed on the planning CT using ITK [26] and Elastix [27] deformable registration software. This ignores a possible interplay effect between robot and patient movements though [28]. When the log files are present, the synchrony between marker data (external marker or internal fiducial) and robot position is used to link the actual robot position to the different breathing phases. Then, for each CT phase a specific dose calculation is performed, using only the “active” beams (taking into account the actual position of the robot). Again a dose summation using deformable registration is performed to reconstruct the actually delivered dose. It is also possible to increase the time resolution by interpolating the deformation maps to generate intermediate CT datasets, although this has not proven to be clinically relevant for all studied cases. As shown in figure 2, any baseline shift is taken into account. The selection of the respiratory phase is based on the minimum and maximum level, defined in figure 2. These values follow the trend of the baseline.

For Tomotherapy treatments there are no specific log files, but one can calculate dose on the daily MVCT using the reconstructed sinogram (available from the patient archive). This does not take into account any patient movements during the treatment.

Figure 2. Information available in the log files. The x-axis provides the time in ms (with an arbitrary origin), while the y-axis shows the breathing amplitude in arbitrary units. The graph illustrates how the base line drift is taken into account when selecting the individual breathing phases. The respiratory phase is selected by scaling between the min and the max line (taking into account the difference between inspiration and expiration). As these lines are following the drift in the base line, this will be correctly taken into account when selecting the phase. An example of this selection is shown in the zoom below. The "E" denotes the start of the exhale and the "I" that of the inhale.

Introduction of Moderato in clinical routine

The main purpose of the software was to have an independent dose recalculation for Cyberknife and Tomotherapy plans. In our department a systematic dose recalculation is performed for the conformal plans (performed on our Varian™ Clinacs), using the commercial software package IMSURE QA™ (Standard Imaging, Middleton, USA) that recalculates the monitor units in the prescription point. For Tomotherapy and Cyberknife treatments a more accurate system is needed providing a full 3D dose validation. Therefore, the MCDE algorithm, programmed at the University of Ghent, was reprogrammed, using an object oriented strategy, as explained above. But next to that we decided that this system shouldn't add additional work in the dosimetry department. Once a plan is finalized it is exported to a dicom server running on the Linux host of Moderato. The directory containing the incoming dicom files is continuously scanned and from the moment all data for a specific patient are available the system launches a Monte Carlo calculation automatically. The status of all cases can be visualized on the so-called Dashboard of Moderato projected on a big screen in the planning room. This window also allows a quick visual check if the export was correctly performed and if all dicom files are available. Once the calculation is finished and the results are available a flag is activated in our patient flow system (RT-Flow™ Surgiqual Institute, Grenoble, France), indicating that the patient plan is ready for validation by the physicist and the physician. One simple click activates the visualization screen containing the

isodoses, the DVH data and a table containing dose-volume information for relevant dose-volume points of all delineated organs. This sheet can then directly be included in a Record and Verify system. At the same time the system is removed from the Dashboard. This procedure allows a systematic validation of all Cyberknife and Tomotherapy patients, using the 192 CPU cores on the 3 Linux servers.

MRI-only dose calculation in Moderato

It is well known that MRI provides an optimal soft-tissue differentiation and allows more accurate target volume delineation in modern radiotherapy [29]. Current dose calculation algorithms require electron density, thus MRI and CT data need to be registered, increasing uncertainty, when propagating contours. A direct dose calculation on MRI images can reduce the uncertainty and also simplifies the treatment planning process. Recently introduced radiotherapy specific MRI systems allow positioning the patient in the actual treatment position [29]. A number of research groups have focused on converting MRI datasets to pseudo-CT images that can be used for attenuation corrections in PET/MRI or for treatment planning, assigning bulk densities [31], atlas-based methods [31] or direct conversion of MRI grey levels, using dedicated MRI sequences (e.g. ZTE or DUTE) [32].

As described in a recently submitted paper [33], we are currently working on several scientific projects on MRI-only treatment planning. Moderato plays an important role in the dosimetrical validation of the pseudo-CTs, generated by the atlas-based deformation method, which is an optimization of the method originally introduced by Dowling et al. [31]. We are specifically focusing on Head and Neck patients and thus on the impact of air cavities when using small beams (Cyberknife and Tomotherapy).

Results

Modeling and commissioning of our 3 Tomotherapy units

As the profiles and PDDs in the watertank were almost superimposing perfectly (within 1 %) and as this paper is not really focusing on these modeling issues a detailed comparison is not shown. Instead, we prefer to describe the setup and results we obtained for a direct comparison between TPS and Moderato for individual beams on a phantom.

One example is shown in figure 3.a but the same test was performed for all field sizes (1.0, 2.5 and 5.0 cm). A density override was used both in the TPS and in Moderato excluding the impact of the IVDT for these test cases. A worst case scenario was considered by defining a lung density of 0.1 g/cm^3.

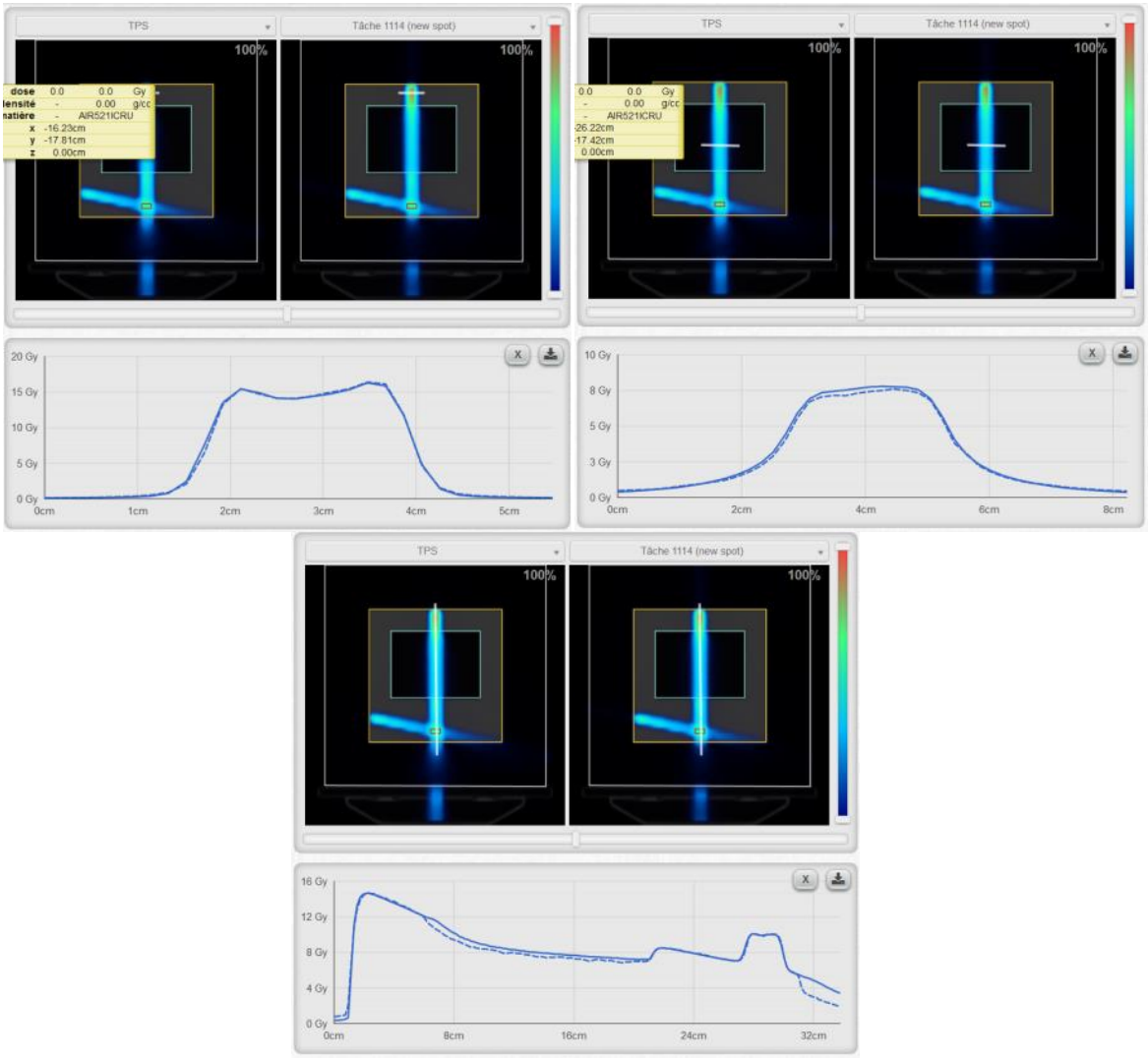

Figure 3. The dose visualisation GUI of Moderato, illustrating the direct comparison between Moderato and the Tomotherapy TPS for an individual beam on a "lung" phantom (the second beam is added because the TPS does not allow defining a single beam). Two profiles are shown. The first profile illustrates the agreement between TPS and Moderato in water. In the lung cavity a difference is observed (confirmed by the PDD below). This difference is because of the limitations of collapsed cone algorithms in this low density (0.1 g/cm^3) region. The differences in the air surrounding the phantom are caused by a different IVDT, but these differences are not relevant.

The profile illustrated in figure 3 is in the direction perpendicular to the leaf and jaw motion, testing the modeled leaf sides, which has proven to be the most critical parameter (actual position read from the xml machine archive, but also the Tongue and Groove). The agreement obtained was (in absolute dose) as good as perfect for all studied cases (within 1 %). The leaf sides extracted from the xml files of our 3 Tomotherapy units were almost identical. So a common model was used for the 3 units.

A comparison of the PDD through the lung cavity is an interesting test for the collapsed cone algorithm used in the Tomotherapy treatment planning system. Even for this very low lung density the precision of the TPS is more than acceptable (see figure 3.b).

To determine the impact of the leaf sides as a function of offset a "picket fence" test was planned on the same phantom as described above. Dose was systematically prescribed to several PTVs while minimizing the dose in the regions between the GTVs in order to force the system to close intermediate leaves.

The result of this comparison is shown in figure 4, again comparing absolute dose, illustrating a perfect agreement (within 1 %).

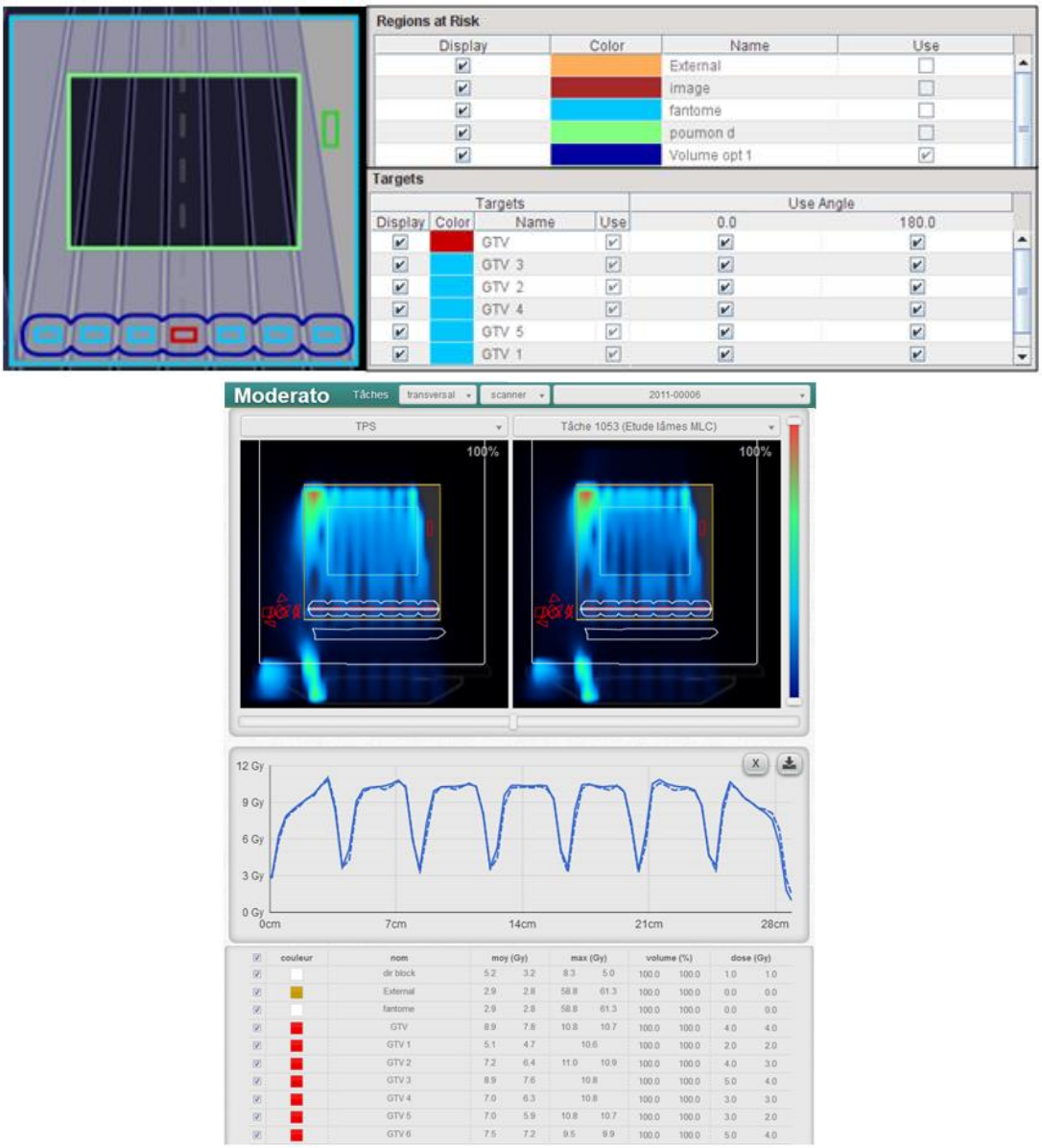

Figure 4: Picket fence test. The image above shows the TPS interface and the definition of the 7 GTVs. Below the results, illustrating an almost perfect agreement between Moderato and TPS. The travel direction of the MLC is perpendicular to the plane. This test is evaluating the leaf sides and the position (perpendicular to the leaf motion). A test parallel to the leaf motion is not necessary as a binary MLC is used.

These results encouraged us to start recalculating patient plans. Again the comparison is absolute and we used the stoichiometric IVDT curve obtained by Demol et al [22]. This curve differs from the IVDT used in the TPS to ensure an independent dose recalculation. One example of such a comparison is shown in figure 5.a for a breast treatment.

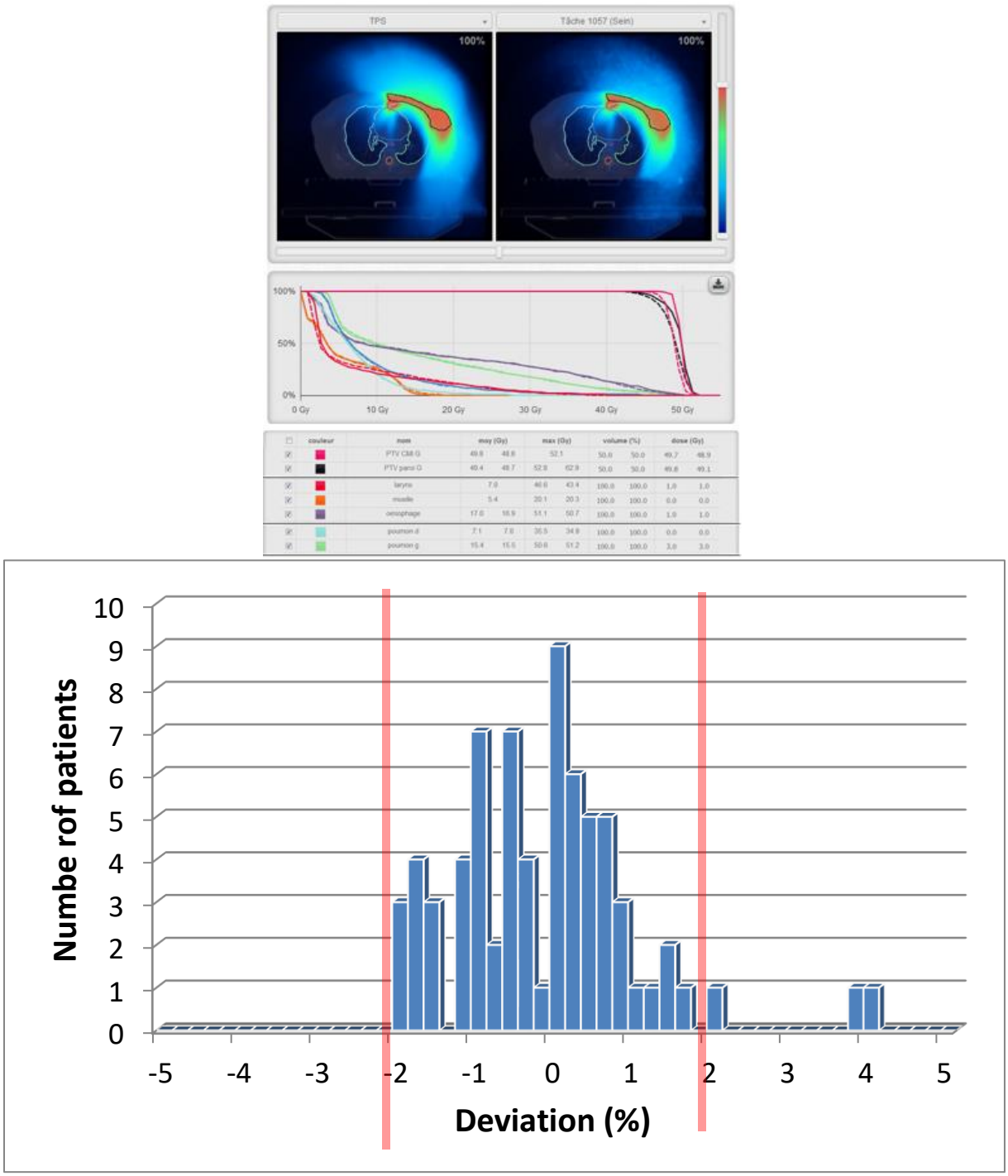

Figure 5. Comparison for a breast patient (above). Below a histogram for 25 targets in 23 patients (mixing different clinical indications) illustrating the agreement of the Tomotherapy model in Moderato. For one patient (having two PTVs) a difference of 4 % is observed because of a problem with the CT data. For all other patients, an agreement between TPS and Moderato within 2 % is obtained.

A study on 23 patients (25 PTVs) is shown in figure 5c. For all patients an agreement between TPS and Moderato within 2 % was obtained for all relevant dose-volume parameters. A gamma test for these cases is considered irrelevant as there is no positioning uncertainty as all doses are calculated on the same scoring grid. For all studied cases, the ray-tracing option provided almost identical dose distributions to the full Monte Carlo simulation through the MLC (within 1 %). As the Tomotherapy system uses a binary MLC (individual leaves are

always fully open or fully closed), the leaf scatter is less important, which explains the fact that the ray-tracing provides correct results.

For one specific breast case an important difference (4 %) between TPS and Moderato was observed. As all treatment parameters were identical to a number of other breast cases, this difference was really patient specific. The only difference with the other patients was the large CT reconstruction diameter (70 cm). Inspecting the scan revealed high HU in a ring surrounding the patient (leading to voxels in air having a density > 0.1 g/cm^3). Removing this CT artifact again led to a perfect agreement.

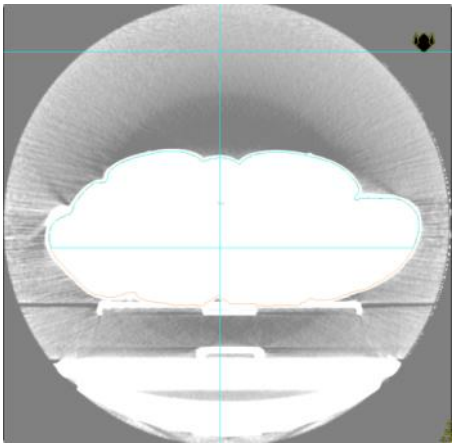

Figure 6. CT data for a large reconstruction diameter (70 cm), giving rise to a ring artifact modeled as high density air in the TPS. The air surrounding the patient has an increasing density when increasing the diameter. At the extreme diameter of 70 cm air has a density of 0.1 g/cm^3. This leads to an overestimation of the attenuation of the beam before entering into the patient. As this effect depends on the IVDT, a large difference (4 %) was obtained between Moderato and the TPS for this specific patient.

Modeling and commissioning of the Cyberknife unit

The modeling of the Cyberknife unit was described by Wagner et al. [24]. In current paper only clinical applications are shown. For most cases the agreement was within 2 %, when comparing to the Monte Carlo results obtained using the Cyberknife TPS (Multiplan). Multiplan allows a direct comparison between the two calculation algorithms available in the TPS (ray-tracing and Multi Plan Monte Carlo). Remark that for the Cyberknife M6, Multiplan uses a third algorithm namely a Pencil Beam algorithm for the MLC plans. Two examples, for different indications, are shown in figure 7.

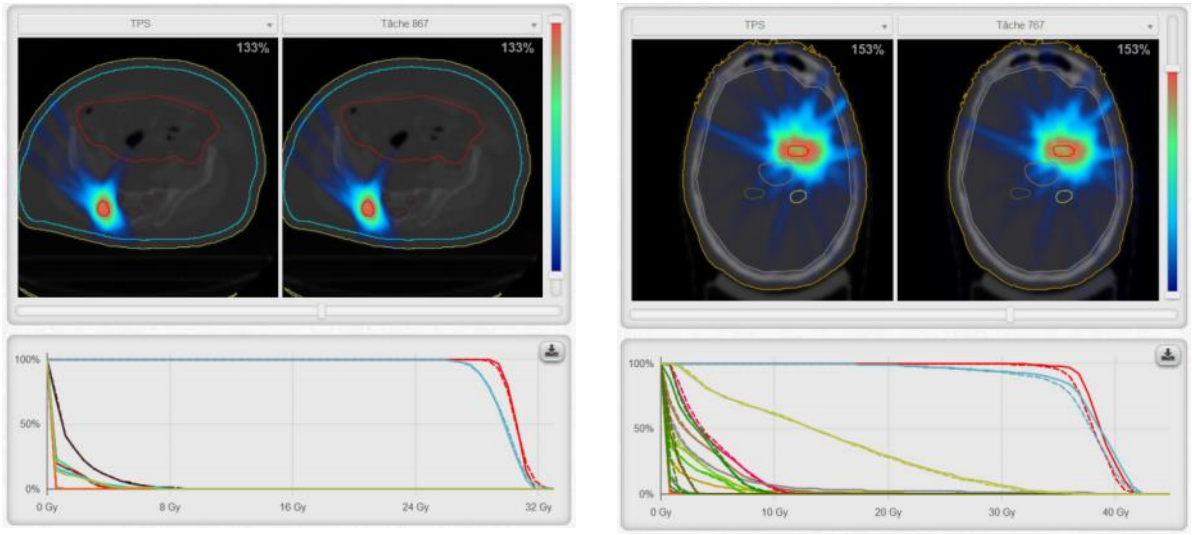

Figure 7. Comparison between Moderato and Cyberknife TPS for two Cyberknife treatments. The first case (left) is a bone metastasis in the pelvic region (iliac), while the second is a brain metastasis. Especially for the first case, small collimators are used (down to 7.5 mm). For the first case the agreement is within 0.5 % at all dose-volume levels. For the second case a difference of 1.8 % is observed for the PTV50.

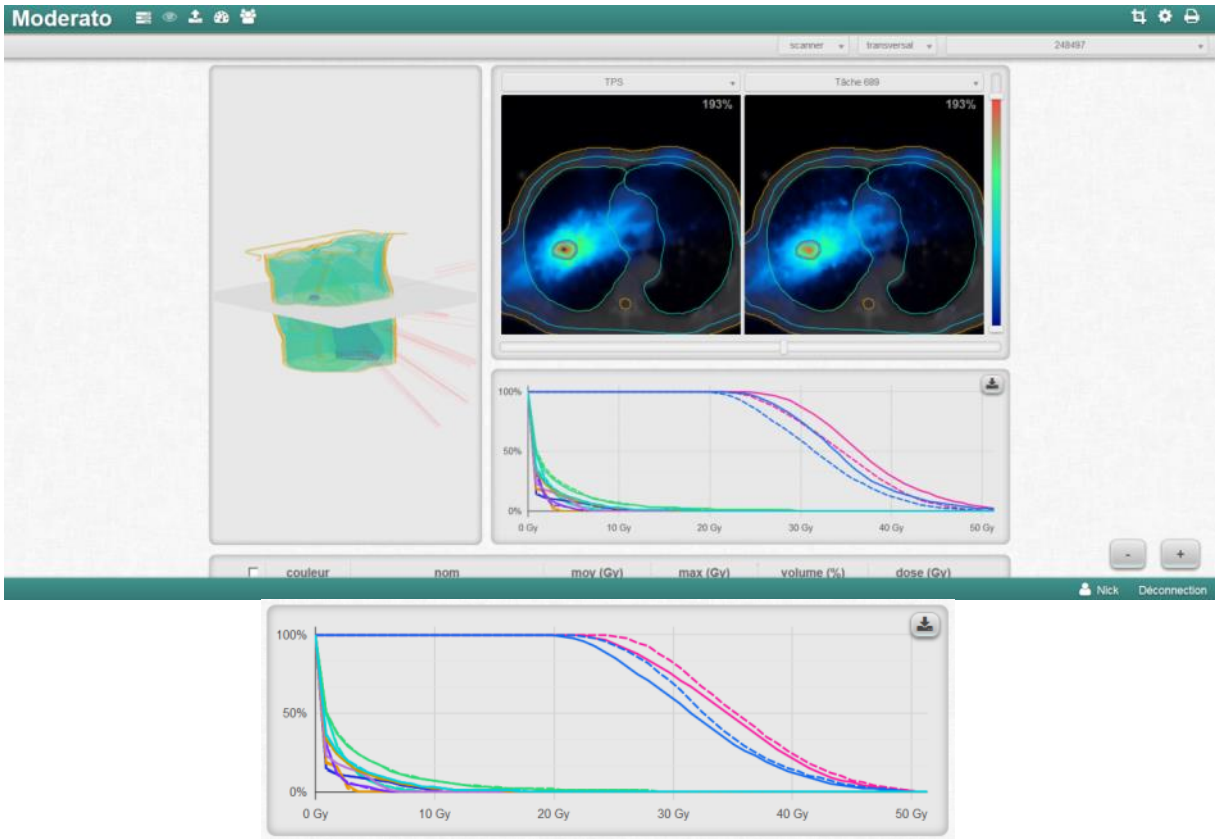

Figure 8. Comparison between Multiplan Monte Carlo (left on isodose plot, and solid line in DVH) and Moderato for a Cyberknife treatment of a small lung lesion surrounded by low density lung tissue, illustrating the impact of using different energy cut-off values for secondary electrons. A PTV50 difference of 6 % is observed between TPS and Moderato. In the figure below, the original Moderato results, calculated with an ECUT of 10 keV (solid line), are compared to a calculation using ECUT = 50 keV. Modifying ECUT does explain most of the deviation.

Even for lung patients, when the difference between the ray-tracing and Monte Carlo options in Multiplan can be very large, the agreement between Multiplan Monte Carlo and Moderato is within 2%. Only for very extreme cases, namely small lung tumors surrounded by low

density lung tissue a more important difference is obtained (PTV50 differs by 6 %), because of the different energy cut-off value used for the secondary electron transport (see figure 8).

Repeating the Moderato calculation with a higher ECUT value (50 keV instead of 10 keV) resolves most of the problem, although there still remains a small difference. This is probably because of other approximation applied in the TPS Monte Carlo algorithm. For these extreme cases, these differences can be considered as clinically acceptable.

4D dose calculation: delivered dose

An example for a specific liver patient treated on Cyberknife is provided, showing a comparison between the planned and the actually delivered dose deformed on the planning CT (see figure 9). The differences are very small (within 2 % of the prescribed dose), because of the limited motion, which is probably because of the treatment belt, systematically used for liver patients in our department. This example illustrates the feasibility of the above described method, all results were obtained automatically.

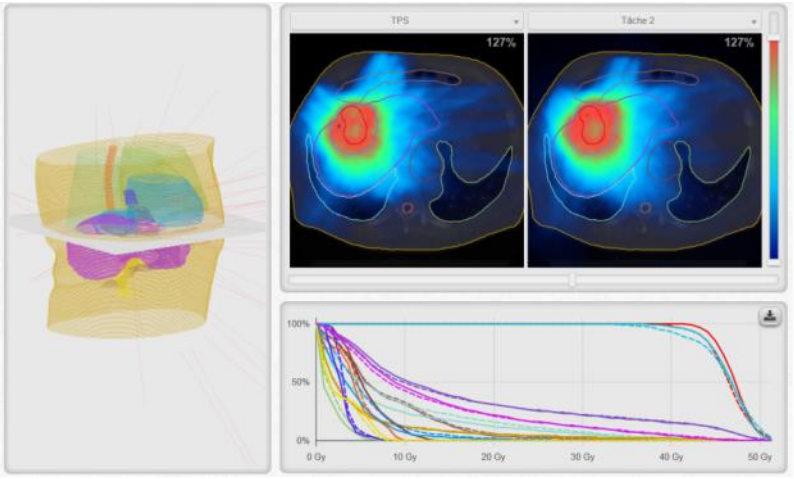

Figure 9. Comparison between planned and delivered dose (both obtained using Moderato) for a liver lesion treated on Cyberknife using the Synchrony tracking system. For the GTV50 a 1.5 % difference is observed (delivered dose < planned dose), while in the colon delivered dose is 4 % higher when normalizing to the local dose (1.5 % when normalizing to the prescription dose). This is the impact of tracking the tumor without taking into account the deformations (beams getting closer to the OAR than during planning).

Dose calculations on MRI

An example of a Monte Carlo calculation on a pseudo-CT dataset is shown in figure 10. The atlas-based method provides in general an agreement within 2 %, when comparing DVHs on actual CT and pseudo-CT. As described in a dedicated paper, for very specific cases [34], when the deformation method cannot accurately reproduce the patient geometry, more important deviations (> 5 %) can be obtained though. One specific example is a patient having part of the skull removed. As illustrated in figure 11, for this case, a simple atlas-based method can never provide an accurate pseudo-CT. For these atypical anatomies the conversion method should fall back to a direct conversion of MRI grey levels, using tissue segmentation e.g.. The same can be said about air cavities that can vary largely from one patient to another.

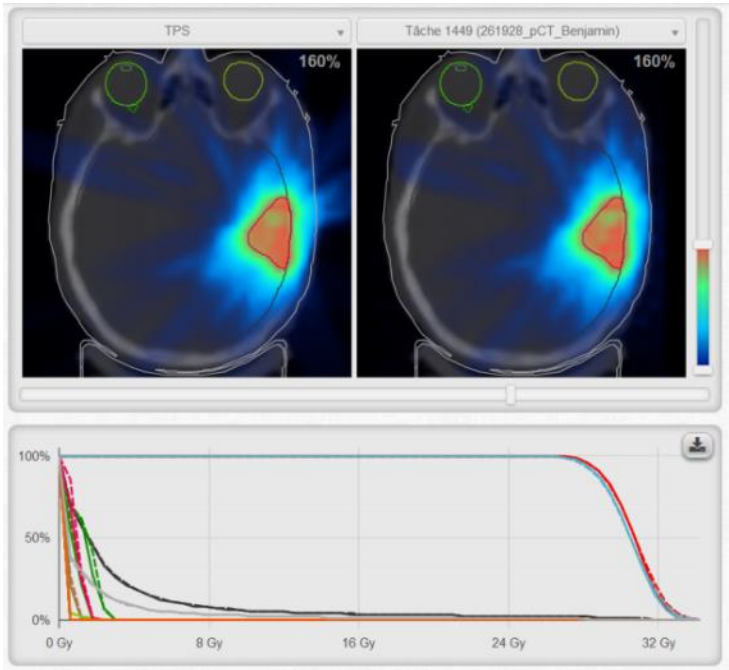

Figure 10: Comparison of dose distributions obtained on a pseudo-CT compared to the real CT, using Moderato. The DVHs are all in agreement within 0.5 %, proving the point that the pseudo-CT can be considered equivalent to the actual CT and would lead to an identical treatment plan. Comparable results are obtained for 90 % of our head and neck patients.

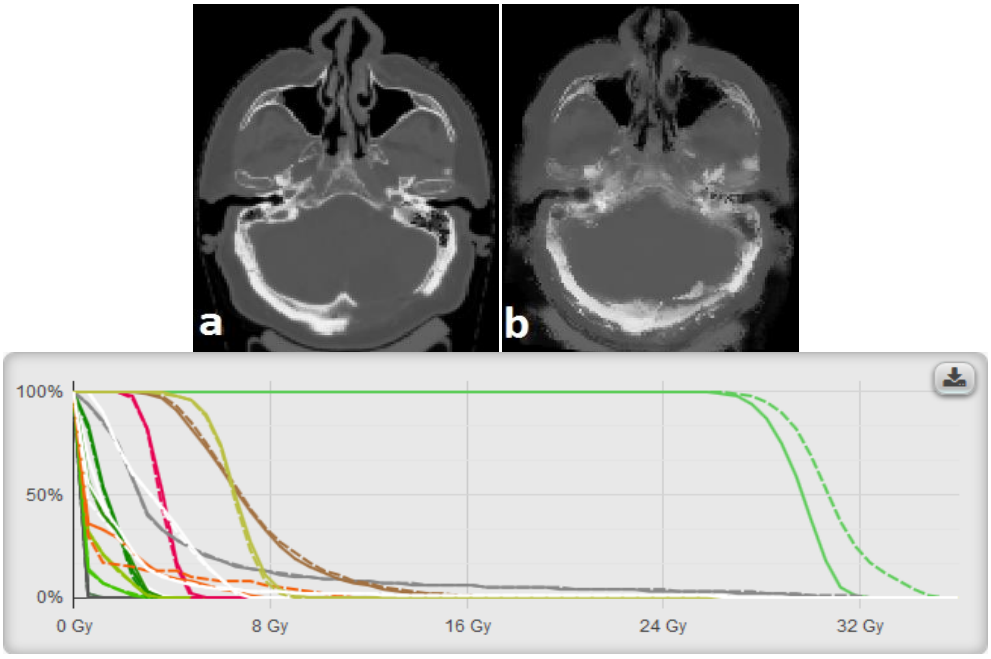

Figure 11: Comparison between actual CT (a) and pseudo-CT (b) for a patient that underwent surgery resulting in the removal of part of the skull. The atlas-based deformation method is not able to reproduce the hole in the skull in the pseudo-CT, which clearly leads to important dose deviations (> 5 %) in the GTV (located next to the hole), as shown in the DVHs below (full line = actual CT).

Discussion

An independent dose validation is a legal requirement in France, for all treatments when this is technically feasible. Up to now, all conventional conformal treatments are validated using a commercial system such as IMSURE QA. Although the system is easy to implement in clinical routine it lacks precision when more advanced treatments need to be validated, as it is

using an approximate algorithm to validate a more advanced dose calculation engine. Many radiotherapy departments have developed in-house software systems for these validations, mostly based on Monte Carlo algorithms. To our knowledge most of these systems are not used on a daily basis though, or in any case not for every individual patient. This demands more than a precise algorithm, namely a robust user-friendly system that does not add additional burden to the workflow in the dosimetry department. This is the focus of current paper. Moderato is a Monte Carlo platform that can be accessed by using a simple web page, for uploading patient data, launching Monte Carlo calculations and evaluating the plan comparison in a very user-friendly way. The automation has even further increased the ease of use. Simply exporting the finalized plan data (which is a task that is already performed when exporting to the PACS) to a specific dicom server; launches the calculation using default parameters, and the status can be followed in real-time. The only additional task is handled during the plan validation by the physicist, who needs to open the visualization page of the GUI and print the report for inclusion in our R&V system (four clicks).

It is often a point of discussion if treatment plans provided by modern TPS algorithms should still be validated by an independent algorithm, as these systems often use advanced dose calculation algorithms such as collapsed cone or even Monte Carlo. Current paper describes the importance of this validation. Even for the small number of patients and even knowing that the dose calculation algorithm used in the Tomotherapy TPS is very precise, an independent dose verification tool has already proven useful for this specific case, illustrating an IVDT problem for large reconstruction diameters.

One can even consider adding additional functionality to the software. Currently, we are working on the automation of the dose prescription step (PTV dose and OAR constraints) which will allow Moderato to automatically validate the plan quality and to highlight specific constraint violations in the table below the DVHs in the Moderato GUI.

A next step is to focus on delivered dose, using all available information saved during the treatment sessions (such as daily images, log files, reconstructed sinogram …). The main limitation of current technique is that everything is based on the 4D planning CT, which is just a snapshot of the breathing motion, not necessarily representative for motion during the actual treatment. Once 4D cone beam CT or even 4D MRI will be available during the treatment, the precision of our dose reconstruction method can even be further increased. As we are interested in a database system containing all patient treatments (“rapid learning”) [34] to construct clinical decision support systems, we need to ensure that the quality of the data is guaranteed. Replacing planned by delivered dose is an important step towards high quality data and can be linked to clinical outcome and toxicity data. The usage of MRI is a second important brick in the construction of a predictive system. That’s why we need to be able to calculate on MRI images and why this is also an important ingredient of Moderato. A dose calculation on a pseudo-CT is not specific though for our Monte Carlo tool, as any TPS can be used for this purpose. We are currently working on a more direct introduction of the MRI images into Moderato. One option could be to convert MRI grey values of a dedicated MRI sequence (ZTE e.g.) into cross sections or by using the hydrogen content as an intermediate parameter as explained in Demol et al. [22].

Conclusion

In current paper the introduction in clinical routine of a Monte Carlo based platform for quality control in radiotherapy was described. The main focus is the possibility to verify the planned dose distribution for every individual patient without adding additional burden to the dosimetrists and medical physicists of the department. This is obtained by a high degree of automation. This allows in routine validation of all patients treated by Tomotherapy and/or Cyberknife, two treatment modalities that demand very precise dose calculation algorithms. Compared to a conventional monitor unit validation tool that only provides the dose in the isocentre, the MC platform provides 3D dose information in the form of isodose information and DVH data. The possibility of switching between different Monte Carlo engines allows simulating different treatment modalities, always using the most adapted algorithm. Next to that, log files, daily images and 4D CT data can be used for calculation of actually delivered dose and dose can also be calculated on MRI. For the moment we are still using pseudo-CT data, but in the near future a more direct link between MRI grey levels and Monte Carlo cross sections will be introduced.

Acknowledgements

Part of the work presented in current paper has been financed by a Siric OncoLille project and a “PhysiCancer” project of the INCA in France.

References

[1] Chen L, Chen LX, Huang SM, Sun WZ, Sun HQ, Deng XW. Independent verification of monitor unit calculation for radiation treatment planning system. Chin J Cancer. 2010; 29(2):217-22

[2] Georg D, Nyholm T, Olofsson J, Kjaer-Kristoffersen F, Schnekenburger B, Winkler P, Nyström H, Ahnesjö A, Karlsson M. Clinical evaluation of monitor unit software and the application of action levels. Radiother Oncol. 2007; 85(2):306-15

[3] Stern RL, Heaton R, Fraser MW, Goddu SM, Kirby TH, Lam KL, Molineu A, Zhu TC; AAPM Task Group 114. Verification of monitor unit calculations for non-IMRT clinical radiotherapy: report of AAPM Task Group 114. Med Phys. 2011; 38(1):504-30

[4] Chan J, Russell D, Peters VG, Farrell TJ. Comparison of monitor unit calculations performed with a 3D computerized planning system and independent "hand" calculations: results of three years clinical experience. J Appl Clin Med Phys. 2002; 3(4):293-301

[5] Fan J, Li J, Chen L, Stathakis S, Luo W, Du Plessis F, Xiong W, Yang J, Ma CM. A practical Monte Carlo MU verification tool for IMRT quality assurance. Phys Med Biol. 2006; 51(10):2503-15

[6] Ahmad SB, Sarfehnia A, Paudel MR, Kim A, Hissoiny S, Sahgal A, Keller B. Evaluation of a commercial MRI Linac based Monte Carlo dose calculation algorithm with geant 4. Med Phys. 2016; 43(2):894.

[7] Fonseca TC, Campos TP. SOFT-RT: Software for IMRT simulations based on MCNPx code. Appl Radiat Isot. 2016; pii: S0969-8043(15)30400-0

[8] Jabbari I, Monadi S. Development and validation of MCNPX-based Monte Carlo treatment plan verification system. J Med Phys. 2015; 40(2):80-9

[9] Chetty IJ, Curran B, Cygler JE, DeMarco JJ, Ezzell G, Faddegon BA, Kawrakow I, Keall PJ, Liu H, Ma CM, Rogers DW, Seuntjens J, Sheikh-Bagheri D, Siebers JV. Report of the AAPM Task Group No. 105: Issues associated with clinical implementation of Monte Carlo-based photon and electron external beam treatment planning. Med Phys. 2007; 34(12):4818-53

[10] Reynaert N, Van der Marck S C, Schaart D R, Van der Zee W, Van Vliet-Vroegindeweij C, Tomsej M, Jansen J, Heijmen B, Coghe M and De Wagter C. Monte Carlo Treatment Planning for photon and electron beams (Topical Review), Rad. Phys. Chem. 2007; 76(4):643-686

[11] Reynaert N, Coghe M, De Smedt B, Paelinck L, Vanderstraeten B, De Gersem W, Van Duyse B, De Wagter C, De Neve W, Thierens H. The importance of accurate linear accelerator head modelling for IMRT Monte Carlo calculations. Phys Med Biol. 2005; 50(5):831-46

[12] Reynaert N, De Smedt B, Coghe M, Paelinck L, Van Duyse B, De Gersem W, De Wagter C, De Neve W, Thierens H. MCDE: a new Monte Carlo dose engine for IMRT. Phys Med Biol. 2004; 49(14):N235-41

[13] Sterpin E, Tomsej M, De Smedt B, Reynaert N, Vynckier S. Monte carlo evaluation of the AAA treatment planning algorithm in a heterogeneous multilayer phantom and IMRT clinical treatments for an Elekta SL25 linear accelerator. Med Phys. 2007; 34(5):1665-77

[14] Paelinck L, Smedt BD, Reynaert N, Coghe M, Gersem WD, Wagter CD, Vanderstraeten B, Thierens H, Neve WD. Comparison of dose-volume histograms of IMRT treatment plans for ethmoid sinus cancer computed by advanced treatment planning systems including Monte Carlo. Radiother Oncol. 2006; 81(3):250-6

[15] Vanderstraeten B, Reynaert N, Paelinck L, Madani I, De Wagter C, De Gersem W, De Neve W, Thierens H. Accuracy of patient dose calculation for lung IMRT: A comparison of Monte Carlo, convolution/superposition, and pencil beam computations. Med Phys. 2006; 33(9):3149-58

[16] Walters B, Kawarakow I, Rogers D W O., DOSXYZnrc users manual, NRCC Report No. PIRS-794revB, 2004; unpublished

[17] Rogers D W O, Walters B, Kawrakow .I BEAMnrc user manual, NRCC Report No. PIRS-0509ArevK, 2006; unpublished

[18] Vanderstraeten B, Olteanu AM, Reynaert N, Leal A, De Neve W, Thierens H. Evaluation of uncertainty-based stopping criteria for monte carlo calculations of intensity-modulated radiotherapy and arc therapy patient dose distributions. Int J Radiat Oncol Biol Phys. 2007; 69(2):628-37

[19] De Smedt B, Fippel M, Reynaert N, Thierens H. Denoising of Monte Carlo dose calculations: smoothing capabilities versus introduction of systematic bias. De Smedt B, Fippel M, Reynaert N, Thierens H. Med Phys. 2006; 33(6):1678-87

[20] De Smedt B, Vanderstraeten B, Reynaert N, De Neve W, Thierens H. Investigation of geometrical and scoring grid resolution for Monte Carlo dose calculations for IMRT. Phys Med Biol. 2005; 50(17):4005-19

[21] Sarrut D, Bardiès M, Boussion N, Freud N, Jan S, Létang JM, Loudos G, Maigne L, Marcatili S, Mauxion T, Papadimitroulas P, Perrot Y, Pietrzyk U, Robert C, Schaart DR, Visvikis D, Buvat I. A review of the use and potential of the GATE Monte Carlo simulation code for radiation therapy and dosimetry applications. Med Phys. 2014; 41(6):064301. doi: 10.1118/1.4871617.

[22] Demol B, Viard R, Reynaert N. Monte Carlo calculation based on hydrogen composition of the tissue for MV photon radiotherapy. J Appl Clin Med Phys. 2015; 16(5):5586

[23] Vanderstraeten B, Chin PW, Fix M, Leal A, Mora G, Reynaert N, Seco J, Soukup M, Spezi E, De Neve W, Thierens H. Conversion of CT numbers into tissue parameters for Monte Carlo dose calculations: a multi-centre study. Phys Med Biol. 2007; 52(3):539-62

[24] Wagner A, Crop F, Lacornerie T, Vandevelde F, Reynaert N. Use of a liquid ionization chamber for stereotactic radiotherapy dosimetry. Phys Med Biol. 2013; 58(8):2445-59

[25] Chen Q, Chen Y, Chen M, Chao E, Sterpin E, Lu W. A slit method to determine the focal spot size and shape of TomoTherapy system. Med Phys. 2011; 38(6):2841-9

[26] Johnson H J, McCormick M, Ibánez L The ITK software guide. Kitware Inc.,. 2013 www.itk.org

[27] Klein S, Staring M, Murphy K, Viergever M A, Pluim J P W, elastix: a toolbox for intensity based medical image registration, IEEE Transactions on Medical Imaging. 2010; 29(1), 196 - 205

[28] Litzenberg DW, Hadley SW, Tyagi N, Balter JM, Ten Haken RK, Chetty IJ. Synchronized dynamic dose reconstruction. Med Phys. 2007; 34(1):91-102

[29] Devic S. MRI simulation for radiotherapy treatment planning. Review paper. Int J Radiat Oncol Biol Phys. 2010; 78(5):1555-62.

[30] Pasquier D, Betrouni N, Vermandel M, Lacornerie T, Lartigau E, Rousseau J. MRI alone simulation for conformal radiation therapy of prostate cancer: technical aspects. Conf Proc IEEE Eng Med Biol Soc. 2006; 1:160-3

[31] Dowling JA, Lambert J, Parker J, Salvado O, Fripp J, Capp A, Wratten C, Denham JW, Greer PB. An atlas-based electron density mapping method for magnetic resonance imaging (MRI)-alone treatment planning and adaptive MRI-based prostate radiation therapy. Int J Radiat Oncol Biol Phys. 2012; 83(1):e5-11

[32] Johansson A, Karlsson M, Nyholm T. CT substitute derived from MRI sequences with ultrashort echo time. Med Phys. 2011; 38(5):2708-14.

[33] Demol B, Boydev C, Korhonen J, Reynaert N. Dosimetric characterization of MRI-only treatment planning for brain tumors in atlas-based pseudo-CT images generated from standard T1-weighted MR images. Med. Phys. 2016; Under revision

[34] Lambin P, Roelofs E, Reymen B, Velazquez ER, Buijsen J, Zegers CM, Carvalho S, Leijenaar RT, Nalbantov G, Oberije C, Scott Marshall M, Hoebers F, Troost EG, van Stiphout RG, van Elmpt W, van der Weijden T, Boersma L, Valentini V, Dekker A. 'Rapid Learning health care in oncology' - an approach towards decision support systems enabling customised radiotherapy'. Radiother Oncol. 2013; 109(1):159-64.

References

[1] Wild CP. World Cancer Report 2014 n.d.

[2] Barton MB, Jacob S, Shafiq J, Wong K, Thompson SR, Hanna TP, et al. Estimating the demand for radiotherapy from the evidence: A review of changes from 2003 to 2012. Radiother Oncol 2014;112(1):140–4.

[3] Tyldesley S, Delaney G, Foroudi F, Barbera L, Kerba M, Mackillop W. Estimating the need for radiotherapy for patients with prostate, breast, and lung cancers: verification of model estimates of need with radiotherapy utilization data from British Columbia. Int J Radiat Oncol Biol Phys 2011;79(5):1507–15.

[4] ICRU. Prescribing, Recording, and Reporting Photon Beam Therapy, Report 50. 1993.

[5] ICRU. Prescribing, Recording, and Reporting Photon Beam Therapy, Report 62 (Supplement to ICRU report 50). 1999.

[6] ICRU. Prescribing, Recording, and Reporting Photon Beam IMRT, Report 83. vol. 10. 2010.

[7] Grégoire V, Mackie TR. State of the art on dose prescription , reporting and recording in Intensity-Modulated Radiation Therapy (ICRU report No . 83) Recommandations de l ' ICRU sur la prescription , le rapport et l ' enregistrement de la dose en radiothérapie avec modulation d ' intensité (RCMI) 2019;15(83):555–9.

[8] Lambin P, Roelofs E, Reymen B, Velazquez ER, Buijsen J, Zegers CML, et al. "Rapid Learning health care in oncology" - An approach towards decision support systems enabling customised radiotherapy. Radiother Oncol 2013;109(1):159–64.

[9] Ovsas BEM, Oughan JEM, Wen JEANO, Oia LARC, Elefsky MIJZ, Anks GEH, et al. Who enrolls onto clinical oncology trials? A radiation patterns of care study analysis. Int J Rad Oncol Biol Phys 2019;68(4):1145–50.

[10] Grand MM, Brien PCO, Bag L, Rmc H. Obstacles to participation in randomised cancer clinical trials : A systematic review of the literature. J Med Imaging Radiat Oncol 2012;56:31–9.

[11] Abernethy AP, Etheredge LM, Ganz PA, Wallace P, German RR, Neti C, et al. Rapid-Learning System for Cancer Care. J Clin Oncol 2019;28(27).

[12] Jaffray DA, Lindsay PE, Brock KK, Deasy JO, Tomé WA. Accurate Accumulation of Dose for Improved Understanding of Radiation Effects in Normal Tissue. Int J Radiat Oncol Biol Phys 2010;76(3 SUPPL.):135–9.

[13] Vinod S, Min M, Jameson MG, Holloway L. A review of interventions to reduce inter-observer variability in volume delineation in radiation oncology. J Med Imaging Radiat Oncol 2016;60:393–406.

[14] Rash C, Barillot I, Remeijer P, Touw A, van Herk M, J L. Definition of the prostate in CT and MRI - a multi-observer study. Int J Rad Oncol Biol Phys 1999;43(1):57–66.

[15] Thiagarajan A, Caria N, Scho H, Iyer NG, Wolden S, Wong RJ, et al. Target Volume Delineation in Oropharyngeal Cancer : Impact of PET , MRI , and Physical Examination. Int J Rad Oncol Biol Phys 2011;83(1):220–7.

[16] Thorwarth D. Functional imaging for radiotherapy treatment planning : current status and future directions — a review. Br J Radiol 2015;88(March).

[17] Nyholm T, Nyberg M, Karlsson MG, Karlsson M. Systematisation of spatial uncertainties for comparison between a MR and a CT-based radiotherapy workflow for prostate treatments. Radiat Oncol 2009;4(1).

[18] Ulin K, Urie M, Cherlow J. Results of a multi-institutional benchmark test for cranial CT-MR image registration. Int J Rad Oncol Biol Phys 2010;77(5):1584–9.

[19] Edmund JM, Nyholm T. A review of substitute CT generation for MRI-only radiation therapy. Radiat Oncol 2017;12(1):1–15.

[20] Demol B, Viard R, Reynaert N. Monte carlo calculation based on hydrogen composition of the tissue for MV photon radiotherapy. J Appl Clin Med Phys 2015;16(5):117–30.

[21] Boydev C, Demol B, Pasquier D, Saint-Jalmes H, Delpon G, Reynaert N. Zero echo time MRI-only treatment planning for radiation therapy of brain tumors after resection. Phys Medica 2017;42:332–8.

[22] Demol B, Boydev C, Korhonen J, Reynaert N. Dosimetric characterization of MRI-only treatment planning for brain tumors in atlas-based pseudo-CT images generated from standard T 1-weighted MR images. Med Phys 2016;43(12):6557–68.

[23] Klein EE, Hanley J, Bayouth J, Carolina N, Simon W, Dresser S, et al. Task Group 142 report : Quality assurance of medical accelerators. Med Phys 2009;36(September):4197–212.

[24] Smilowitz JB, Das IJ, Feygelman V, Fraass BA, Kry SF, Marshall IR, et al. Commissioning and QA of Treatment Planning Dose Calculations — Megavoltage Photon and Electron Beams. J App Clin Med Phys 2015;16.

[25] Papanikolaou N, Battista JJ, Boyer AL, Kappas C, Klein E, Mackie TR, et al. AAPM Report No. 85: Tissue inhomogeneity corrections for megavoltage photon beams. 2004.

[26] Kupelian K, Langen M, Zeidan O, Meeks S, Willoughby T, Wagner T, et al. Daily variations in delivered doses in patients treated with radiotherapy for localized prostate cancer. Med Phys 2006;66(3):876–82.

[27] Lee L, Quynh-Thu L, Xing L. Retrospective IMRT dose reconstruction based on cone-beam CT and MLC log-file. Int J Radiat Oncol Biol Phys 2008;70(2):634–44.

[28] Swaminath A, Massey C, Brierley JD, Dinniwell R, Wong R, Kim JJ, et al. Accumulated Delivered Dose Response of Stereotactic Body Radiation Therapy for Liver Metastases. Int J Radiat Oncol Biol Phys 2015;93(3):639–48.

[29] Shelley LEA, Scaife JE, Romanchikova M, Harrison K, Forman JR, Bates AM, et al. Delivered dose can be a better predictor of rectal toxicity than planned dose in

prostate radiotherapy. Radiother Oncol 2017;123(3):466–71.

[30] Lou J, Huang P, Ma C, Zheng Y, Chen J, Liang Y, et al. Parotid gland radiation dose-xerostomia relationships based on actual delivered dose for nasopharyngeal carcinoma. J Appl Clin Med Phys 2018;19(3):251–60.

[31] Esch A Van, Clermont C, Devillers M, Iori M, Huyskens DP. On-line quality assurance of rotational radiotherapy treatment delivery by means of a 2D ion chamber array and the Octavius phantom. Med Phys 2007;34(10):3825–37.

[32] Low DA, Harms WB, Mutic S, Purdy JA. A technique for the quantitative evaluation of dose distributions. Med Phys 1998;25(5):656–61.

[33] Zhen H, Nelms BE, Tomé W a. Moving from gamma passing rates to patient DVH-based QA metrics in pretreatment dose QA. Med Phys 2011;38(10):5477.

[34] InCA. Institut National du Cancer - Critères d ' agrément pour la pratique de la radiothérapie externe. 2008.

[35] Brock KK, Mutic S, McNutt TR, Li H, Kessler ML. Use of image registration and fusion algorithms and techniques in radiotherapy: Report of the AAPM Radiation Therapy Committee Task Group No. 132: Report. Med Phys 2017;44(7):e43–76.

[36] Zhong H, Chetty IJ. Caution Must Be Exercised When Performing Deformable Dose Accumulation for Tumors Undergoing Mass Changes During Fractionated Radiation Therapy. Radiat Oncol Biol 2017;97(1):182–3.

[37] Reynaert N, Crop F, Sterpin E, Kawrakow I, Palmans H. On the conversion of dose to bone to dose to water in radiotherapy treatment planning systems. Phys Imaging Radiat Oncol 2018;5(August 2017):26–30.

[38] Lebredonchel S, Lacornerie T, Rault E, Wagner A, Reynaert N, Crop F. About the non-consistency of PTV-based prescription in lung. Phys Medica 2017;44:177–87.

[39] Lacornerie T, Lisbona A, Mirabel X, Lartigau E, Reynaert N. GTV-based prescription in SBRT for lung lesions using advanced dose calculation algorithms. Radiat Oncol 2014;9(1):223.

[40] Reynaert N, van der Marck SC, Schaart DR, Van der Zee W, Van Vliet-Vroegindeweij C, Tomsej M, et al. Monte Carlo treatment planning for photon and electron beams. Radiat Phys Chem 2007;76(4):643–86.

[41] Chen Q, Westerly D, Fang Z, Sheng K, Chen Y. TomoTherapy MLC verification using exit detector data. Med Phys 2012;39(1):143–52.

[42] Sevillano D, Mínguez C, Sánchez A, Sánchez-Reyes A. Measurement and correction of leaf open times in helical tomotherapy. Med Phys 2012;39(11):6972–80.

[43] Deshpande S, Xing A, Metcalfe P, Holloway L, Vial P, Geurts M. Clinical implementation of an exit detector-based dose reconstruction tool for helical tomotherapy delivery quality assurance. Med Phys 2017;44(10):5457–66.

[44] Saito M, Kadoya N, Sato K, Ito K, Dobashi S, Takeda K, et al. Comparison of DVH-based plan veri fi cation methods for VMAT : ArcCHECK-3DVH system and dynalog-based dose reconstruction. J App Clin Med Phys 2017;18(4):206–14.

[45] Sun W, Zhang D, Peng Y, Kang D, Wang B, Deng X. Retrospective dosimetry study of intensity- modulated radiation therapy for nasopharyngeal carcinoma : measurement- guided dose reconstruction and analysis. Radiat Oncol 2018;13(42):1–9.

[46] Handsfield LL, Jones R, Wilson DD, Siebers J V., Read PW, Chen Q. Phantomless patient-specific TomoTherapy QA via delivery performance monitoring and a secondary Monte Carlo dose calculation. Med Phys 2014;41(10).

[47] Sterpin E, Salvat F, Cravens R, Ruchala K, Olivera GH, Vynckier S. Monte Carlo simulation of helical tomotherapy with PENELOPE. Phys Med Biol 2008;53(8):2161–80.

[48] Kadoya N, Kon Y, Takayama Y, Matsumoto T, Hayashi N, Katsuta Y, et al. Quantifying the performance of two different types of commercial software programs for 3D patient dose reconstruction for prostate cancer patients: Machine log files vs. machine log files with EPID images. Phys Medica 2018;45(January):170–6.

[49] Au IWL, Ciurlionis L, Campbell N, Goodwin D. Validation of the Mobius system for patient-specific quality assurance using introduced intentional errors. Australas Phys Eng Sci Med 2017;40(1):181–9.

[50] McDonald DG, Jacqmin DJ, Mart CJ, Koch NC, Peng JL, Ashenafi MS, et al. Validation of a modern second-check dosimetry system using a novel verification phantom. J Appl Clin Med Phys 2017;18(1):170–7.

[51] Zhuang AH, Olch AJ. Sensitivity study of an automated system for daily patient QA using EPID exit dose images. J Appl Clin Med Phys 2018;19(3):114–24.

[52] Bresciani S, Poli M, Miranti A, Maggio A, Di Dia A, Bracco C, et al. Comparison of two different EPID-based solutions performing pretreatment quality assurance: 2D portal dosimetry versus 3D forward projection method. Phys Medica 2018;52(May):65–71.

[53] Mijnheer B, Beddar S, Izewska J, Reft C. In vivo dosimetry in external beam radiotherapy. Med Phys 2013;40(7):1–19.

[54] Nailon WH, Welsh D, Mcdonald K, Burns D, Forsyth J, Cooke G, et al. EPID - based in vivo dosimetry using Dosimetry Check ™ : Overview and clinical experience in a 5 - yr study including breast , lung , prostate , and head and neck cancer patients n.d.

[55] Mccowan PM, Asuni G, Uytven E Van, Vanbeek T, Mccurdy BMC, Loewen SK, et al. Clinical Implementation of a Model-Based In Vivo Dose Verification System for Stereotactic Body Radiation Therapy e Volumetric Modulated Arc Therapy Treatments Using the Electronic Portal Imaging Device. Int J Radiat Oncol Biol Phys 2016;97(5):1077–84.

[56] Qin A, Gersten D, Liang J, Liu Q, Grill I, Guerrero T, et al. A clinical 3D / 4D CBCT - based treatment dose monitoring system 2018(September 2017):166–76.

[57] Chao M, Penagaricano J, Yan Y, Moros EG, Corry P, Ratanatharathorn V. Voxel-based dose reconstruction for total body irradiation with helical tomotherapy. Int

J Radiat Oncol Biol Phys 2012;82(5):1575–83.

[58] Branchini M, Fiorino C, Oca ID, Belli ML, Perna L, Muzio N Di, et al. Validation of a method for ‘‘ dose of the day ’’ calculation in head-neck tomotherapy by using planning ct-to-MVCT deformable image registration. Phys Medica 2017.

[59] Thomas SJ, Romanchikova M, Harrison K. Recalculation of dose for each fraction of treatment on TomoTherapy. Br J Radiol 2015;89.

[60] Thomas SJ, Eyre KR, Tudor GSJ, Fairfoul J. Dose calculation software for helical tomotherapy, utilizing patient CT data to calculate an independent three-dimensional dose cube. Med Phys 2012;39(1):160–7.

[61] Sterzing F, Uhl M, Hauswald H, Schubert K, Skora-Perez G, Chen Y, et al. Dynamic jaws and dynamic couch in Helical Tomotherapy. Int J Rad Oncol Biol Phys 2010;76(4):1266–73.

[62] Ahnesjö A. Collapsed cone convolution of radiant energy for photon dose calculation in heterogeneous media. Med Phys 1989;16(4):577–92.

[63] Mackie TR, Scrimger JW, Battista JJ. A convolution method of calculating dose for 15MV x rays. Med Phys 1985;12(2).

[64] Ahnesjo A, Aspradakis MM. Dose calculations for external photon beams in radiotherapy. Phys Med Biol 1999;44:R99–155.

[65] Accuray. Cyberknife Robotic Radiosurgery system - Physics Essentials Guide. 2017.

[66] Ma CM, Li JS, Pawlicki T, Jiang SB, Deng J, Lee MC, et al. A Monte Carlo dose calculation tool for radiotherapy treatment planning. Phys Med Biol 2002;47(10):1671–89.

[67] Ma C, Li J, Deng J. Implementation of Monte Carlo Dose calculation for CyberKnife treatment planning. J Phys Conf Ser 2008;102.

[68] Jeleń U, Söhn M, Alber M. A finite size pencil beam for IMRT dose optimization. Phys Med Biol 2005;50(8):1747–66.

[69] Kawrakow I, Rogers D. The EGSnrc code system: Monte Carlo simulation of electron and photon transport. NRCC Rep PIRS-701 (Nov 7, 2003) 2010:2001–9.

[70] Rogers DWO, Faddegon BA, Ding GX, Ma CM, We J, Mackie TR. BEAM: A Monte Carlo code to simulate radiotherapy treatment units. Med Phys 1995;22(5):503–24.

[71] Rogers DWO, Walters B, Kawrakow I. BEAMnrc Users Manual. Source 2005.

[72] Walters B, Kawrakow I, Rogers DWO. DOSXYZnrc Users Manual. NRCC Rep PIRS-0794 2016(April):1–125.

[73] Rogers DWO, Kawrakow I, Seuntjens JP, Walters BRB, Mainegra-Hing E. NRC user codes for EGSnrc. NRCC Rep PIRS-702 (Rev B) 2013;702:1–92.

[74] Das IJ, Ding GX, Ahnesjö A. Small fields: nonequilibrium radiation dosimetry. Med Phys 2008;35(1):206–15.

[75] International Atomic Energy Agency. Dosimetry of Small Static Fields Used in External Beam Radiotherapy. 2017.

[76] Wagner A, Crop F, Lacornerie T, Vandevelde F, Reynaert N. Use of a liquid ionization chamber for stereotactic radiotherapy dosimetry. Phys Med Biol 2013;58(8):2445–59.

[77] Kawrakow I. egspp: the EGSnrc C++ class library. NRCC Rep PIRS-899 2005(April 2005):1–54.

[78] Reynaert N, De Smedt B, Coghe M, Paelinck L, Van Duyse B, De Gersem W, et al. MCDE: A new Monte Carlo dose engine for IMRT. Phys Med Biol 2004;49(14).

[79] Vanderstraeten B, Chin PW, Fix M, Leal A, Mora G, Reynaert N, et al. Conversion of CT numbers into tissue parameters for Monte Carlo dose calculations: A multi-centre study. Phys Med Biol 2007;52(3):539–62.

[80] Reynaert N, Demol B, Charoy M, Bouchoucha S, Crop F, Wagner A, et al. Clinical implementation of a Monte Carlo based treatment plan QA platform for validation of Cyberknife and Tomotherapy treatments. Phys Medica 2016;32(10):1225–37.

[81] Chen Q, Chen Y, Chen M, Chao E, Sterpin E, Lu W. A slit method to determine the focal spot size and shape of TomoTherapy system. Med Phys 2011;38(6):2841–9.

[82] Wagner A, Crop F, Mirabel X, Tailly C, Reynaert N. Use of an in-house Monte Carlo platform to assess the clinical impact of algorithm-related dose differences on DVH constraints. Phys Medica 2017;42:319–26.

[83] Crop F, Lacornerie T, Mirabel X, Lartigau E. Workflow optimization for robotic stereotactic radiotherapy treatments: Application of Constant Work In Progress workflow. Oper Res Heal Care 2015;6:18–22.

[84] Fontenot JD. Evaluation of a novel secondary check tool for intensity- modulated radiotherapy treatment planning. J Appl Clin Med Phys 2014;15(5):207–15.

[85] Hardcastle N, Oborn BM, Haworth A. On the use of a convolution-superposition algorithm for plan checking in lung stereotactic body radiation therapy. J Appl Clin Med Phys 2016;17(5):99–110.

[86] Thwaites D. Accuracy required and achievable in radiotherapy dosimetry: Have modern technology and techniques changed our views? J Phys Conf Ser 2013;444(1).

[87] Pettersen MN, Aird E, Olsen DR. Quality assurance of dosimetry and the impact on sample size in randomized clinical trials. Radiother Oncol 2008;86(2):195–9.

[88] Müller A, Guido S. Introduction to Machine Learning with Python. O'Reilly; 2017.